THE UNIVERSITY *of* EDINBURGH

Manganese-Enhanced Magnetic Resonance Imaging in Cardiometabolic Disorders

Dr. Shruti Shree Joshi
MBBS MRCP

A thesis presented for the degree of Doctor of Philosophy

The University of Edinburgh

2023

To my dearest Mummy
You are my inspiration and you are in everything I do

Contents

Declaration

This thesis represents the research I undertook at the Centre for Cardiovascular Science, University of Edinburgh and the Edinburgh Heart Centre, Royal Infirmary of Edinburgh between February 2020 and August 2023. Research conducted in this thesis was supported by the British Heart Foundation (FS/CRTF/20/24087 and RE/18/5/34216) and an investigator-initiated award from AstraZeneca (ESR-19-20118). The research was performed in accordance with the Declaration of Helsinki and the regulation of various Research Ethics Committees.

Data presented here have either been published (chapters 3,4 and 6) or are being submitted to peer-reviewed journals (chapter 5).

I contributed to the study design, drafted the protocol, obtained research ethics approval, recruited and scanned patients, performed all the image and data analysis for the studies included in chapters 4-6. A proportion of the patients included in chapters 4 and 5 were co-recruited from the Leicester Biomedical Research Centre (Prof Gerry McCann) but all the image and data analyses were carried out by myself.

Chapter 3 has been included in a previous doctorate thesis presented by Dr. Trisha Singh. I was involved in patient recruitment, image and data analysis for this study along with Dr. Singh. Apart from this, no other content of this thesis has been previously accepted in applications for a degree and all sources of information have been acknowledged appropriately.

This thesis is of my own composition and has not been submitted for any other degree or professional qualification. I have no personal disclosures.

Dr. Shruti Shree Joshi

23rdOctober 2023

Lay Summary

Diabetes is among top ten leading causes of death worldwide and the number of people living with diabetes is going up every year. People with diabetes have a higher risk of developing heart failure and people with both diabetes and heart failure have worse outcomes when compared to patients with heart failure without diabetes. It is well established that the movement of calcium within the heart muscle changes in heart failure but exactly how and why this happens is not completely understood. We currently use magnetic resonance imaging (MRI) to assess the heart muscle but it does not provide information regarding this movement of calcium within the heart muscle. We explored a new imaging technique called manganese-enhanced magnetic resonance imaging to better understand the underlying abnormalities in the heart muscle and pancreas in diabetes. This new technique uses manganese contrast agent that offers the possibility to track the changes in calcium movement within the heart muscle, something which we can't do using currently available tests. Moreover, insulin production in the pancreas is also a calcium dependent process and we currently don't have any non-invasive tests to assess these insulin producing cells. Manganese enhanced magnetic resonance imaging may offer a non-invasive method of assessing these cells in the pancreas. The safety of this technique has already been established in multiple previous studies.

First, we assessed whether this new method of imaging the heart is robust enough to be used clinically and we looked at the repeatability and reproducibility of this technique. We found that this technique has excellent repeatability and reproducibility and is suitable for clinical use. Second, we used this technique to study the differences in calcium movement in the heart muscle in healthy volunteers versus patients with diabetes but without any known heart disease. We found that patient with either type 1 or type 2 diabetes have

abnormal calcium movement in the heart muscle even in the absence obvious heart disease or cardiac failure. Third, using this novel imaging method, we evaluated the differences between the calcium movement in the heart muscle in patients with both heart failure and type 2 diabetes versus patients with heart failure without type 2 diabetes. We demonstrated that patients with both type 2 diabetes and heart failure have deeply suppressed calcium movement in their heart muscle compared to patients with heart failure only. This finding might explain the worse outcomes seen in patients with both type 2 diabetes and heart failure. Finally, we investigated whether this imaging technique can be used to assess the insulin producing cells located within the pancreas and found that manganese-enhanced magnetic resonance imaging can differentiate between patients with type 1 diabetes and healthy volunteers. Although this study was performed in a small number of patients, it highlights the potential role of this novel method to better understand the underlying disease process in diabetes and can provide useful information to help discovery of new drugs to treat type 1 and type 2 diabetes.

Overall, these studies have provided useful insights into the complex interactions at play in diabetes and heart failure, that could drive forward the development of novel therapeutic strategies.

Acknowledgements

I am extremely grateful to everyone who supported me during my time in research. In particular, I would like to thank my PhD supervisors. Firstly, Prof Dave Newby for giving me this opportunity to undertake a PhD. Prof Newby has been incredibly supportive and encouraging throughout my PhD. I have learnt a lot from Prof Newby and been given plenty of opportunities to develop my research skills. Secondly, Prof Marc Dweck for all the guidance and support during my PhD. Thank you for providing me with all the education, training and opportunities. Prof Newby and Prof Dweck are the best PhD supervisors and mentors one could ask for and I am extremely lucky to have worked with them. They have inspired me to exceed my own ambitions. I would also like to thank Prof Scott Semple for his unwavering support for all the imaging studies I undertook during my PhD.

I would like to thank the British Heart Foundation for their support of my work through the Clinical Research Training Fellowship. I am also grateful to all the patients and volunteers for their time and for participating in my research studies. I would also like to thank all my colleagues at the Edinburgh Imaging Facility and Clinical Research Facility – it has been a pleasure to work with you all.

I was also lucky enough to have made some incredible friends during my PhD and I would like to thank all my fellow researchers in the barn for being there for me through all the highs and lows. In particular, I would like to thank Jolien, Kri, Marwa, Beth, Anda and Trisha for their friendship. I really miss our salsa Thursdays!

Finally, to my family. To my mother, Prof Rajani Joshi. You are my inspiration for everything and I would not be who I am without you. You taught me everything in life and provided

rock solid support in all aspects. You always believed in me and inspired me to be the best version of myself. You always wanted me to do medicine and to undertake a PhD and I know how happy you would have been to see me complete this thesis. I can’t thank you enough for being the best mom in the world. I miss you terribly but I know that you are always with me. To my father, Mr. Sunil Joshi, my brother, Shrey Joshi, and my nani, Mrs. Shakuntala Purohit, for their endless love and for their support during some of the toughest times. I would also like to thank my parents-in-law Mr. B.M Calla, Mrs. Veena Kalla and my late grandparents Prof G.R Purohit, Mr. S.K Joshi and Mrs. Laxmi Joshi for their blessings. Last but not the least, I would like to thank my husband, Rahul for being my rock. You have been there for me through some of the roughest times and your humour and kindness has always kept me going. I would not be able to complete this thesis without you.

Abbreviations

CI – confidence interval
DCM – dilated cardiomyopathy
DEMRI – gadolinium delayed-enhancement magnetic resonance imaging
ECV% - extracellular volume fraction
HCM – hypertrophic cardiomyopathy
LVEF – Left ventricular ejection fraction
MEMRI – Manganese-enhanced magnetic resonance imaging
MnDPDP – manganese dipyridoxyl diphosphate
MOLLI – modified Look-Locker inversion recovery
MRI – Magnetic resonance imaging
ROI – region of interest
SD – standard deviation
SERCA1a – sarcoplasmic reticulum Ca^{2+}-ATPase
ShMOLLI – shortened modified Look-Locker inversion recovery
T1DM – type 1 diabetes mellitus
T2DM – type 2 diabetes mellitus

Abstract

Background and aims

Cardiometabolic disorders include cardiovascular diseases and metabolic conditions such as diabetes mellitus and represent a leading cause of morbidity and mortality worldwide. Identification of specific biological pathways driving progression of these disorders may unveil targets for preventing and treating these diseases. Dysregulated myocardial and pancreatic beta-cell calcium handling may be a key mediator and driver of these disorders.

Manganese is a calcium analogue which has paramagnetic properties. Cellular uptake of manganese by voltage gated L-type calcium channels causes T1 shortening and intracellular contrast enhancement on magnetic resonance. Manganese-enhanced magnetic resonance imaging therefore represents a novel non-invasive method of assessing intracellular calcium handling. It has been used previously to assess myocardial viability and to assess myocardial calcium uptake in ischaemic and non-ischaemic cardiomyopathies. However, no prior studies have used manganese-enhanced magnetic resonance imaging to evaluate perturbations in myocardial calcium handling in patients with subclinical or clinically overt diabetic cardiomyopathy and it has never been used to assess pancreatic functional beta-cell mass in patients with type 1 diabetes.

The aims of this thesis were 1) to assess the reproducibility and repeatability of manganese-enhanced magnetic resonance imaging, 2) to determine whether myocardial calcium uptake is altered in patients with either type 1 or type 2 diabetes without known

cardiac disease, 3) to study the differences between myocardial calcium handling in patients with both heart failure and type 2 diabetes versus patients with heart failure without type 2 diabetes, and 4) to investigate whether manganese-enhanced magnetic resonance imaging can be used as a non-invasive and reproducible measure pancreatic beta-cell function.

Methods

In study one, we assessed the intra-observer and inter-observer repeatability and scan-rescan reproducibility of cardiac manganese-enhanced magnetic resonance imaging. Twenty healthy volunteers, 20 patients with acute myocardial infarction, 18 patients with hypertrophic and 10 patients with non-ischemic dilated cardiomyopathy underwent manganese-enhanced magnetic resonance imaging. Native T1 values and myocardial manganese uptake (Ki) were assessed for intra and inter-observer repeatability. Scan-rescan reproducibility was assessed in 10 healthy volunteers.

In study two, we compared myocardial manganese uptake in patients with either type 1 or type 2 diabetes without cardiac disease versus healthy volunteers. Manganese-enhanced cardiac magnetic resonance imaging was performed in people with type 1 diabetes (n=19), type 2 diabetes (n=30) and healthy volunteers (n=28), all without prevalent cardiac disease.

In study three, we studied the differences between myocardial manganese uptake in patients with heart failure with or without type 2 diabetes. Twenty patients with both heart failure and type 2 diabetes and 20 patients with heart failure but without a diagnosis of type 2 diabetes underwent manganese-enhanced magnetic resonance imaging.

In study four, 20 people with type 1 diabetes mellitus (10 with low (≥50 pmol/L) and 10 with very low (<50 pmol/L) C-peptide concentrations) and 15 healthy volunteers underwent manganese-enhanced magnetic resonance imaging of the pancreas following an oral glucose load. Scan-rescan reproducibility was performed in 10 participants.

In all the studies, cardiac and pancreatic manganese uptake (Ki) was measured using a two-compartment model, Patlak formulation.

Results

Intra-observer and inter-observer correlation was excellent in healthy volunteers for mean native T1 mapping (Lin's correlation coefficient [LCC] 0.97 and 0.97 respectively) and myocardial manganese uptake (LCC: 0.99 and 0.96 respectively). Scan-rescan correlation for native T1 and myocardial manganese uptake was also excellent. Similarly, there was strong intra-observer agreement for native T1 and myocardial manganese uptake in patients with acute myocardial infarction (LCC: 0.97 and 0.97 respectively), hypertrophic (LCC: 0.98 and 0.97 respectively) and dilated cardiomyopathy (LCC: 0.99 and 0.95 respectively).

In study two, we showed that myocardial manganese uptake was 23% and 22% lower in those with type 1 and 2 diabetes compared to healthy volunteers (Ki 6.43±0.77, 6.47±0.99 and 8.33±0.77 mL/100 g/min, respectively; P<0.001). There were no differences in left ventricular systolic and diastolic function (ejection fraction, global longitudinal strain, and peak early diastolic strain rate) between groups.

In study three, we observed that myocardial manganese uptake was lower in patients with both heart failure and type 2 diabetes compared to patients with heart failure only (4.69±0.71 versus 5.48±0.88, p=0.03). There was no difference in left ventricular systolic function between the two groups.

In study four, we demonstrated that mean pancreatic manganese uptake was 31±6 mL/100 g of tissue/min in healthy volunteers (median 32 [interquartile range 23-36] years, 6 women), falling to 23±4 and 13±5 mL/100 g of tissue/min ($p \leq 0.002$ for both) in people with type1 diabetes mellitus (52 [44-61] years, 6 women) and low or very low plasma C-peptide concentrations respectively. Furthermore, pancreatic manganese uptake correlated strongly with plasma C-peptide concentrations in people with type1 diabetes mellitus ($r=0.73$, $p<0.001$).

Conclusions

We have demonstrated excellent intra-observer and inter-observer repeatability and scan-rescan reproducibility for manganese-enhanced T1 mapping and kinetic modelling. Therefore, it has potential for future clinical applications. We have shown significant dysregulation of myocardial calcium handling in patients with either type 1 or type 2 diabetes mellitus in the absence of any apparent cardiac disease. Hence, abnormal calcium uptake may be an early pathologic feature of the diabetic heart, reduced to a similar extent in both type 1 and type 2 diabetes mellitus. In patients with heart failure, we observed a greater reduction in myocardial calcium uptake in patients with both heart failure and type 2 diabetes mellitus versus patients with heart failure without type 2 diabetes. This suggests that type 2 diabetes mellitus has a profound effect on myocardial calcium handling in patients with heart failure. Finally, we showed that manganese-

enhanced magnetic resonance imaging provides a reproducible non-invasive imaging technique to assess functional beta-cell mass in people with type 1 diabetes mellitus.

Overall, we have demonstrated that dysregulated myocardial calcium handling plays an important role in the pathophysiology of diabetic cardiomyopathy and beta-cell dysfunction in type 1 diabetes. Furthermore, manganese-enhanced magnetic resonance imaging is a promising novel imaging technique for the diagnosis and risk stratification of a variety of cardiometabolic disorders. It has the potential to be used as a non-invasive biomarker to monitor disease progression and tracking response to novel therapies.

CHAPTER 1. Introduction

Adapted from:

-Joshi SS, Singh T, Newby DE, Singh J. Sodium-glucose co-transporter 2 inhibitor therapy: mechanisms of action in heart failure. Heart. 2021 Feb 26;107(13):1032–8. doi: 10.1136/heartjnl-2020-318060. Epub ahead of print. Erratum in: Heart. 2021 Nov;107(22):e15. PMID: 33637556; PMCID: PMC8223636.

1.1 OVERVIEW

Cardiometabolic disorders include cardiovascular diseases and metabolic conditions, such as diabetes mellitus, and represent a leading cause of morbidity and mortality worldwide. Identification of specific biological pathways driving progression of these disorders may unveil targets for treatment of disease or even preventing development of the disease itself. Dysregulated myocardial and pancreatic beta-cell calcium handling may be a key driver for these disorders.

Manganese is a calcium analogue which has paramagnetic properties. Cellular uptake of manganese by voltage gated L-type calcium channels causes T1 shortening and intracellular contrast enhancement on magnetic resonance. Manganese-enhanced magnetic resonance imaging therefore represents a novel non-invasive method of assessing intracellular calcium handling. It has been used previously to assess myocardial viability and to assess myocardial calcium uptake in ischaemic and non-ischaemic cardiomyopathies. However, no prior studies have used manganese-enhanced magnetic resonance imaging to evaluate perturbations in myocardial calcium handling in patients with subclinical or clinically overt diabetic cardiomyopathy and it has never been used prospectively for pancreatic functional beta-cell mass imaging.

This chapter provides a synopsis of cardiometabolic disorders, highlights the contribution of previously published work, and discusses the future potential applications of manganese-enhanced magnetic resonance imaging.

1.2 CARDIOMETABOLIC DISORDERS

Cardiometabolic disorders include cardiovascular disease, diabetes mellitus, chronic renal failure and non-alcoholic fatty liver disease (1). These disorders are the number one cause of death in the world and their incidence is rising sharply globally with a major public health impact (2,3). Cardiometabolic disorders are primarily caused by an unhealthy lifestyle and risk factors including a sedentary lifestyle and obesity (2). Early diagnosis at a subclinical stage and identifying individuals at risk may offer an opportunity to alter the natural history of these disorders and prevent the development of complications and reduce the overall associated mortality. Diabetes mellitus and associated complications are discussed in more detail in subsequent sections.

1.3 DIABETES MELLITUS

Diabetes mellitus is a spectrum of chronic metabolic disorders characterised by pancreatic beta cell dysfunction, insulin resistance and hyperglycaemia (4). The existence of diabetes mellitus has been known since before the Middle Ages and descriptions have been found in the Egyptian papyri, in ancient Indian and Chinese medical literature, as well as, in the work of ancient Greek and Arab physicians. In the 2nd century AD, Aretaeus of Cappadocia coined the term ‘diabetes’ and provided its first accurate description, and in 17th century, Thomas Willis added the term ‘mellitus’ to describe the extremely sweet taste of diabetic urine (5). Our understanding of diabetes mellitus has markedly improved since then, but diabetes related morbidity and mortality has remained high with the incidence of diabetes rising sharply every year. In 2021, there were 537 million people living with living with diabetes in the world which is around 1 in 10 of the world’s adult population (6). This figure is expected to rise to 643 million by 2030 (6). Notably, almost half (46%) of people living with diabetes remain undiagnosed and 240 million people are estimated to be living with undiagnosed diabetes worldwide (7). In 2019, diabetes was the direct cause of 1.5 million

deaths and 48% of all deaths due to diabetes occurred before the age of 70 years (8). Diabetes mellitus is divided into four broad categories by the American Diabetes Association: type 1 diabetes, type 2 diabetes, gestational diabetes, and diabetes due to other specific causes like monogenic diabetes syndromes (9). Type 2 diabetes accounts for 90% of all cases of diabetes. Life expectancy is reduced by more than 20 years for people with type 1 diabetes and up to 10 years for people with type 2 diabetes (10).

1.4 TYPE 2 DIABETES MELLITUS: GLOBAL BURDEN AND PATHOPHYSIOLOGY

The World Health Organisation (WHO) defines type 2 diabetes as a chronic metabolic condition characterised by elevated levels of blood glucose, insulin resistance, and relative lack of insulin, which leads to multiorgan damage over time (8). The current worldwide prevalence of type 2 diabetes mellitus is 463 million, 9.3% of the world population, and this is expected to rise to 693 million by 2045 (7). Furthermore, the incidence of type 2 diabetes is also rising in people under the age of 30 (4). The key contributors to the rise in type 2 diabetes include sedentary lifestyle, obesity and high caloric diets.

The pathophysiology of type 2 diabetes involves two main disease processes: defective insulin secretion by pancreatic beta cells and the inability of insulin sensitive tissues to respond to insulin, also known as insulin resistance (11). Glucose metabolism is regulated by a feedback loop between pancreatic beta cells and insulin-sensitive tissue. Insulin released from beta cells in response to a rise in the circulating blood glucose concentrations, mediates uptake of glucose, fatty acids and amino acids by insulin sensitive tissues. In the presence of insulin resistance, beta cells produce more insulin in order to maintain normal glucose tolerance. However, if beta cells are incapable of increasing insulin production, plasma glucose concentrations rise, leading to the clinical syndrome of type 2 diabetes (12). Type 2 diabetes is associated with various

microvascular and macrovascular complications and as a result, people with type 2 diabetes have a two-fold to four-fold increase in mortality, compared with the general population (13).

1.5 TYPE 1 DIABETES MELLITUS: GLOBAL BURDEN AND PAHTOPHYSIOLOGY

Type 1 diabetes is an autoimmune condition characterised by the destruction of pancreatic beta cells resulting in complete insulin deficiency (14). Currently, there are 9-million people living with type 1 diabetes worldwide (15). Type 1 diabetes constitutes approximately 5-10% of all cases of diabetes and often involves children and young adults. Concerningly, the incidence of type 1 diabetes is increasing by 4% each year and in children under five, the incidence of type 1 diabetes is rising by 5% each year (16).

The destruction of beta cells in type 1 diabetes involves a T cell-mediated autoimmune response which results in lymphocytic infiltration of the islets of Langerhans thereby leading to pancreatic beta cell damage (17). This precedes the clinical manifestation of the disease, and impaired insulin secretion can be detected several years prior to the onset of hyperglycaemia (18–20). Furthermore, beta cell mass is reduced by 80-90% at the time of diagnosis. The degree of beta-cell dysfunction at this time often exceeds the percentage beta-cell loss, suggesting additional functional impairment in insulin secretion in these individuals (21–23). Interestingly, it is now recognised that there are micro-secretors of insulin and that preservation of insulin secretion in these cases is associated with decreased complications (24). However, a limited understanding of the underlying pathophysiology of pancreatic beta cell loss in type 1 diabetes has hindered the development of any curative treatments. Moreover, there are no non-invasive imaging techniques currently available to assess disease progression and track response to treatment in these patients. Therefore, the mainstay of management for type 1 diabetes

involves lifelong insulin treatment, patient education and disease monitoring. However, despite insulin treatment, the life expectancy of people with type 1 diabetes could be reduced by 10-15 years owing to the associated micro and macrovascular complications (25).

1.6 COMPLICATIONS ASSOCIATED WITH DIABETES MELLITUS

Diabetes mellitus is associated with multiorgan damage and can cause a plethora of microvascular and macrovascular complications. Microvascular complications include peripheral neuropathy (nervous system damage), nephropathy (renal impairment) and retinopathy (eye damage) and diabetes-related macrovascular complications include cardiovascular disease, stroke and peripheral vascular disease (26). Cardiovascular disease accounts for 65% of all deaths in people with diabetes and are discussed in further detail in the following sections.

1.7 CARDIOVASCULAR COMPLICATIONS OF DIABETES MELLITUS

One of the most deleterious consequences of developing diabetes mellitus is a 2-2.5 times increased risk of developing cardiovascular disease (27). In a meta-analysis of 4,549,481 people with diabetes mellitus, almost one third suffered from cardiovascular disease and half of all deaths were attributable to cardiovascular complications (28). The cardiovascular complications associated with diabetes mellitus include coronary artery disease, cerebrovascular disease and heart failure.

1.7.1 CORONARY ARTERY DISEASE

The prevalence and severity of coronary artery disease is worse in people with diabetes when compared with age-matched non-diabetic people (29). Hyperglycaemia, dyslipidaemia and insulin resistance associated with diabetes mellitus can lead to impaired

platelet function, vascular smooth muscle dysfunction and abnormal coagulation (30). People with diabetes also tend of have lipid-rich atherosclerotic plaques that are more vulnerable to rupture than the plaques seen in non-diabetic individuals (31). However, lifestyle interventions like weight loss can lead to a reduction in the incidence of coronary artery disease in people with diabetes (32).

1.7.2 CEREBROVASCULAR DISEASE

People with diabetes have both cerebral microvascular and macrovascular disease and are 2-6 times more susceptible to a stroke event. Furthermore, people with diabetes and hyperglycaemia are more likely to die or suffer major disability following an acute ischaemic stroke (33). Although it is clear that diabetes increases the risk of stroke, cerebrovascular remodelling can be reversed with good glycaemic control. The UKPDS 34 study demonstrated that intensive glycaemic control with metformin is associated with a reduction in the incidence of stroke and myocardial infarction (34).

1.7.3 HEART FAILURE

Despite the popular belief that atherosclerosis is the predominant cause of cardiovascular disease in diabetes mellitus, recent data from the United Kingdom National Diabetes Audit which included 2.7 million patients with diabetes showed that heart failure is the commonest cardiovascular complication of diabetes mellitus and a major cause of premature mortality (35). Patients with diabetes have over twice the risk of developing heart failure, and heart failure patients with diabetes are four times more likely to die than those without diabetes (36). Large population-based studies have shown that even after adjusting for risk factors commonly associated with diabetes mellitus like age, sex, coronary artery disease, hypertension and dyslipidaemia, diabetes still confers a two-fold added risk for the development of heart failure (37,38). This observation led to the

identification of diabetes mellitus as an independent risk factor for heart failure and the recognition of the distinct clinical entity of ‘diabetic cardiomyopathy’, a term originally coined by Lundbaek in 1954. So far, large studies involving multifactorial risk factor management in people with diabetes mellitus have failed to show a reduction in the incidence of heart failure in these patients (39).

The problems of heart failure associated with diabetes are further compounded by the fact that several therapeutic glucose-lowering agents are either ineffective or harmful. Thiazolidinediones, such as pioglitazone, activate peroxisome proliferator-activated receptor gamma (PPAR gamma) to improve insulin sensitivity. However, they also cause increased sodium and fluid retention, thereby leading to a 42% increased risk of incident heart failure (40). In contrast, dipeptidyl peptidase 4 inhibitors appear to have a neutral effect on major adverse cardiovascular events although one agent of this class, saxagliptin, has been associated with a 27% increase in hospitalisation for heart failure and a 22% increase in cardiovascular mortality (41). A meta-analysis of more than 24,000 individuals from four large clinical trials reported that the use of insulin for type 2 diabetes was associated with a 27% increase in all-cause mortality and 23% increase in hospitalisation for heart failure (42). Looking at 100,000 individuals in the ‘real-world’ setting of an administrative database, such treatment was associated with an odds ratio of 2.02 for all-cause mortality and 1.42 for heart failure hospitalisation (42). Sodium-glucose co-transporter 2 inhibitors are the only class of glucose lowering drugs that have shown a reduction in heart failure mortality and are associated with a 30-35% reduction in heart failure hospitalisations (43). However, the mechanism underlying this benefit seen with sodium-glucose co-transporter 2 inhibitors remains unclear.

1.8 DIABETIC CARDIOMYOPATHY: DEFINITION AND STAGES

First described in 1972, ‘diabetic cardiomyopathy’ is defined as the presence of abnormal myocardial structure and performance in the absence of other cardiac risk factors like coronary artery disease, hypertension, and significant valvular disease, in people with diabetes mellitus (44). Further evidence for the existence of diabetic cardiomyopathy came from the Framingham Heart study in 1974 that demonstrated a 5-fold higher incidence of heart failure in diabetic women and 2.4-fold higher incidence in diabetic men (45).

Four stages of diabetic cardiomyopathy are described and are summarised in the table below. These stages also overlap with stages A-D of the American Heart Association/ American College of Cardiology classification. Patients in stage A usually have normal cardiac structure and function or subclinical cardiac structure and function abnormalities. Approximately 36% of patients in stage A progress to symptomatic heart failure. Stage B usually comprises of asymptomatic structural heart disease (for example – left ventricular hypertrophy, systolic or diastolic dysfunction). Late stages of diabetic cardiomyopathy include stages C and D and are characterised by symptomatic heart failure with structural heart disease.

TABLE 1.1. STAGES OF DIABETIC CARDIOMYOPATHY

Diabetic Cardiomyopathy Stage	Clinical Manifestations
Stage 1	Diastolic heart failure with normal ejection fraction.
Stage 2	Symptomatic heart failure with combined systolic and diastolic dysfunction.
Stage 3	Symptomatic heart failure to which hypertension, microvascular disease and/or viral disease have contributed. No coronary artery disease.
Stage 4	Symptomatic heart failure with contribution from multiple confounders including coronary artery disease.

1.9 DIABETIC CARDIOMYOPAHTY: PATHOPHYSIOLOGY

The pathophysiology of diabetic cardiomyopathy is not completely understood and various hypotheses have been proposed. The key proposed underlying mechanisms are discussed in this section and are summarised in **Figure 1.1**.

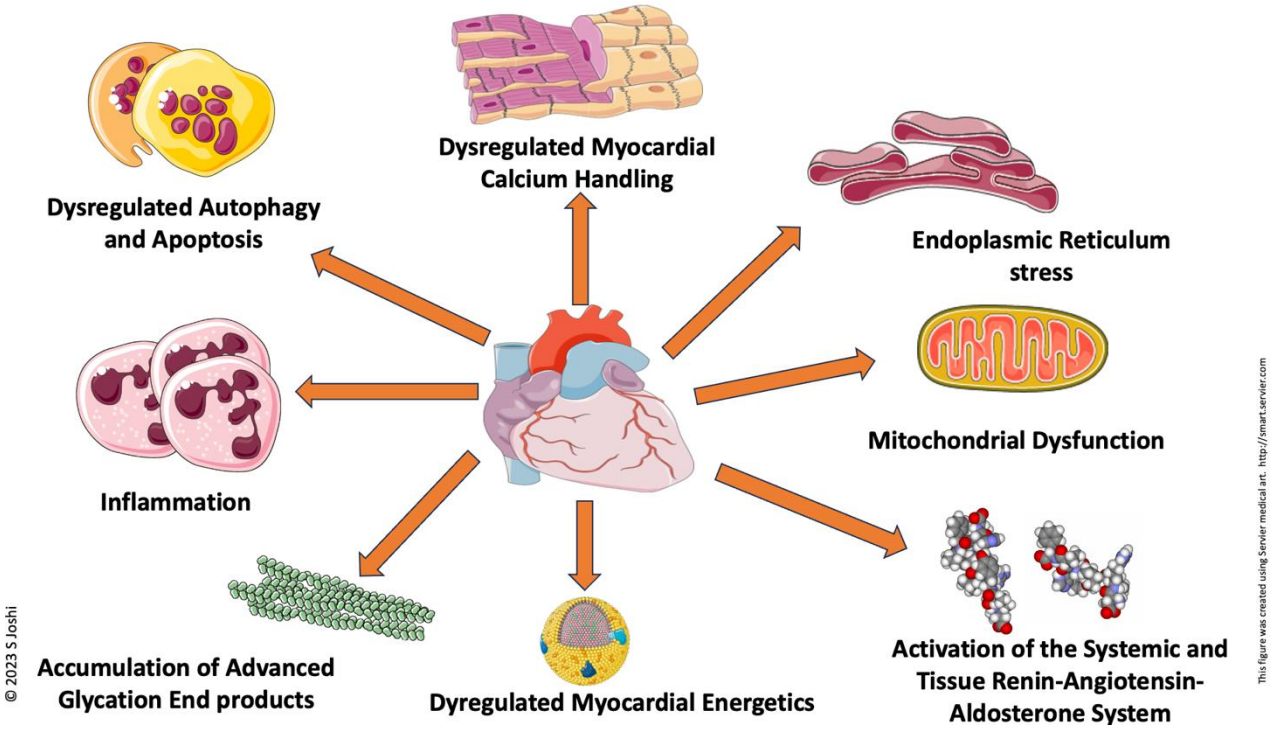

Figure 1.1. **Different Theories Proposed to Explain the Pathophysiology of Diabetic Cardiomyopathy**

1.9.1 DYSREGULATED MYOCARDIAL ENERGETICS

Under physiological conditions, nearly 95% of cardiac energy (in the form of adenosine triphosphate, ATP) is derived from mitochondrial oxidative metabolism and 5% from the citric acid cycle (46). Normally, the heart displays considerable metabolic substrate flexibility, using various molecules like free fatty acids, glucose, ketone bodies, lactate and some amino acids. However, the presence of hyperglycaemia and insulin resistance impairs the heart's ability to use glucose as a substrate for ATP production and it subsequently switches to free fatty acids (47). This energy substrate switch is accompanied by impaired oxidative phosphorylation and a mitochondrial proton leak thereby leading to an increased production of reactive oxygen species, which eventually causes myocardial oxidative damage and facilitates the development of diabetic cardiomyopathy (47). Furthermore, ketones, such as beta-hydroxybutyrate, could act as

super-fuels by producing ATP more efficiently than glucose or free fatty acids (48). Therefore, they could potentially play an important role in maintaining myocardial homeostasis in this setting of restricted fuel selection and low energetic reserve. However, diabetes mellitus is often associated with decreased ketogenesis because of systemic insulin resistance and hyperinsulinaemia (49). This, in turn, is thought to further contribute to myocardial dysfunction in diabetic cardiomyopathy.

1.9.2 INFLAMMATION

A proinflammatory response involving cells like neutrophils, mast cells, dendritic cells, macrophages, and eosinophils has been proposed as a potential mechanism to explain the pathophysiology of diabetic cardiomyopathy (50). Hyperglycaemia promotes cytokine and chemokine release, which activates a common signalling pathway involving a transcription factor, called the nuclear factor kappa-B (NF- κB). Activation of NF- κB via toll-like receptor (TLR) 4 results in further downstream release of pro-inflammatory cytokines. Cytokines and chemokines released as part of this cascade cause oxidative myocardial damage, with remodelling and fibrosis eventually leading to myocardial dysfunction (50).

1.9.3 DYSREGULATED CARDIAC APOPTOSIS AND AUTOPHAGY

Increased cardiac apoptosis has been postulated to play a significant role in the development of diabetic cardiomyopathy and biopsied diabetic heart tissue expresses 85-fold more cardiomyocyte apoptosis than control healthy heart tissue (51). Increased cardiac apoptosis occurs as a result of increased endoplasmic reticulum stress which occurs in response to oxidative stress, lipotoxicity, inflammation and the accumulation of misfolded proteins. Furthermore, dysregulated endoplasmic reticulum homeostasis inhibits cellular protein synthesis and degradation of misfolded or damaged proteins ultimately

increasing cell apoptosis and autophagy (52). This is thought to contribute to the development of diabetic cardiomyopathy.

1.9.4 ACTIVATION OF THE RENIN-ANGIOTENSIN-ALDOSTERONE SYSTEM

Hyperglycaemia and insulin resistance can lead to an increase in the activation of the systemic and tissue renin-angiotensin-aldosterone system, and this is thought to play an important role in the pathogenesis of diabetic cardiomyopathy (53). Serum angiotensin II concentrations correlate with postprandial glucose concentrations in insulin resistance and type 2 diabetes. Moreover, the proinflammatory angiotensin II type 1 receptor is upregulated and the anti-inflammatory angiotensin II type 2 receptor is downregulated in early diabetes mellitus. Activation of the renin-angiotensin-aldosterone impairs insulin metabolic signalling and induces systemic and cardiac insulin resistance (54). These abnormalities can promote cardiac remodelling, fibrosis and diastolic dysfunction seen in diabetic cardiomyopathy.

1.9.5 ACCUMULATION OF ADVANCED GLYCATION END PRODUCTS IN THE MYOCARDIUM

Hyperglycaemia is characterised by an increased production and accumulation of advanced glycation end products in the heart leading to myocardial structural alterations by increases in nonenzymatic glycation, oxidation of lipids and proteins, myocardial collagen production and fibrosis (55). A combination of these pathological processes can promote myocardial fibrosis and diastolic dysfunction ultimately leading to diabetic cardiomyopathy (56).

1.9.6 IMPAIRED MYOCARDIAL CALCIUM HANDLING

Myocardial calcium homeostasis is a finely balanced mechanism, essential for efficient excitation-contraction coupling. During systole, calcium is actively transported into the cardiomyocyte via the L-type voltage-gated calcium channels where it binds to ryanodine receptors on the sarcoplasmic reticulum resulting in ‘calcium-induced calcium release’. This, in turn, activates calcium-sensitive contractile proteins (troponin C, troponin NC) which leads to myocyte contraction (57). In the setting of diabetes mellitus, there is an upregulation of both sodium hydrogen exchanger 1 and sodium glucose co-transporter 1 resulting in markedly increased intra-cytosolic sodium content. This promotes calcium influx via the membrane bound sodium-calcium exchanger transporters and calcium efflux from the mitochondria (into the cytosol) via mitochondrial sodium-calcium exchanger transporters. The elevated baseline intracellular calcium content results in reduced calcium transients and smaller sarcoplasmic reticulum calcium stores in diabetic cardiomyocytes, thereby inhibiting contractile function and the development of diabetic cardiomyopathy (58). Although there is strong pre-clinical evidence from animal studies to support this hypothesis, this has not been tested in a clinical study.

1.10 THE NEED FOR UNDERSTANDING THE UNDERLYING MECHANISMS OF MYOCARDIAL AND PANCREATIC DYSFUNCTION IN DIABETES MELLITUS

Mortality associated with atherosclerotic cardiovascular disease can be reduced in people with diabetes mellitus by lifestyle interventions like strict glycaemic control, weight reduction and pharmacologic treatment for dyslipidaemia (59). However, large studies involving multifactorial risk factor management in patients with diabetes mellitus have failed to show a reduction in the incidence of heart failure in these patients (60). Therefore, heart failure has emerged as a major cause of death in the setting of diabetes mellitus. This also suggests that mechanisms involved in the development of heart failure differ

from those involved in the pathophysiology of diabetes associated atherosclerotic disease. A better understanding of these underlying abnormalities may aid early diagnosis at a subclinical stage and may provide an opportunity to test pharmacological interventions that may slow disease progression and improve patient outcomes.

People with type 1 diabetes with advanced pancreatic beta cell dysfunction are at a higher risk of developing cardiovascular complications despite adequate glycaemic control compared to people with type 1 diabetes with ongoing endogenous insulin secretion (61). Therefore, the opportunity to preserve or to enhance beta cell function in type 1 diabetes may maximise beta cell activity and provide several physiological advantages such as a reduction in the rate of associated cardiovascular complications. Recent studies have also demonstrated the presence of 'insulitis', inflammatory pathologic changes in islet cells in pre-clinical stages of type 1 diabetes (62). Hence, a better knowledge of pre-clinical stages of beta cell dysfunction in type 1 diabetes may help identify 'at risk' patients and developing targeted therapy to halt the progression of disease.

1.11 THE ROLE OF CALCIUM IN MYOCARDIAL CONTRACTION

Calcium plays a central role in the excitation contraction coupling in the heart: a phenomenon responsible for myocardial contraction. Calcium enters the cardiomyocytes predominantly via the voltage gated L-type calcium channels in the transverse tubules, which, in turn, leads to further calcium release form the sarcoendoplasmic reticulum (**Figure 1.2**). During systole, calcium is actively transported into the cardiomyocyte via the L-type voltage-gated calcium channels where it binds to ryanodine receptors on the sarcoplasmic reticulum resulting in 'calcium-induced calcium release'. This calcium release then binds troponin, causing sliding of the thick and thin filaments, sarcomeric shortening, finally resulting in cardiac contraction and ejection of blood. During diastole, calcium is

actively transported into sarcoplasmic reticulum by calcium-adenosine triphosphatase (SERCA2a), along with its passage into the extracellular space via the sodium-hydrogen exchanger and mitochondrial uptake (63). Calcium's essential role in excitation-contraction coupling makes it central to pathophysiological and adaptive mechanisms of defective contractile function and impaired relaxation in various cardiomyopathies.

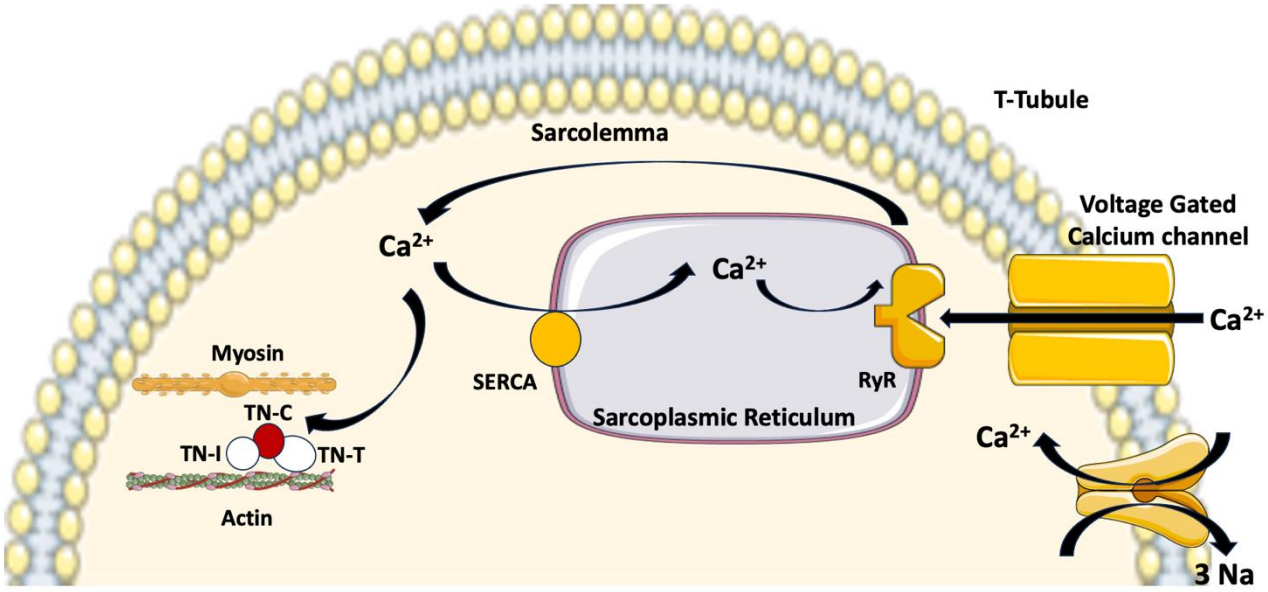

Figure 1.2. Myocardial Excitation Contraction Coupling. SERCA: Sarcoendoplasmic Reticulum Calcium ATPase, T-Tubule: Transverse tubule, TN-T: Troponin T, TN-C: Troponin C, TN-I: Troponin I.

1.12 THE ROLE OF CALCIUM IN PANCREATIC INSULIN SECRETION

Insulin is the key hormone responsible for maintaining glucose homeostasis and is secreted by the beta cells of the pancreatic islets of Langerhans. Insulin secretion from pancreatic beta cells occurs in a dose-dependent fashion in response to a rise in the circulating blood glucose levels (for example: after a meal). The four main components of this glucose stimulated insulin secretion are: Glucose transporter 2 (GLUT2) dependent glucose uptake, glucose metabolism, adenosine triphosphate (ATP)-dependent potassium channel closure and the opening of L-type voltage-gated calcium channels causing insulin granule fusion and exocytosis (64). Voltage-gated calcium channels are normally closed and ATP sensitive potassium are normally open, and these channels are located on the plasma membrane of the pancreatic beta cells (65). When the blood glucose concentration is high, glucose molecules enter the pancreatic beta cells via the GLUT2 transporter. Metabolism of glucose inside the beta cells produces ATP, which increases the intracellular ATP to adenosine diphosphate (ADP) ratio. The ATP-sensitive potassium channels close when the ATP to ADP ratio is high. As a result, potassium ions are unable to diffuse out of the cell and this creates an action potential which, in turn, leads to the opening of the voltage-gated calcium channels allowing the calcium ions to diffuse inside the beta cells. After entering the beta cells, calcium ions cause the insulin containing granules to move towards and fuse with the cell surface membrane, releasing insulin by exocytosis into the hepatic portal vein (66). This is illustrated in **Figure 1.3** below.

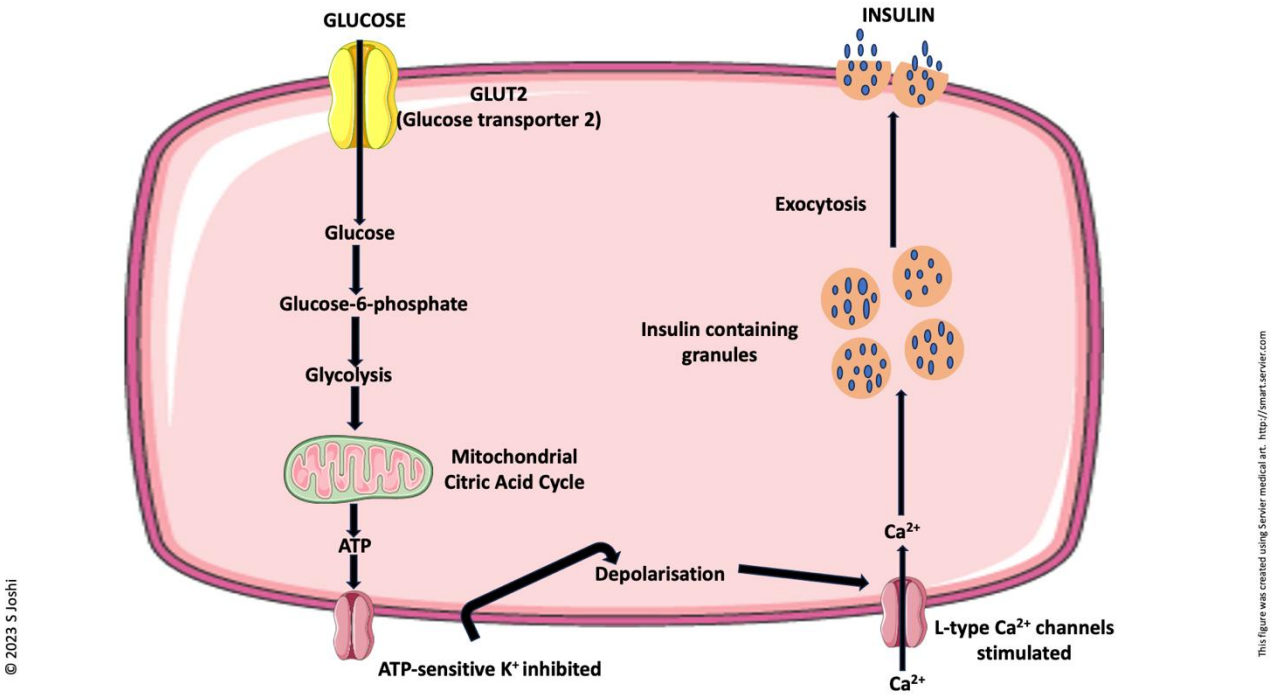

Figure 1.3. Insulin secretion from pancreatic beta-cells. ATP – Adenosine triphosphate, K^+ - potassium ions, Ca^{2+} - Calcium ions.

1.13 IMAGING OF CALCIUM DEPENDENT PROCESSES: MANGANESE-ENHANCED MAGNETIC RESONANCE IMAGING

Manganese-enhanced magnetic resonance imaging is a novel non-invasive imaging method to quantify myocardial and pancreatic calcium handling.

1.13.1 MANGANESE AS A MAGNETIC RESONANCE IMAGING CONTRAST AGENT

Manganese is a naturally occurring trace element and serves as a cofactor in the activation of several enzymes required for various physiological processes in the human body (67). Manganese also plays an important role in protecting mitochondrial membranes from oxidative stress through superoxide dismutase. It is present in most human diets and some of the manganese rich foods include mussels, spinach, brown rice etc. It is primarily metabolised via the kidneys and the liver (68).

Manganese was the first compound used as a magnetic resonance imaging contrast agent. Like gadolinium, it is paramagnetic and causes shortening of T1 relaxation of water protons, providing contrast in tissues where it accumulates, offering excellent anatomical delineation (69). Furthermore, it is a calcium analogue and is taken up by the tissues like the heart, pancreas, kidney, liver and brain that have functional L-type voltage gated calcium channels and sodium-hydrogen exchangers (70).

1.13.2 MANGANESE BASED CONTRAST FORMULATIONS

There are various non-chelated, chelated and partially chelated formulations of manganese as described below (71).

Non-Chelated Manganese Formulations

Manganese chloride is a non-chelated manganese-based contrast agent that dissociates into manganese and chloride ions after administration and manganese ions enter tissues via voltage-gated calcium channels. However, it competes with calcium and can cause myocardial depression and toxicity especially with higher doses. Low dose (5 μmol/kg) intravenous manganese chloride was found to be safe in 15 healthy volunteers (72) but its long term and extra cardiac safety has not been established and therefore, it is not approved for use in humans. EVP 1001-1 (Eagle Vision Pharmaceuticals, Downingtown, United States of America) is another non-chelated form of manganese contrast agent. It is co-administered with calcium gluconate which results in short plasma half-life and rapid myocardial uptake with little redistribution. This approach reduces the toxic effects of high dose manganese ions and achieves adequate T1 shortening for imaging (73). EVP 1001-1 is also not currently approved for clinical use.

Partially Chelated Manganese Formulations

Manganese dipyridoxyl diphphosphate (MnDPDP, mangafodipir) is a partially chelated form of manganese. In this formulation, manganese is partially chelated by dipyridoxyl diphosphate and circulates within a protein bound complex. After intravenous injection, mangafodipir releases manganese ions into plasma by dephosphorylation and transmetallation with zinc thereby allowing rapid intracellular manganese uptake and clearance. This approach mitigates the toxicity seen with non-chelated forms of manganese-based contrast media (71). Manganese dipyridoxyl diphosphate (previously marketed as Teslascan) was removed from the market in 2012 as it was felt to be commercially non-viable by the manufacturers. However, with recent clinical research studies exploring the role of manganese-enhanced imaging in various pathological conditions, this is likely to change and partially chelated manganese-based contrast agents are likely to become available soon for cardiac, pancreatic and liver imaging (74).

Fully Chelated Manganese Formulations

O-carboxymethyl chitosan-Manganese-diethylenetriamine pentaacetate [CMCS-(Mn-DTPA)] is a fully chelated form of manganese and provides extracellular contrast similar to gadolinium-based contrast media. It is stable enough to prevent any release of manganese ions and therefore is unable to serve as an intracellular contrast agent (75).

1.13.3 SAFETY

The human body has inbuilt mechanisms in place to handle manganese and therefore the risk of manganese accumulation and toxicity with manganese-based contrast agents is low. However, based on early pre-clinical studies, there have been concerns regarding the safety of non-chelated manganese-based contrast agents, such as manganese chloride, as they can compete too strongly with myocardial calcium uptake and cause hypotension and cardiac arrest (70). In contrast, partially chelated manganese-based contrast media

like manganese dipyridoxyl diphosphate are well tolerated and have demonstrated an excellent safety profile (76–78). Manganese dipyridoxyl diphosphate was initially developed for staging hepatobiliary cancers and has since been used for multiple clinical studies without any safety concerns (Teslascan, EMEA. 2005).

Manganese toxicity from chronic environmental overexposure is recognised and is known as ‘manganism’. It has only been described in context of major environmental or occupational exposure over a long time period and can result in manganese accumulation in the globus pallidus and present as headaches, gait disturbance and extra-pyramidal symptoms (79).

1.14 MANGANESE-ENHANCED T1 MAPPING AND QUANTIFYING TISSUE MANGANESE UPTAKE

Physiologically, T1 magnetic resonance images represent characteristics of the tissue of interest. In magnetic resonance imaging, the longitudinal (spin-lattice) relaxation time (T1) of water protons is a fundamental tissue property. T1 mapping techniques measure this longitudinal or spin-lattice relaxation time, which is determined by how rapidly protons re-equilibrate their spins after being excited by a radiofrequency pulse (80). Due to its paramagnetic properties, manganese causes shortening of T1 relaxation time of water protons. Therefore, manganese-enhanced imaging is best quantified using the T1-mapping method. Following intravenous infusion, there is an initial reduction in blood pool T1 which normalises to baseline by 30 minutes. Myocardial and pancreatic T1 values also rapidly decline initially after manganese infusion, but in contrast to blood pool, there is a plateau phase in the myocardial and pancreatic T1 values which is likely secondary to ongoing intracellular uptake and accumulation until hepatic and renal excretion is complete (70).

Tissue manganese uptake can be quantified using tracer kinetic modelling; the commonest approach being Patlak two-compartment model. The multi-timepoint approach produces information about the exchange rate of the compartments that rapidly and reversibly exchange with plasma (81). Moreover, this can be used to assess the rate constant of any type of irreversible process within any organ system. This approach is further described within the methods section of this thesis.

1.15 MANGANESE-ENHANCED MAGNETIC RESONANCE IMAGING OF THE HEART

The effectiveness of manganese in imaging the healthy human myocardium was first demonstrated by Skjold et al in 2004 (82). Since then, manganese-enhanced imaging has been utilised in various clinical studies investigating a wide range of cardiac conditions (76–78). **Figure 1.4** shows myocardial manganese-enhanced magnetic resonance imaging in a healthy volunteer. Manganese-enhanced magnetic resonance imaging can identify viable myocardium in ischaemic heart disease more accurately compared to gadolinium enhanced imaging (83). Manganese-enhanced magnetic resonance imaging is also a non-invasive measure of myocardial calcium handling in patients with non-ischaemic cardiomyopathy and takotsubo syndrome (77,84). Furthermore, manganese-enhanced magnetic resonance imaging is capable of tracking changes in myocardial calcium handling over a period of time (77).

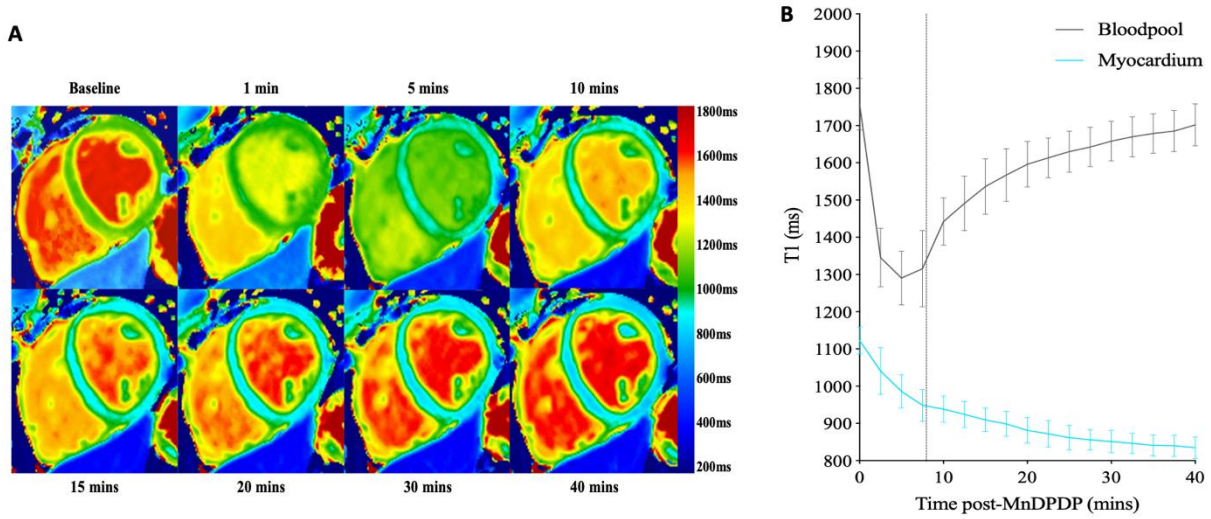

Figure 1.4. Manganese-enhanced magnetic resonance imaging in healthy myocardium. Panel A: T1-maps at mid ventricular level in a healthy volunteer at different time points before and after intravenous manganese contrast infusion. Panel B: Reduction in T1 values (ms) in blood pool and myocardium over 40 minutes after manganese contrast infusion

1.16 MANGANESE-ENHANCED MAGNETIC RESONANCE IMAGING OF THE PANCREAS

Manganese is taken up into the pancreatic beta-cells via voltage-gated calcium channels. Manganese and calcium ions compete during insulin secretion, thereby leading to pancreatic enhancement with manganese contrast which is dependent on the functional beta cell mass. **Figure 1.5** shows pancreatic manganese-enhanced imaging in a healthy volunteer. The specificity of this technique for pancreatic beta cells has been demonstrated in various pre-clinical studies using pharmacological treatments, such as nifedipine, tolbutamide and diazoxide, that activate or inactivate the voltage-gated calcium channels in the pancreatic beta cells. Several animal studies have suggested that manganese

uptake in the pancreas is specific to beta cells as opposed to exocrine cells or other islet cell populations. Streptozotocin specifically targets pancreatic beta cells, entering through glucose transporter 2, causing beta cell necrosis (85). There is a marked decrease in pancreatic manganese uptake in streptozotocin-treated mice compared to the non-diabetic mice. Tolbutamide and diazoxide target beta cell adenosine triphosphate-sensitive potassium channels (K_{ATP}), but not exocrine pancreas cells, and selectively activate or inactivate beta cell voltage-gated calcium channels respectively. Following treatment, pancreatic manganese uptake is increased by tolbutamide and decreased by diazoxide (86–88). Furthermore, in a retrospective analysis of abdominal manganese-enhanced magnetic resonance imaging, Botsikas et al found lower enhancement of pancreatic signal in people with type 2 diabetes (89). This is likely in keeping with 20-30% reduction in pancreatic beta-cell mass that is observed in people with type 2 diabetes. These studies suggest that it is very likely that pancreatic enhancement seen with manganese is predominantly due to manganese uptake in functional beta cells (89–91).

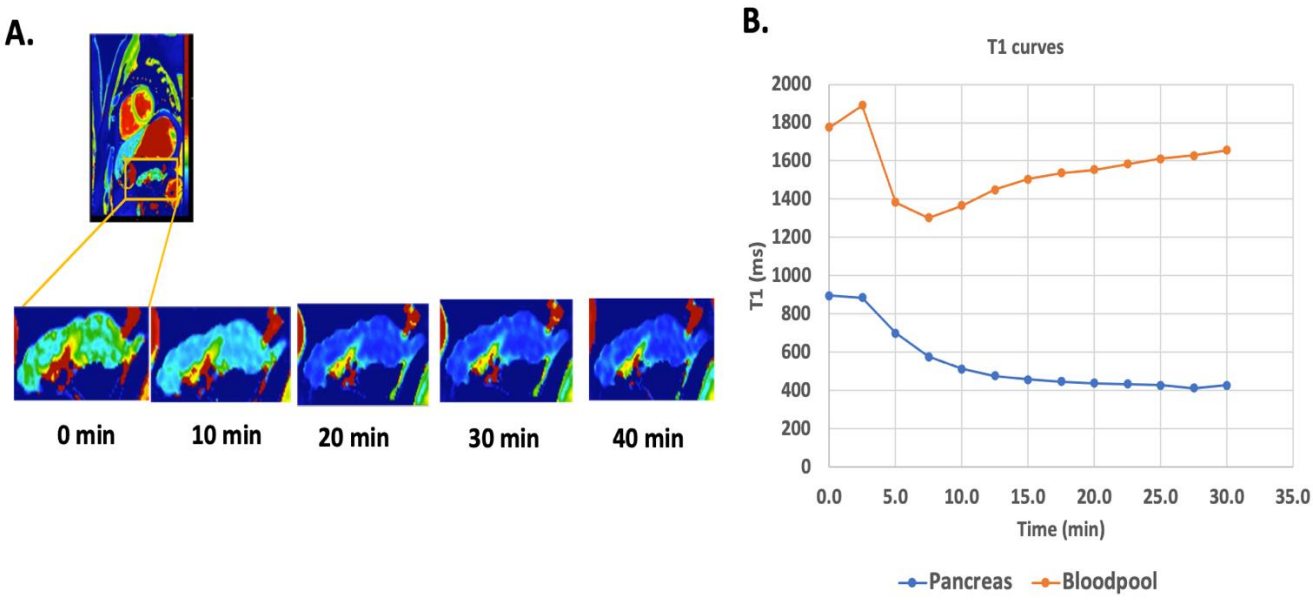

Figure 1.5. Manganese-enhanced Magnetic Resonance Imaging in Healthy Pancreas. Panel A: Pancreatic T1 maps at different time points before and after manganese infusion. Panel B: Reduction in T1 values (ms) in blood pool and pancreas over 40 minutes after manganese contrast infusion

1.17 SUMMARY

The prevalence of cardiometabolic disorders has reached a pandemic scale. People with cardiometabolic disorders have a higher mortality compared to the general population which is mainly driven by cardiovascular complications. Even in the absence of traditional risk factors like coronary artery disease, people with type 1 and type 2 diabetes mellitus are still twice as likely to develop heart failure. This has led to the identification of diabetic cardiomyopathy as a distinct clinical entity. Furthermore, people with type 1 diabetes with advanced pancreatic beta cell dysfunction are at a higher risk of developing cardiovascular complications compared to people with type 1 diabetes with ongoing endogenous insulin secretion. Therefore, the opportunity to preserve or to enhance beta cell function in type 1 diabetes may maximise beta cell activity and provide several physiological advantages such as a reduction in the rate of associated cardiovascular complications.

Despite a wealth of research interest, the underlying pathophysiology of diabetic cardiomyopathy remains uncertain. Similarly, there is limited understanding of the mechanism of pancreatic beta cell dysfunction in type 1 diabetes, and this has hindered the development of effective treatments. Evidence from pre-clinical studies suggests that dysregulated myocardial and pancreatic beta cell calcium handling could explain the pathophysiology of these cardiometabolic conditions. The focus of this thesis is to understand the underlying pathophysiology of diabetic cardiomyopathy and pancreatic beta cell dysfunction in type 1 diabetes using a novel imaging technique: manganese-enhanced magnetic resonance imaging. Manganese is a calcium analogue and is taken up in tissues with functional voltage gated calcium channels like the cardiomyocytes and pancreatic beta cells, providing intracellular contrast. Therefore, manganese-enhanced magnetic resonance imaging can be a non-invasive biomarker for myocardial and pancreatic beta cell calcium handling.

1.18 AIMS

The aims of this thesis are as follows:

1) To assess the reproducibility and repeatability of manganese-enhanced magnetic resonance imaging (Chapter 3).

2) To determine whether myocardial calcium uptake is altered in patients with type 1 or type 2 diabetes without known cardiac disease (Chapter 4).

3) To study the differences between myocardial calcium handling in patients with both heart failure and type 2 diabetes mellitus versus patients with heart failure without type 2 diabetes mellitus (Chapter 5).

4) To investigate whether manganese-enhanced magnetic resonance imaging can be used as a non-invasive and reproducible measure of pancreatic beta-cell function (Chapter 6).

1.19 HYPOTHESES

This thesis examines a novel approach to the diagnosis and risk stratification of patients with cardiometabolic disorders. The following hypotheses are tested.

1) Manganese-enhanced magnetic resonance is a repeatable and reproducible imaging technique (Chapter 3).

2) There is abnormal myocardial calcium handling in patients with type 1 and type 2 diabetes mellitus without apparent cardiovascular disease and this can be detected using manganese-enhanced magnetic resonance imaging (Chapter 4).

3) Patients with both type 2 diabetes mellitus and heart failure have more profound dysregulation of myocardial calcium handling compared to the patients with heart failure without type 2 diabetes mellitus (Chapter 5).

4) There is marked dysregulation of pancreatic beta cell calcium homeostasis in patients with type 1 diabetes mellitus and this dysregulation is directly proportional to plasma C-peptide concentrations (Chapter 6).

CHAPTER 2. Methods

2.1 ETHICAL AND REGULATORY CONSIDERATIONS

Ethical approval for all studies was granted by the United Kingdom National Research Ethics Service (20/NS/0037, 17/WM/0192, 20/WM/0304, 20/SS/0001 and 17/SS/0055). All patients provided written informed consent at the time of recruitment. All studies were conducted in accordance with the Declaration of Helsinki, and were sponsored by the Academic and Clinical Central Office for Research and Development (ACCORD), which is a partnership between the University of Edinburgh and the NHS Lothian Health Board.

2.2 AGENTS AND MATERIALS

2.2.1 Gadolinium-based contrast agent

Only the patients included in Chapter 1 (Repeatability and Reproducibility of Cardiac Manganese-Enhanced Magnetic Resonance Imaging) underwent gadolinium-enhanced magnetic resonance imaging and for this, 0.1 mmol/kg of gadobutrol (Gadovist®, Bayer Pharma AG, Germany) was used, as per manufacturers' recommended administration parameters for clinical use.

2.2.2 Manganese dipyridoxyl diphosphate (MnDPDP, mangafodpir trisodium)

Manganese-enhanced magnetic resonance imaging for all the studies was performed using Manganese dipyridoxyl diphosphate (5 μmol/kg). MnDPDP is a partially chelated manganese-based contrast agent and is free of toxicity seen with the non-chelated manganese-based contrast media like manganese chloride ($MnCl_2$). It was previously marketed by GE Healthcare for liver and pancreas imaging under the trade name of Teslascan™ but was withdrawn from both European and American markets due to a lack of commercial demand. Teslascan™ contains 10 μmol MnDPDP/mL and is now a generic product. Whilst not in current commercial use, clinical grade MnDPDP was reconstituted (Exova SL Pharma, Wilmington, Delaware, USA) to identical pharmaceutical particulars of

Teslascan™ with the only exception of being 5 times more concentrated, using active pharmaceutical ingredient sourced from an independent pharmaceutical company (Albany Molecular Research Inc. New York, USA). The final product constitutes a concentration of 50 μmol MnDPDP/mL and the dose administered for all the clinical studies was 0.1 μmol/Kg bodyweight given at a rate of 0.4-1.2 mL/min (20-60 μmol/min).

2.2.3 Fortisip Compact

Fortisip Compact (Nutricia, United Kingdom) is a high energy (2.4 Kcal/mL), ready to drink nutritional supplement. Subjects undergoing pancreatic magnetic resonance imaging were given 125 mL of Fortisip Compact as an oral glucose load half an hour prior to their scans in order to stimulate pancreatic beta-cell insulin secretion (Chapter 6).

2.2.4 Connecting-Peptide (C-Peptide) Assay

Patients with type 1 diabetes underwent plasma C-peptide testing as part of study four (Chapter 6). Plasma C-peptide concentrations were measured using an immunoassay (ARCHITECT C-peptide assay, Abbott, USA). The ARCHITECT C-peptide assay measures C-peptide rapidly, accurately and precisely in human plasma, serum and urine (92). Internal assay validation demonstrated a coefficient of variation of 7% at 7 pmol/L and of 15% at 4 pmol/L. C-peptide is secreted from the beta-cells of islets of Langerhans of the pancreas when proinsulin is cleaved into insulin and C-peptide. Clinically, measurement of plasma C-peptide is used as a marker of endogenous pancreatic beta-cell function, however, there is evidence to suggest that plasma C-peptide concentrations do not correlate with beta-cell mass in humans (93).

2.3 PARTICIPANT COHORTS

All subjects were >18 years of age and exclusion criteria for all patient cohorts included contraindications to magnetic resonance imaging (described in section 2.4.2), renal failure (estimated glomerular filtration rate <30 mL/min/1.73 m^2), an inability to consent, New York Heart Association class IV heart failure, pregnancy or breast feeding, obstructive liver disease, high degree atrioventricular block, history of torsades de pointes, prolonged QTc interval.

2.3.1 Patients with type 1 diabetes mellitus

People with a confirmed diagnosis of type 1 diabetes mellitus, aged ≥18 years were identified and approached through the Edinburgh Centre for Endocrinology and Diabetes, Royal Infirmary of Edinburgh, Edinburgh, United Kingdom. The diagnosis of type 1 diabetes was made by an endocrinologist based on the National Institute for Health and Care Excellence criteria (94). All enrolled patients were established on stable therapy prior to recruitment. We specifically recruited 10 people with low (>50 pmol/L) and 10 people with very low (<50 pmol/L) baseline plasma C-peptide concentrations.

2.3.2 Patients with type 2 diabetes mellitus

People with type 2 diabetes were prospectively enrolled from primary care services or Edinburgh Centre for Endocrinology and Diabetes in Edinburgh and Leicestershire, United Kingdom. The diagnosis of type 2 diabetes was made either by the patient's general practitioner (GP) or an endocrinologist based on the National Institute for Health and Care Excellence criteria (95). All patients with type 2 diabetes were on stable therapy prior to their study scans and did not have any known cardiovascular disease.

2.3.3 Patients with heart failure with or without type 2 diabetes mellitus

People aged ≥18 years with left ventricular systolic dysfunction with an ejection fraction <50% with or without type 2 diabetes mellitus were recruited from the Edinburgh Heart Centre, NHS Lothian, United Kingdom. All patients had an echocardiogram prior to magnetic resonance imaging to confirm the diagnosis of left ventricular systolic impairment. Half of the patients in this cohort had both a diagnosis of type 2 diabetes and heart failure and the other half only had heart failure but did not have a diagnosis of type 2 diabetes mellitus.

2.3.4 Patients with non-ischemic dilated cardiomyopathy

Patients ≥18 years of age with dilated cardiomyopathy were recruited from the Edinburgh Heart Centre, NHS Lothian, United Kingdom. Non-ischaemic dilated cardiomyopathy was defined as left ventricular dilatation (left ventricular end-diastolic volume >117% adjusted for age and body-surface area) and presence of left ventricular systolic dysfunction (ejection fraction <50%), in the absence of coronary artery disease or abnormal loading conditions like hypertension and valvular heart disease. All patients were required to have stable New York Heart Association class I-III heart failure, on stable therapy in the preceding month. Patients in this cohort were included in the repeatability study.

2.3.5 Patients with hypertrophic cardiomyopathy

Subjects ≥18 years of age with hypertrophic cardiomyopathy were recruited from the Edinburgh Heart Centre, United Kingdom. Hypertrophic cardiomyopathy was diagnosed either on echocardiogram or magnetic resonance imaging according to the European Society of Cardiology guidelines (left ventricular thickness ≥ 15 mm in any segment) in the absence of abnormal loading conditions (like hypertension, valvular heart disease or congenital heart disease). Patients in this cohort were included in the repeatability study.

2.3.6 Patients with myocardial infarction

Adult patients (≥18 years of age) who had suffered acute ST-elevation myocardial infarction were identified from the coronary care unit, Edinburgh Heart Centre, Royal Infirmary of Edinburgh. Patients were required to have angiographically proven left main stem, left anterior descending or multivessel disease and ischemic cardiomyopathy with a left ventricular ejection fraction <50% by echocardiography. Patients in this cohort were included in the repeatability study.

2.3.7 Healthy volunteers

Healthy volunteers ≥18 years of age were recruited either via advertisement at the Edinburgh Heart Centre or Glenfield hospital, Leicester, United Kingdom. Healthy volunteers had no known pre-existing medical conditions.

2.4 IMAGE ACQUISITION

2.4.1 ECHOCARDIOGRAPHY

Transthoracic echocardiography is a safe, non-invasive technique and is the first-line imaging investigation for many cardiac conditions including heart failure. Indeed, the most common reason for referral for echocardiography is left ventricular function assessment. Left ventricular function is usually evaluated by measuring the ejection fraction. Ejection fraction is the percentage of blood ejected from the ventricle during systole in relation to total end-diastolic volume (96). The left ventricle doesn't have a specific geometric shape and therefore assessing its function can be challenging. Hence, usually a combination of echocardiographic parameters like fractional shortening, 'eyeballing of left ventricular function', ejection fraction calculation using the Simpson's biplane method, stroke volume, contractility (dp/dt), is used in clinical practice (97). Simpson's biplane method, also known as the biplane method of discs, is the commonest method used to assess left ventricular

ejection fraction by echocardiography in clinical practice. This method requires tracing the left ventricular endocardial border in the apical four and two chamber views in both end-diastole and end-systole. The tracings are used to divide the left ventricular cavity into a predetermined number of discs. The disc volumes are calculated based on the endocardial tracings and it determines the left ventricular ejection fraction using the formula below:

$$\text{Ejection fraction (\%)} = \frac{\text{End diastolic volume} - \text{End systolic volume}}{\text{End diastolic volume}} \times 100$$

However, this method has some limitations and relies heavily on good image quality to allow reliable tracing of the endocardial borders (98). Furthermore, it can be challenging to calculate the left ventricular ejection fraction using this method in the presence of dyssynchrony (e.g.: left bundle branch block) and arrhythmia. Other echocardiographic techniques to assess left ventricular systolic function (like fractional shortening, dp/dt measurement and stroke volume) are prone to error and are not generally used in isolation.

Overall, echocardiography provides two-dimensional images with high temporal resolution and offers structural and functional information for left ventricular systolic function assessment. Some of the limitations of echocardiography include poor reproducibility and the image quality is dependent on multiple factors like anatomy, patient position and respiration and operator skill or expertise (99).

Transthoracic echocardiography was performed using a dedicated echocardiogram machine (Affiniti 70, Philips, Amsterdam, Netherlands) at the Edinburgh Clinical Research Facility by a British Society of Echocardiography-accredited cardiac sonographer.

Research transthoracic echocardiograms were undertaken by this sonographer according to the British Society of Echocardiography guidelines (100). Left ventricular ejection fraction was calculated using the Simpson's biplane method (101).

2.4.2 MAGNETIC RESONANCE IMAGING

Magnetic resonance imaging is a non-invasive imaging modality that produces three dimensional detailed anatomical images. Magnetic resonance scanners employ magnets to produce a strong magnetic field that forces protons in the body to align with that field. When a radiofrequency pulse is applied, the protons spin out of equilibrium, straining against the pull of the magnetic field. When the radiofrequency pulse is turned off, the magnetic resonance sensors are able to detect the energy released as the protons realign with the magnetic field. The time it takes for the protons to realign with the magnetic field, as well as the amount of energy released depends on the proton density in the tissue and tissue relaxation times (102). Therefore, magnetic resonance imaging provides excellent soft tissue characterisation and quantification of cardiac volumes and flow. Furthermore, magnetic resonance imaging is safe and does not involve ionising radiation. However, some of its limitations include the relative or absolute contraindications to entering the magnetic field (like implantable cardiac devices, cochlear implants, metallic foreign body in the eye, cerebral, carotid or aortic aneurysm clips etc), claustrophobia, the costs involved, and the requirement of specific software and trained staff.

T1 Mapping

T1 mapping involves registering the course of recovery of longitudinal (spin lattice) magnetisation of water protons and involves prior preparation with radiofrequency pulses to change the magnetisation. Recovery of longitudinal magnetisation follows an exponential course and T1 value is the time when recovery of magnetisation has reached

63% of its original state (103). The rate of T1 recovery is different in healthy and diseased tissue and can therefore help with tissue characterisation. T1 mapping can be performed in native tissue (without contrast) or after the injection of contrast agents (post contrast T1). A T1 map is generated by combining multiple images acquired in diastole, but with different inversion times, to assess T1 relaxation. The resulting T1-map is a two-dimensional image where every pixel represents the T1 value for the respective voxel, displayed as signal intensity (104). A pre-determined colour scheme for different T1 values can be applied using image analysis software to aid visual discrimination between different tissue types.

MOdified Look-Locker Inversion recovery (MOLLI) and Shortened Modified Look-Locker Inversion recovery (ShMOLLI) are the most common T1-mapping sequences used. MOLLI samples T1 using single short steady-state free precision readouts several times during its recovery, using magnetisation inversion. T1 is estimated using the resulting data points to generate a best-fit T1 decay curve (105). ShMOLLI uses the same principles as MOLLI but samples fewer data points in a shorter breath-hold (105). SAturation recover single-SHot Acquisition (SASHA) and SAturation Pulse Prepared Heart-rate independent Inversion-REcovery (SAPPHIRE) are the other T1-mapping sequences. SASHA sequence enables a more direct estimation of T1 by using saturation pulses without inversion-pulse preparation, effectively removing the previous cycle's magnetisation and by sampling it once during recovery. SAPPHIRE sequence uses a combination of saturation followed by inversion pulses to reduce susceptibility to variations in heart rate and rhythm (105). All these T1-mapping techniques demonstrate excellent reproducibility but SASHA and SAPPHIRE offer greater accuracy whereas MOLLI and ShMOLLI offer greater precision (106). Measurement of T1 values using either MOLLI or ShMOLLI sequences at 3T offers excellent reproducibility (107). MOLLI T1-mapping sequence was used for scanning

patients with type 1 diabetes, type 2 diabetes and patients with heart failure (Chapters 4, 5 and 6) and ShMOLLI sequence was used for scanning patients with myocardial infarction, hypertrophic cardiomyopathy and ischaemic or non-ischaemic cardiomyopathies (Chapter 3).

CARDIAC MAGNETIC RESONANCE IMAGING

Cardiac magnetic resonance imaging is the gold standard measure of myocardial function and anatomy as it provides high temporal and spatial resolution, does not require geometric assumptions and has high signal to noise ratio. Left ventricular mass and volumes (end diastolic volume and end systolic volume) are independent predictors of adverse remodelling and are associated with cardiovascular events, and, therefore, are essential measures required for the management of patients with cardiomyopathies (108,109).

The advantages of cardiac magnetic resonance imaging include 3-dimensional images, high resolution and tissue characterisation. In contrast to echocardiography, cardiac magnetic resonance imaging provides sequential 3-domensional cine images of the heart from base to apex throughout the cardiac cycle. This facilitates the summation of cross-sectional volumes from each of the short-axis tomographic cuts, thereby providing accurate end-diastolic and end-systolic volumes (110). The accuracy of cardiac magnetic resonance measures of left ventricular parameters has been validated in several studies using post-mortem human hearts (111,112) imaged ex-vivo and in in-vivo animal studies (113,114). Furthermore, reproducibility of left ventricular measurements is crucial for evaluating changes over time and cardiac magnetic resonance imaging displays excellent interstudy (i.e., test-retest reliability), intra- and inter-observer variability (115–117). While cardiac magnetic resonance provides high-quality imaging, it can be time-consuming, may

not be suitable for claustrophobic patients (~5%) and may not provide optimal imaging in patients with faster heart rates or atrial fibrillation. However, despite these limitations, cardiac magnetic resonance is currently the most accurate and reproducible method of quantifying left ventricular mass and volumes (118) and it plays a key role in the diagnosis and prognostication of various cardiomyopathies.

Manganese-enhanced cardiac magnetic resonance imaging was performed using 3-Tesla scanners (Siemens Skyra, Erlangen, Germany and MAGNETOM Skyrafit, Siemens Healthineers, Erlangen, Germany) with electrocardiographic gating and an 18-channel phased-array cardiac receiver coil. The magnetic resonance imaging protocol included localisers, steady-state free precession cine images in four-, three- and two-chamber views and a stack of short-axis slices covering the entire left ventricle. T1 mapping was performed pre-contrast in a mid-short-axis slice position using either Modified Look-Locker Inversion recovery sequence (MOLLI, Siemens MyoMaps, Erlangen, Germany) or ShMOLLI sequence (Shortened Modified Look-Locker Inversion recovery sequence (Siemens Healthcare, Germany) (80). An intravenous infusion of manganese dipyridoxyl diphosphate (5 μmol/kg (0.1 mL/kg) at 1 mL/min; Exova SL Pharma, Wilmington, DE, USA) was commenced and repeated T1 maps were performed at the same location every 2.5 min for 30 min (**Figure 2.1**).

PANCREATIC MAGNETIC RESONANCE IMAGING

Subjects fasted from midnight and, on the following morning, were given a standardised glucose load (125 mL of Fortisip compact, 2.4 Kcal/mL [Nutricia] supplement drink) half an hour prior to their imaging to stimulate pancreatic beta-cell insulin secretion. People with type 1 diabetes mellitus withheld any quick-acting insulin prior to the scan.

Magnetic resonance imaging was performed using a 3-Tesla scanner (MAGNETOM Skyrafit; Siemens Healthineers) with a dedicated 30-channel body matrix coil. Manganese-enhanced magnetic resonance imaging was performed using intravenous manganese dipyridoxyl diphosphate (5 µmol/kg (0.1 mL/kg) at 1 mL/min; Exova SL Pharma) administered over 10 min. Localisers, half-Fourier single-shot turbo spin-echo (HASTE) and standard breath-hold cine sequences of the heart were followed by T1 mapping sequences of the pancreas. Pancreatic T1 mapping was performed prior to contrast using a breath-held modified Look-Locker inversion recovery acquisition and every 2.5 min for 30 min after commencing the intravenous manganese dipyridoxyl diphosphate infusion (**Figure 2.1**). Pancreas and left ventricular blood pool T1 values were compared.

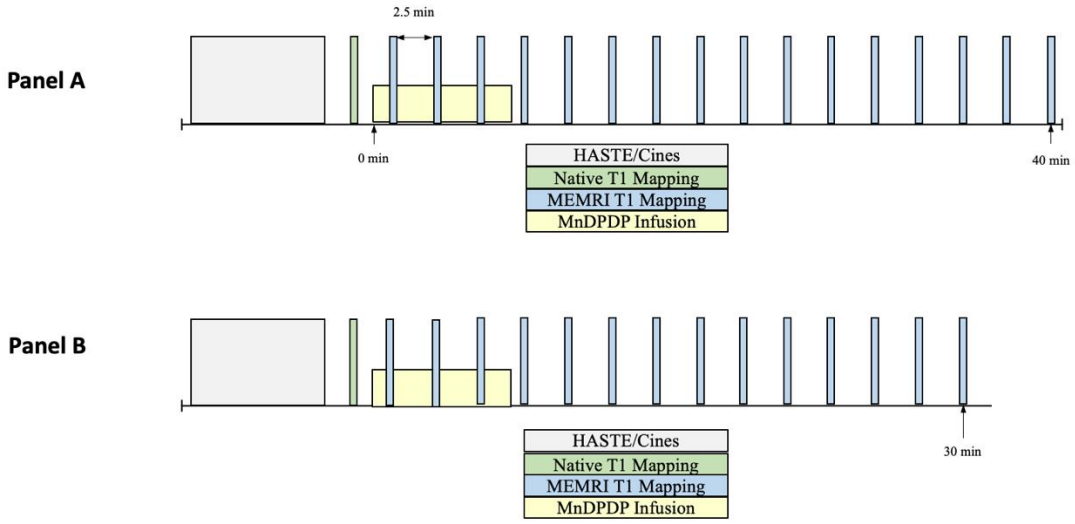

Figure 2.1. Manganese-enhanced magnetic resonance imaging protocols. Panel A. Protocol for patients with ischaemic cardiomyopathy, non-ischaemic cardiomyopathy and hypertrophic cardiomyopathy. Panel B. Protocol for patients with either type 1 or type 2

diabetes mellitus, patients with heart failure and healthy volunteers. MEMRI – Manganese-enhanced magnetic resonance imaging, MnDPDP – Manganese dipyridoxyl diphosphate.

2.5 IMAGE ANALYSIS

2.5.1 Cardiac Magnetic Resonance Imaging

Image analysis was performed at an imaging core lab (Queen's Medical Research Institute, University of Edinburgh) offline and blinded to all participant details. Cardiac chamber volumes, mass and function (including myocardial strain analysis) were assessed using Circle CVI (Circle Cardiovascular Imaging, CVI42 v5.13.5 Calgary, Canada). Endocardial and epicardial borders were manually defined on the short-axis cine images for volumetric and wall motion measurements. For serial T1-mapping before and after MnDPDP infusion, regions of interest were drawn within the mid-ventricular inferoseptal segment and the left ventricular blood pool for all the T1 maps from 0 to 30 minutes. Left ventricular septal sampling yields the greatest precision and minimises the effect of considerable variations of regional T1 values because of the artefact-prone left ventricular free wall myocardium (119–121). Manganese-enhanced cardiac T1-map analysis technique used in all studies is illustrated in **Figure 2.2**. Cardiac manganese uptake was calculated using manganese kinetic modelling as described in section 2.5.3.

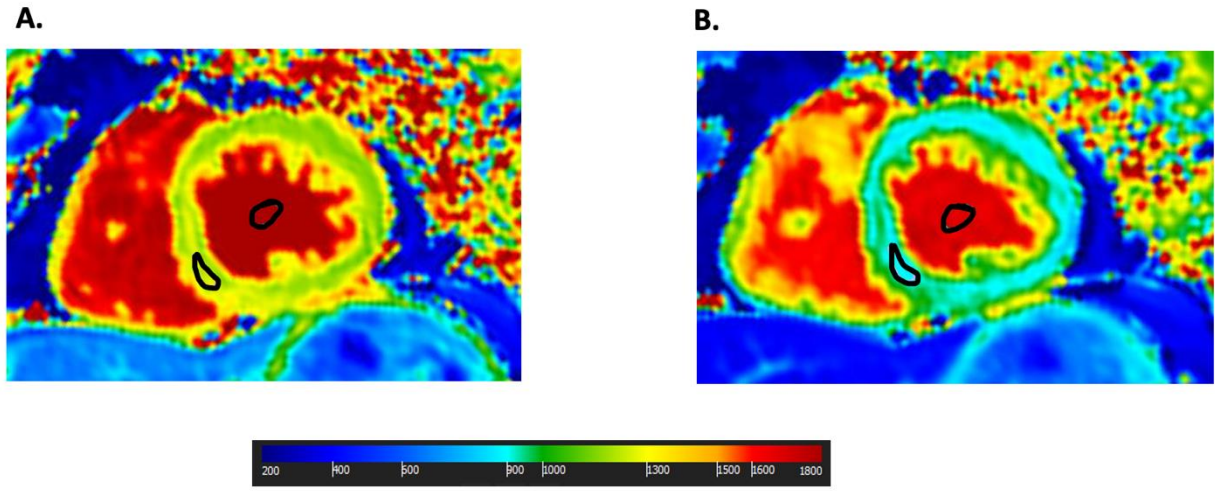

FIGURE 2.2. Cardiac Manganese T1-mapping analysis. Regions of interest were drawn in the mid-ventricular inferoseptal segment and the left ventricular blood pool from 0 to 30 minutes. Panel A – example T1 map at baseline (0 min) and Panel B – example T1 map at 30 min.

2.5.2 Pancreatic Magnetic Resonance Imaging

Magnetic resonance images were analysed offline using Circle CVI (Circle Cardiovascular Imaging, CVI42 v5.13.5). T1 relaxations times were measured in the pancreas and left ventricular blood pool. For this, regions of interest were drawn within the head, body and tail of the pancreas and compared with regions of interest drawn within the left ventricular blood pool. This is illustrated in the figure below (**Figure 2.3**). Pancreatic manganese uptake was calculated using Patlak formulation as described in section 2.5.3.

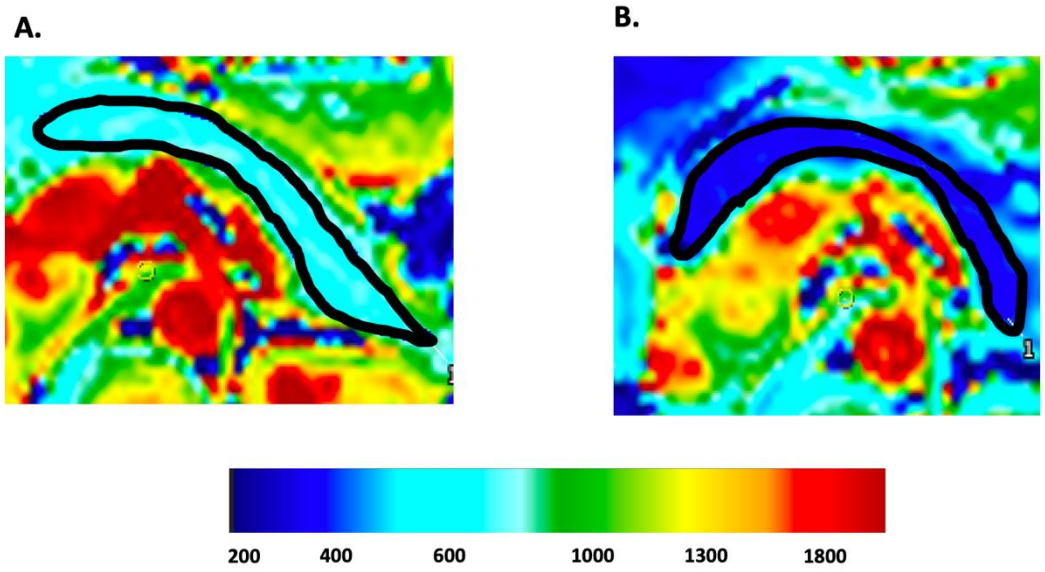

Figure 2.3. Pancreatic Manganese T1-mapping analysis. Regions of interest were drawn within the head body and tail of the pancreas and the left ventricular blood pool from 0 to 30 minutes. Panel A – example pancreatic T1 map at baseline (0 min) and Panel B – example pancreatic T1 map at 30 min.

2.5.3 Manganese Kinetic Modelling

Patlak et al were the first to provide a graphical analysis of unidirectionality of transfer and of the influx constant, using brain uptake data (81). The multi-timepoint approach produces information about the exchange rate of the compartments that rapidly and reversibly exchange with plasma. Moreover, this can be used to assess the rate constant of any type of irreversible process within any organ system. The Patlak two-compartment model was used in all the studies to measure the rate of cardiac or pancreatic manganese uptake. This assumes the influx of manganese ions from a reversible (v_e, extracellular and vascular space) into a largely irreversible (v_i, pancreatic beta cells or cardiomyocytes during the imaging period) compartment. This apparent unidirectional influx constant (*Ki*)

for the transfer of manganese from plasma to irreversible compartments v_i, can be measured, using the equation below:

$$\frac{C_t(t)}{C_a(t)} = Ki\frac{\int_0^t C_a(\tau)d\tau}{C_a(t)} + v_e$$

where C_t and C_a are the manganese concentration in cardiac/ pancreatic tissue and blood pool (arterial input function) respectively. This formula is equivalent to the Patlak model and describes that if a contrast medium is irreversibly trapped in the tissue within the imaging period, the instantaneous tissue concentration (cardiac or pancreatic T1) divided by the instantaneous arterial concentration (blood pool T1) plotted against the integrated arterial concentration divided by the instantaneous arterial concentration, will result in linearisation of the data. The gradient of this line represents the unidirectional manganese influx constant, Ki and is equal to: (K1 x K2) / (K2 + K3) where K1, K2 and K3 are the individual rate constants of this compartmental model. This is demonstrated in **Figure 2.4**.

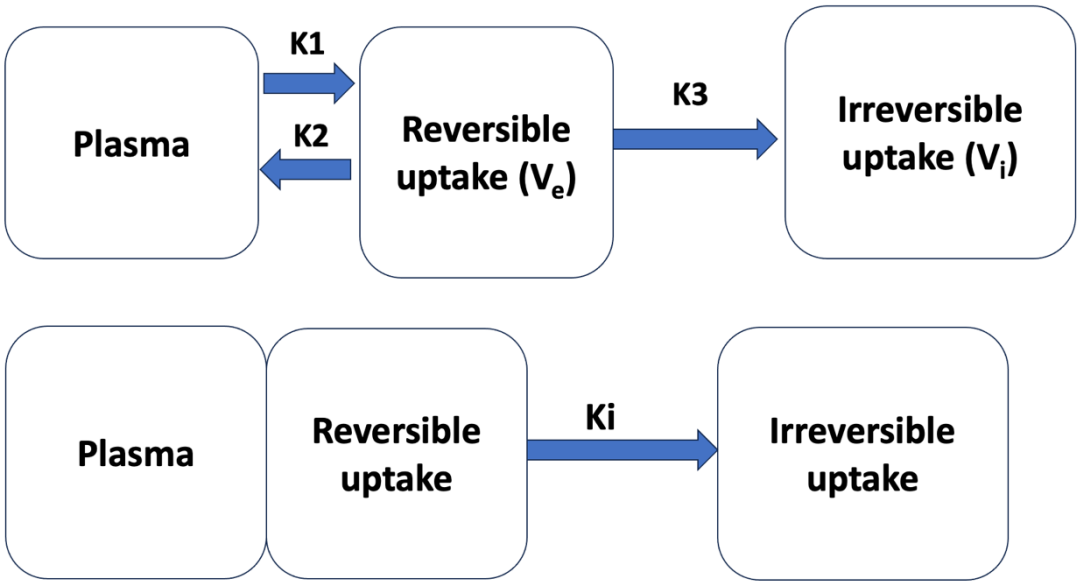

Figure 2.4. Patlak Formulation. Two-compartment model used for Patlak formulation with reversible (Ve) and irreversible (Vi) uptake between combined intravascular/interstitial and intracellular compartments respectively. K1, K2, K3 represent individual transfer constants and Ki represents manganese influx constant. Ki=[(K1 x K2) / (K2 + K3)]. (Adapted from Skjold et al. 2004).

Further details on image analysis are described in relevant results chapters.

2.6 STATISTICAL ANALYSIS

All statistical analyses were performed with R Studio (RStudio, Boston, USA). Categorical baseline variables were presented as number (%) and compared using a Chi-squared test. Continuous data were assessed for normality using either the Shapiro Wilk test or the D'Augustino-Pearson test and presented as mean ± standard deviation or median [interquartile range]. Comparisons between variables were made using paired and unpaired t-tests, Mann-Whitney, Wilcoxon tests and analysis of variance/covariance or Kruskal Wallis tests as appropriate. Tukey's HSD (honestly significant difference) or Bonferroni tests were used for post-hoc analysis where analysis of variance test was applied. Categorical baseline variables were compared using Fisher's exact test.

Statistical significance was taken as two-sided $P<0.05$. Correlation between independent non-parametric variables were assessed with Spearman's rank correlation coefficient. Reproducibility and repeatability analyses were carried out using intra-class correlation coefficient (ICC), Lin's correlation coefficient and Bland Altmann analysis. A positive or negative correlation coefficient with an integer value of 1.0 was considered as perfect correlation, between 0.9-1.0 very strong, between 0.70-0.90 strong, between 0.5-0.6 moderate and 0.1-0.4 weak.

CHAPTER 3. Repeatability and Reproducibility of Cardiac Manganese-Enhanced Magnetic Resonance Imaging

Adapted from:

Singh T, Joshi S, Meah MN, Spath NB, Papanastasiou G, Kershaw LE, Baker AH, Dweck MR, Newby DE, Semple SI. Repeatability and reproducibility of cardiac manganese-enhanced magnetic resonance imaging. Sci Rep. 2023 Feb 27;13(1):3366. doi: 10.1038/s41598-023-29591-z. PMID: 36849509; PMCID: PMC9971197.

3.1 Abstract:

Background

Manganese-enhanced magnetic resonance imaging can provide a surrogate measure of myocardial calcium handling. Its repeatability and reproducibility are currently unknown.

Methods

Sixty-eight participants: 20 healthy volunteers, 20 with acute myocardial infarction, 18 with hypertrophic and 10 with non-ischemic dilated cardiomyopathy underwent manganese-enhanced magnetic resonance imaging. Ten healthy volunteers were re-scanned at 3 months. Native T1 values and myocardial manganese uptake were assessed for intra and inter-observer repeatability. Scan-rescan reproducibility was assessed in 10 healthy volunteers.

Results

Intra-observer and inter-observer correlation was excellent in healthy volunteers for mean native T1 mapping (Lin's correlation coefficient [LCC] 0.97 and 0.97 respectively) and myocardial manganese uptake (LCC: 0.99 and 0.96 respectively). Scan-rescan correlation for native T1 and myocardial manganese uptake was also excellent. Similarly, intra-observer correlations for native T1 and myocardial manganese uptake in patients with acute myocardial infarction (LCC: 0.97 and 0.97 respectively), hypertrophic (LCC: 0.98 and 0.97 respectively) and dilated cardiomyopathy (LCC: 0.99 and 0.95 respectively) were excellent. Limits of agreement were broader in patients with dilated cardiomyopathy.

Conclusion

Manganese-enhanced magnetic resonance imaging has high repeatability and reproducibility in healthy myocardium and high repeatability in diseased myocardium. However, further study is needed to establish robustness in pathologies with diffuse myocardial fibrosis.

3.2 Introduction:

Cardiac magnetic resonance imaging has a major role in the diagnosis, evaluation of myocardial function and tissue characterization of a range of cardiovascular diseases (122–124). Conventional cardiac magnetic resonance with gadolinium enhancement allows for quantification of myocardial fibrosis which has utility in the assessment of viability in ischemic cardiomyopathy. Furthermore, it allows for prognostication in a variety of cardiac conditions including myocarditis, dilated cardiomyopathy, hypertrophic cardiomyopathy, amyloidosis (125–127), arrhythmogenic right ventricular dysplasia (128) and Fabry's disease (129). However, gadolinium-based contrast media only allow for the assessment of the extracellular space.

Magnetic resonance imaging using manganese-based contrast media has the ability to provide intracellular contrast of viable myocardium. Manganese was the first clinical magnetic resonance imaging contrast medium to be used *in vivo*, resulting in shortening of T1 relaxation in the heart, liver, kidneys and pancreas (70). In brief, after intravenous administration in humans, manganese dipyridoxyl diphosphate undergoes dephosphorylation and transmetallation with zinc to release manganese ions into the plasma (130,131). Being, a calcium analogue, manganese is actively taken up by voltage-gated calcium channels in viable myocardium whereas abnormal myocardium has reduced or no uptake. Myocardial manganese uptake can be calculated using Patlak kinetic modelling (81,132,133), thereby providing a measure for myocardial calcium handling (134,135). Indeed, manganese-enhanced T1 mapping can detect dysfunctional myocardial calcium handling in patients with cardiomyopathies and can distinguish between normal and pathological myocardium (77,84,135).

Repeatability of the assessment of manganese-enhanced magnetic resonance imaging and its scan-rescan reproducibility have not been established and is a necessary step for its future clinical application. The aims of this study were to establish the intraobserver and interobserver repeatability of manganese-enhanced T1 mapping and kinetic modelling of myocardial manganese uptake as well as provide early data on overall scan-rescan reproducibility.

3.3 Methods:

3.3.1 Ethics approval and consent to participate:

The study was conducted in accordance with the Declaration of Helsinki, with the favourable ethical opinion of the South-east Scotland Research Ethics Committee 2 (MEMRI-17/SS/0055, MEMORY-20/SS/0001) and with the written informed consent of all participants.

3.3.2 Study population:

Adult (≥18 years of age) healthy volunteers (n=20) were recruited as part of the MEMORY [NCT04623788] and DAPA-MEMRI studies [NCT04591639]. Patients with acute myocardial infarction (n=20), hypertrophic cardiomyopathy (n=18) or non-ischemic dilated cardiomyopathy (n=10) were recruited from the Edinburgh Heart Centre as part of the MEMRI study [NCT03607669]. Patients with acute myocardial infarction were required to have a ST-segment elevation myocardial infarction according to the universal definition of myocardial infarction (136) and angiographically proven coronary artery disease. Patients were required to be clinically stable with reduced left ventricular ejection fraction (≤50% by echocardiography) secondary to one or more acute ischaemic events.

The diagnosis of hypertrophic cardiomyopathy and dilated cardiomyopathy were based on echocardiography or magnetic resonance imaging according to European Society of Cardiology guidelines (137,138). Hypertrophic cardiomyopathy was defined as left ventricular hypertrophy (left ventricular wall thickness ≥15 mm in any segment) in the absence of hemodynamic stresses (138). Non-ischemic dilated cardiomyopathy was defined by the presence of impaired left ventricular systolic function (ejection fraction ≤50% within 12 months) and left ventricular dilatation (left ventricular end-diastolic volume >105 mL/m^2 for men and >96 mL/m^2 for women, adjusted for age and body-surface area), in the absence

of abnormal loading conditions (hypertension and valvular disease) and coronary artery disease (137).

3.3.3 Magnetic Resonance Imaging

All participants were scanned on a Siemens MAGNETOM Skyrafit 3T scanner (Siemens Healthineers, Erlangen, Germany) with a 30-channel body matrix coil. Electrographic gated breath-hold steady-state free procession long-axis cine images in two, three and four chamber views were acquired. Short axis cine images covering the entire left ventricle were taken at 8-mm slice thickness, 2-mm gap, field of view 300 x 400 mm, matrix 208 x 256, repetition time 2.9 ms, echo time 1.2 ms, flip angle 64-790, temporal resolution <50 ms, with 30 phases per cardiac cycle, in-plane image resolution 1.1 x 1.5 mm to 1.3 x 1.7mm.

All participants underwent gadolinium enhanced magnetic resonance imaging, followed by manganese-enhanced imaging. This was performed at least 48 hours apart. Additionally, healthy volunteers underwent repeat manganese-enhanced magnetic resonance imaging, 3 months following baseline imaging.

T1 mapping

For healthy volunteers, T1 mapping was acquired with a modified Look-Locker inversion recovery sequence (139,140) and in patients, T1 mapping was acquired with shortened modified Look-Locker inversion recovery (WIP #1048 Siemens Healthineers), with a 5(3)3) sampling pattern and the following typical parameters: slice thickness 8.0 mm with 1.6-mm gap, field of view=360x280 mm, repetition time 388.8 ms; echo time 1.07 ms, matrix 256×115. To minimize image artefacts, acquisition was performed with the region of interest (the heart) at isocentre, a small shim volume applied around the myocardium, and a large field of view (400 mm). All T1 mapping was acquired with non-rigid motion correction. The

same parameters were used for scan-rescan reproducibility with the chosen slice being matched visually by the supervising cardiologist using appropriate anatomical landmarks to ensure the same location was being analysed.

Late Gadolinium Enhancement

Late gadolinium enhancement images were acquired following intravenous gadobutrol (0.1 mmol/kg; Gadovist, Bayer, Germany) using a single breath hold per slice with a short-axis stack, and long-axis orientations. A full short-axis T1 stack was acquired prior to and 10 min after contrast administration as described previously (84,135).

Manganese infusion

Manganese-enhanced magnetic resonance imaging was conducted with intravenous infusion of manganese dipyridoxyl diphosphate (5 μmol/kg (0.1 mL/kg) at 1 mL/min; Exova SL Pharma, Wilmington, Delaware, USA) and has been described previously (84,135). Following a full short-axis native T1 stack, a single mid-ventricular short-axis slice was identified and performed at this location every 2.5 min for 30 min after starting manganese infusion, at which point a full short-axis T1 stack was repeated (**Figure 3.1**).

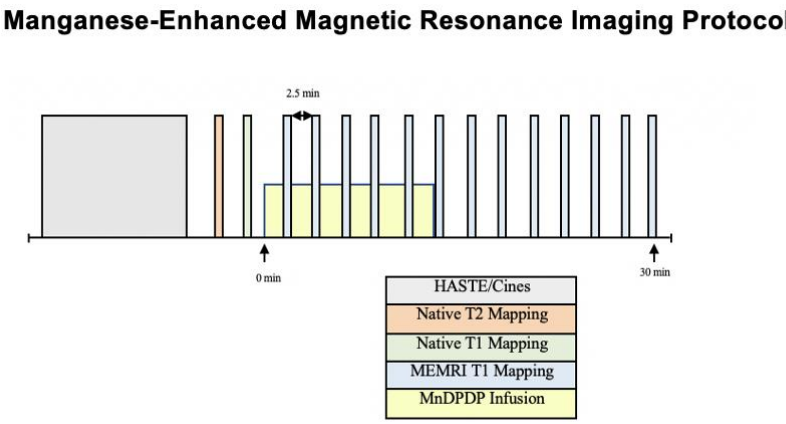

Figure 3.1. Manganese-Enhanced Magnetic Resonance Imaging Protocol.

A single mid-ventricular slice was chosen for healthy volunteers. For patients, the short-axis slice was identified by the supervising cardiologist, guided by late gadolinium enhancement imaging, native T1 maps and cine images to represent abnormal myocardium (**Figure 3.2**). For patients with acute myocardial infarction, infarct area was assessed by late-gadolinium images and to reduce variability, automated reference regions of interest were generated in the infarct region.

For patients with hypertrophic cardiomyopathy, regions of maximal hypertrophy and fibrosis were selected and for dilated cardiomyopathy, a mid-ventricular short-axis slice was selected. The chosen slice was matched visually by the same supervising cardiologist for repeat scanning.

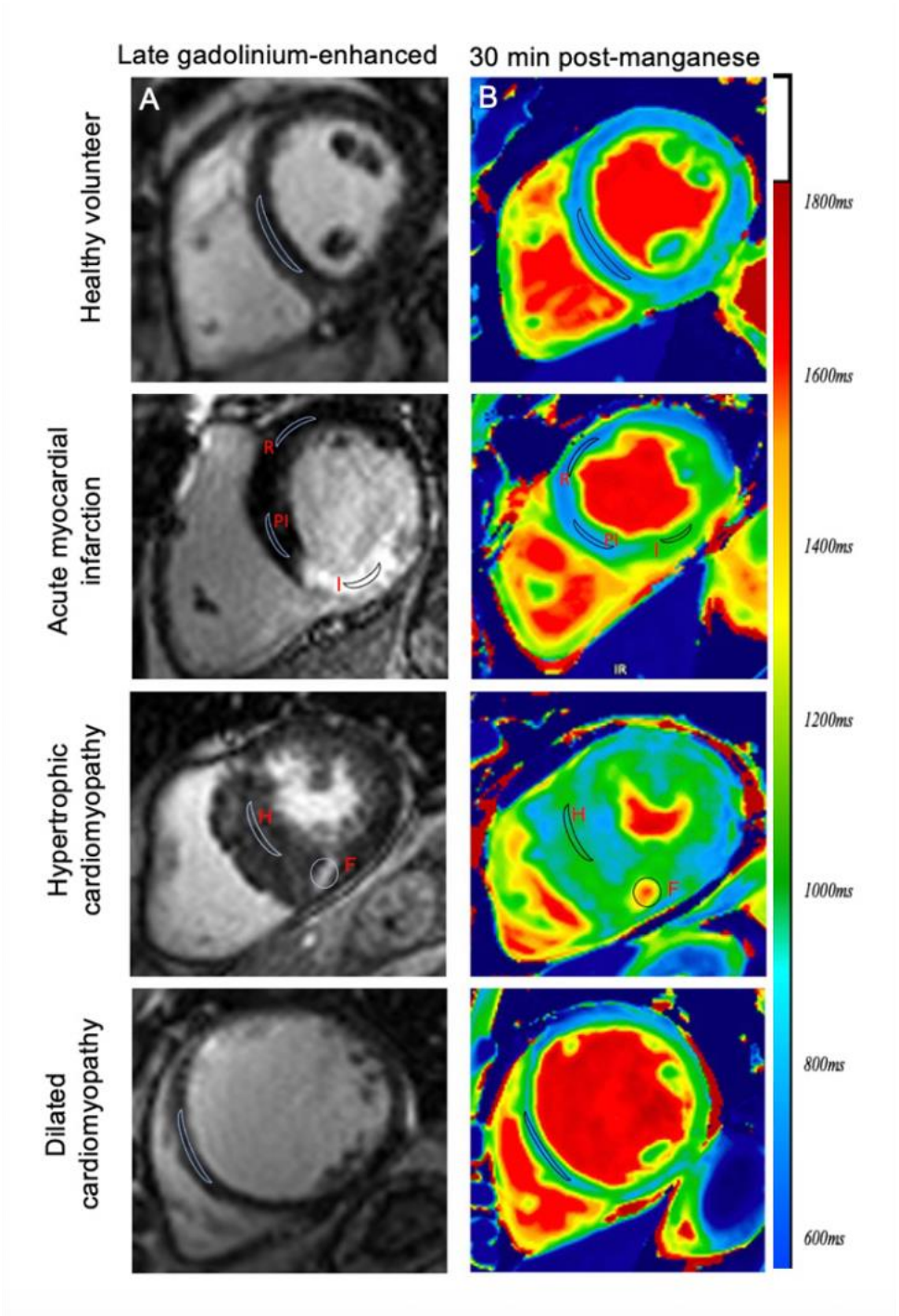

Figure 3.2. Regions of interest in manganese-enhanced magnetic resonance imaging. Late-gadolinium enhanced (A) and 30 min post-manganese T1 maps (B) in healthy volunteers, patients with acute myocardial infarction, hypertrophic and dilated cardiomyopathy. Demonstrating regions of interest in healthy volunteers (septum) and patients with acute myocardial infarction (infarct, I, peri-infarct, PI, and remote, R),

hypertrophic cardiomyopathy (hypertrophied, non-fibrotic, H and fibrotic, F) and dilated cardiomyopathy (septum).

3.3.4 Image analysis

All analyses of T1 maps, late gadolinium enhancement and cine-derived volumetric and functional sequences were performed using Circle CVI (Circle Cardiovascular Imaging, CVI42 v5.3.6, Calgary Canada) as described previously (84,135). Image analysis was performed by two MRI trained observers who were blinded to participant details.

All images were assessed for artefacts caused by susceptibility effects and cardiac or respiratory motion. The presence of artefacts led to the exclusion of all affected myocardial segments. Endocardial and epicardial borders were manually defined on all conventional short-axis images for volumetric and wall motion measurements and were then copied to corresponding T1 map images for analysis with minimal manual adjustments. The left ventricular basal short axis slice was identified as the image containing at least 50% of circumferential myocardium at end diastole. Papillary muscles were included in the mass and excluded from volumetric analysis.

Segmental variation in native and post-manganese T1 and myocardial manganese uptake (Ki) was only assessed in healthy volunteers. T1 values were derived from segments 7-12 (mid-ventricular slice) of a standard 16-segment model, as well as septal (region of interest in mid-septal wall) and global (average of all 6 segments from mid-ventricular slice) values. After contouring, an additional epicardial and endocardial offset of 20% was applied automatically to minimize partial volume effect for all T1 map analyses.

For patients with myocardial infarction, a reference region of interest was manually generated in the remote myocardium, with minimal manual adjustment based on the opposing wall from the late-gadolinium enhancement-defined infarct and wall motion by cine sequences where necessary. Given the lack of established consensus on quantification, a threshold of 2 x SD above remote myocardium was used for area at risk (141). Peri-infarct tissue was defined as late-gadolinium enhancement negative but with elevated T1 in the area at risk (>2 x SD) in the infarct related artery territory. For patients with hypertrophic cardiomyopathy, regions of interest were drawn in areas with hypertrophy and fibrosis (guided by late gadolinium enhancement). In patients with dilated cardiomyopathy, regions were drawn in the mid-septal wall, due to lack of late-gadolinium enhancement (**Figure 3.2**). For serial T1 imaging post manganese, manually drawn regions of interest from the pre-contrast image were transferred to all subsequent post-contrast images to ensure consistency.

3.3.5 Intra and Inter-observer Reproducibility

To test for intra-observer variability, scans were analysed in a random order, twice by the same operator, 6 months apart to reduce the risk of recall bias. To test for inter-observer variability, ten random datasets from each patient cohort and healthy volunteer data set were analysed by a second observer.

3.3.6 Scan-rescan Repeatability

Scan-rescan analysis was performed on a subset of healthy volunteers (n=10) who underwent repeat manganese-enhanced cardiac magnetic resonance imaging 3 months after baseline scanning.

Kinetic modelling

To derive quantitative estimates and to assess differential manganese uptake, kinetic model analysis was performed, as described previously (84,135,142). Kinetic modelling was based on a Patlak two-compartment model formulation (81,133). In brief, the model consists of (i) a reversible compartment (v_e), comparable to intravascular and interstitial space and (ii) an irreversible compartment (v_i) comparable to the intracellular space, in which irreversible accumulation of the contrast agent is anticipated during the imaging period (30 min). The arterial concentration (derived from blood pool T1) represents contrast agent delivery into myocardial tissue and constitutes the arterial input function.

Skjöld *et al* previously derived a Patlak model formulation for cardiac manganese-enhanced magnetic resonance imaging (133), demonstrating that an apparent unidirectional influx constant (Ki) for the transfer of manganese from plasma to irreversible compartments v_i, can be measured, using Equation 1:

$$\frac{C_t(t)}{C_a(t)} = Ki\frac{\int_0^t C_a(\tau)d\tau}{C_a(t)} + v_e \qquad (1)$$

where C_t and C_a are the manganese concentration in myocardial tissue and blood pool (arterial input function) respectively. This formulation is equivalent to the Patlak model (81) and describes that if a contrast medium is irreversibly trapped in the tissue within the imaging period, the instantaneous tissue concentration divided by the instantaneous arterial concentration plotted against the integrated arterial concentration divided by the instantaneous arterial concentration, will result in linearization of the data. The gradient of this line represents the apparent unidirectional influx constant Ki, which equals:

$$K_i = \frac{k_1 \cdot k_3}{k_2 + k_3} \qquad (2)$$

where $k1$, $k2$, and $k3$ are the individual rate constants of the compartmental model presented. A visual representation of the influx constant Ki is given in **Figure 3.3**.

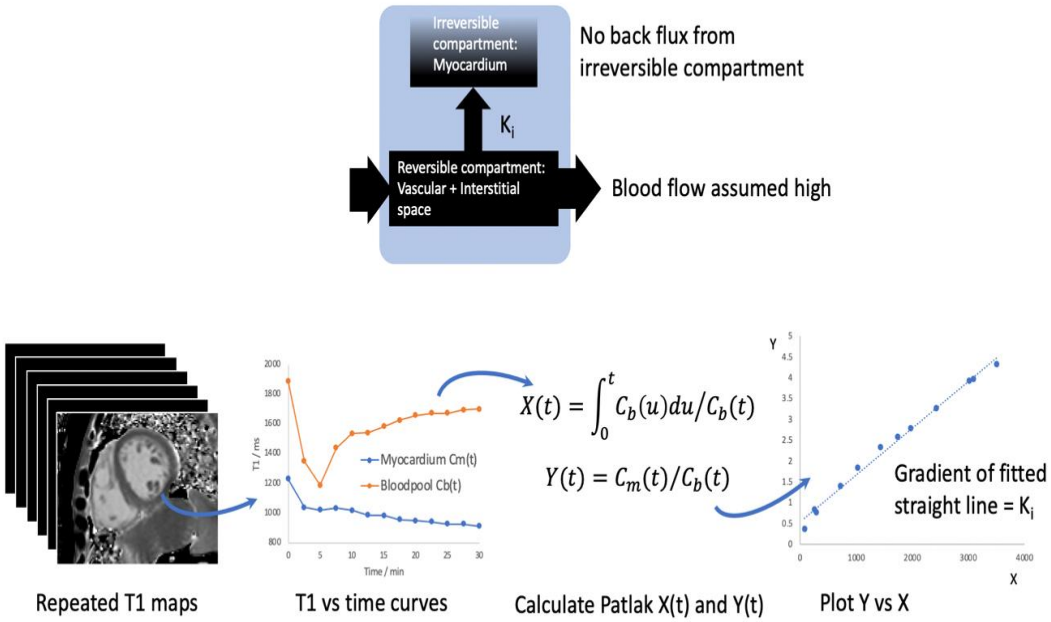

Figure 3.3. Patlak formulation: Patlak formulation – schematic of (A) model compartments and transfer constant K_i , describing passage from reversible to irreversible compartment (B) data analysis

3.3.7 Statistical analysis

Data are expressed as mean ± standard deviation or mean (95% confidence interval) for continuous variables or median [interquartile range] where not normally distributed. Categorical variables are presented as number (percentage). Data were analysed using paired or unpaired Student's *t*-tests, mixed effects model, linear regression analysis and Lin's concordance correlation coefficients. Group variance was examined with the Brown-Forsythe test. Coefficient of variation (%) was defined as the average of means divided by the standard deviation of mean difference. Repeatability and reproducibility were determined using Bland-Altman analysis and bias (mean difference) is presented alongside 95% limits of agreement. Statistical analysis was performed using R Studio (RStudio, Boston, USA) and GraphPad Prism (Version 8.0, GraphPad Software, San Diego, California, USA). Statistical significance was taken as a two-sided P-value <0.05.

3.4 Results:

3.4.1 Manganese Infusion

Seventy-eight infusions of manganese dipyridoxyl diphosphate were completed during the course of the study (mean duration, 10 min). There were no changes in the electrocardiogram, heart rate or blood pressure following manganese dipyridoxyl diphosphate administration (P>0.1 for all). Two healthy volunteers and one patient with dilated cardiomyopathy experienced mild transient nausea for <10 s after commencing manganese dipyridoxyl diphosphate infusion, spontaneously resolving without intervention. Otherwise, administration of manganese dipyridoxyl diphosphate was well tolerated with no adverse reactions reported during or immediately after administration or after seven days of follow up.

3.4.2 Healthy Volunteers

Intra-observer repeatability

In twenty healthy volunteers, a total of 120 segments were analysed. Six segments, predominantly the infero-lateral wall (segment 11), were excluded due to artefact. The mean septal native T1 was 1218±24 ms (**Figure 3.4**). There was regional difference in myocardial native T1, with septal T1 appearing to be higher than global T1 (1218±24 versus 1215±22 ms, P=0.02, **Figure 3.4**). Furthermore, myocardial manganese demonstrated similar segmental variation across the myocardium **(**P= 0.04, **Figure 3.4).**

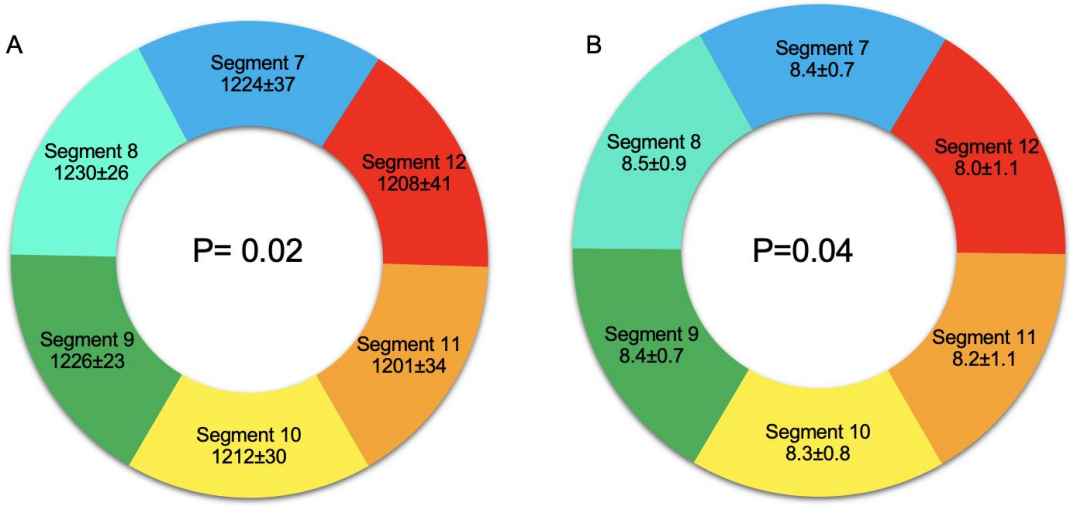

C

Healthy Volunteer	Septal	7	8	9	10	11	12	Global	P value
Mean Native T1 (ms)	1218 ±27	1214 ±41	1230 ±26	1226 ±23	1212 ±30	1201 ±34	1208 ±41	1215 ±25	0.02
Mean Ki (ml/100g/min)	8.4±0.7	8.4±0.9	8.5±0.9	8.4±0.7	8.3±0.8	8.2±1.1	8.0±1.1	8.3±1.1	0.04

Figure 3.4. Intra-observer Repeatability in Healthy Volunteers. (A) Mean native T1 values (m/s) and (B) mean myocardial manganese uptake (Ki-ml/100g/min) per segment in healthy volunteers (n=20). (C) Septal and global values.

There were no differences between mean myocardial septal native and post-manganese T1 on repeat analysis by the same observer (p= 0.75 and 0.63 respectively), with excellent correlation (Lin's concordance correlation: 0.97 and 0.95 respectively, **Table 3.1**). Bland-Altman plots demonstrate excellent intra-observer agreement; however, limits of agreement (LoA) were wider for post-manganese T1 compared with native T1 (880±24 ms, bias: +3.0ms, LoA: - 19.1 to 14.8 versus 1218±24ms, bias +2.2ms, LoA: -12.5 to 8.0, respectively, **Table 3.1**).

Mean myocardial manganese (septal) uptake in healthy volunteers was 8.4±0.7 mL/100 g of tissue/min and similarly had excellent correlation on repeated measurement (Lin's correlation coefficient: 0.99, **Table 3.1**). Coefficient of variation was higher for manganese uptake compared to native and post-manganese T1 (7.1, 1.3 and 3.3 % respectively).

Despite this, Bland-Altman plots highlighting limits of agreement (**Figure 3.5**) demonstrate excellent intra-observer agreement.

Inter-observer repeatability

There were no differences in myocardial native T1 (1218±24 versus 1221±27 ms, bias: +2.9 ms, p= 0.96) and estimates of mean myocardial manganese uptake (8.4±0.7 versus 8.2±0.7 mL/100 g of tissue/min, bias: -0.04, p=0.96) in healthy volunteers, with all showing excellent correlations (**Table 3.1**). Bland-Altman plots highlight excellent inter-observer agreements for native T1, post-manganese T1 and myocardial manganese uptake (**Figure 3.5**).

Scan-rescan Reproducibility

Ten healthy volunteers underwent repeat manganese-enhanced imaging 88 [range: 62-124] days following baseline imaging. There were no differences between repeated scans for mean native T1 (1230±23 versus 1226±15, P=0.60) and myocardial manganese uptake (8.4±0.7 versus 8.5±0.7, P=0.89, **Table 1**). There was excellent correlation between the paired scans for mean native T1 and myocardial manganese uptake (Lin's correlation coefficient: 0.94 and 0.97 respectively, **Table 3.1**). Similarly, Bland-Altman plots demonstrate narrow limits of agreement between the two paired scans (**Figure 3.5, Table 3.1**).

Intra-observer(n=20)	**First measurement**	**Second measurement**	**Mean Difference**	**P value**	**LCC (95% CI)**	**Bland-Altman 95% LoA (95% CI)**	**CoV (%)**
Native T1 (ms)	1218±24 [1189 - 1270]	1220±22 [1187 - 1273]	+2.2	0.75	0.97 (0.92-0.99)	-12.5 (16.8, -8.2) to 8.0 (3.7, 12.3)	1.3
30-min post Manganese T1 (ms)	880±24 [823 - 922]	883±17 [851 - 918]	+3.0	0.63	0.95 (0.78-0.97)	-9.1 (9-14, -3.9) to 14.8 (9.6, 19.9)	3.3

Manganese uptake (Ki, mL/100 g of tissue/min)	8.4±0.7 [7.2 – 10.2]	8.3±0.7 [8.0 – 8.7]	-0.01	0.91	0.99 (0.95-0.99)	- 0.6 (-0.8, -0.3) to 0.5 (0.31, 0.79)	7.1
Inter-observer (n=20)	**First observer**	**Second observer**					
Native T1 (ms)	1218±24 [1189 - 1270]	1221 ± 27 [1183 - 1279]	+ 2.9	0.96	0.98 (0.91-0.99)	- 10.9 9-14.6, -7.2) to 6.8 (2.6, 9.9)	1.8
30-min post Manganese T1 (ms)	880±24 [838 - 930]	885± 28 [809 - 933]	+4.9	0.80	0.91 (078-0.96)	- 19.7 (-23.4, -9.4) to 29.3 (34.5,15.3)	3.9
Manganese uptake (Ki, mL/100 g of tissue/min)	8.4±0.7 [7.2 – 10.2]	8.2±0.7 [7.1- 10.0]	-0.04	0.96	0.96 (0.91-0.99)	- 0.7 (-0.9, -0.3) to 0.6 (0.4, 0.90)	8.9
Scan-Rescan (n=10)	**Baseline scan**	**Repeat scan**					
Native T1 (ms)	1230±23 [1213- 1247]	1226±15 [1213 - 1239]	-4.0	0.60	0.94 (0.76- 0.98)	-12.6 (-25.1, -0.07) to 22.6 (10.1, 35.3)	1.4
30-min post Manganese T1 (ms)	899±28 [871 - 927]	894±27 [867 - 921]	-4.5	0.71	0.92 (0.64-0.95)	-26.8 (-43.2, -12.6) to 15.7 (0.15, 31.3)	2.6
Manganese uptake (Ki, mL/100 g of tissue/min)	8.4±0.7 [8.0 - 8.6]	8.5±0.7 [7.9 - 9.1]	+0.04	0.89	0.97 (0.91-0.99)	- 0.3 (-0.6, -0.1) to 0.3 (-1.7, 1.5)	8.6

TABLE 3.1. Intra-observer, inter-observer repeatability and scan-rescan reproducibility for healthy volunteers.
Mean± standard deviation [95% confidence interval], LCC, Lin's concordance correlation, LoA, limits of agreement, CoV, coefficient of variation.

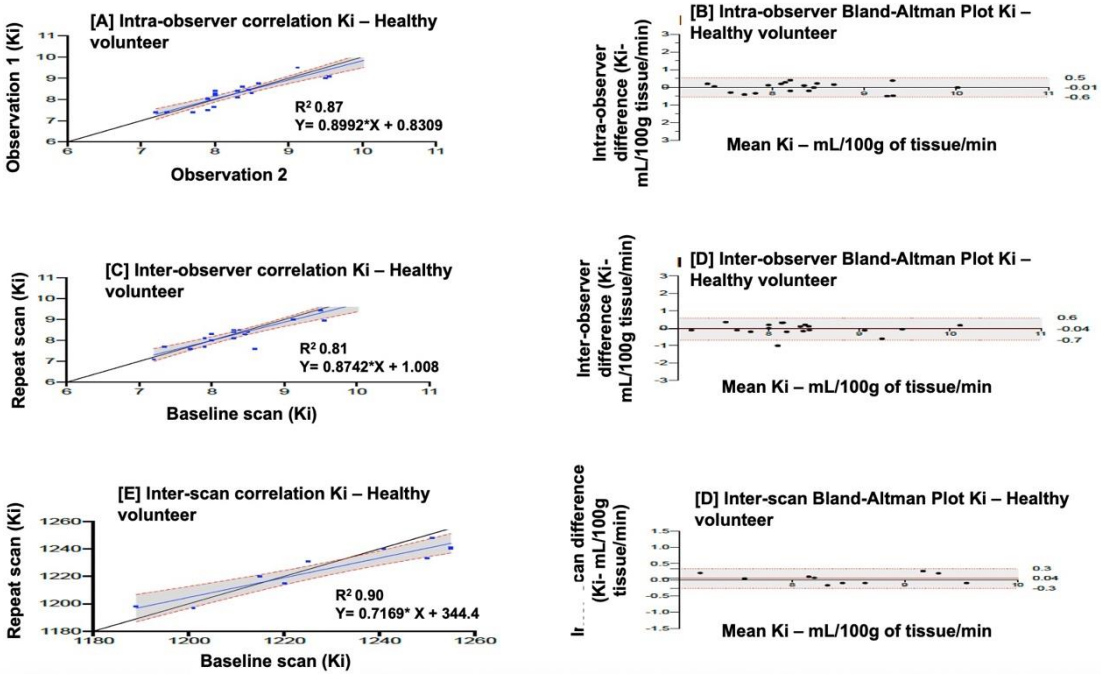

Figure 3.5. Intra, Inter- Observer Repeatability and Scan-Rescan Reproducibility for Myocardial Manganese uptake in Healthy Volunteers.

Linear regression analysis and Bland-Altman plots demonstrating intra-observer repeatability (A, B), inter-observer repeatability (C, D) and scan-rescan reproducibility (E, F) in healthy volunteers.

3.4.3 Patient cohorts

Intra-observer repeatability

The mean native T1 for patients with acute myocardial infarction (infarct), hypertrophic (non-fibrosis) or dilated cardiomyopathy were 1395±72, 1185±35 and 1208±60 ms respectively. On repeated analysis by the same observer, there were no differences between mean myocardial T1 values (p= 0.87, 0.96 and 0.92 respectively, **Table 3.2**). Mean myocardial manganese uptake in patients with acute myocardial infarction (infarct) hypertrophic (non-fibrosis) and dilated cardiomyopathy was 5.3±1.4, 7.6±1.6 and 7.2±1.5 mL/100 g of tissue/min respectively. Repeated analyses demonstrated excellent correlation across all

patient cohorts (Lin's correlation coefficient: 0.98, 0.97 and 0.95 respectively, **Table 3.2**). Bland-Altman plots demonstrate excellent agreement (**Figures 3.6, 3.7 and 3.8**), although patients with dilated cardiomyopathy demonstrated the widest limits of agreement for native, post-manganese T1 and myocardial manganese uptake (-15.6 to 11.4, -22.5 to 18.4 and -0.9 to 0.6 respectively, **Table 3.2**).

Myocardial infarction (n=20)	**First measurement**	**Second measurement**	**Mean Difference**	**P value**	**LCC (95% CI)**	**Bland-Altman (95% LoA)**	**CoV (%)**
Native T1 (ms) Infarct	1395 ± 72 [1246-1501]	1391 ± 74 [1241-1485]	-3.8	0.87	0.97 (0.91-0.99)	-20.0 (-27.4, -13.1) to 12.9 (5.8, 20.1)	4.1
30-min post Manganese T1 (ms) Infarct	1137±79 [996 - 1280]	1133±80 [1009 - 1284]	-4.2	0.87	0.97 (0.91-0.99)	- 18.4 (-24.8, -12.7) to 8.9 (2.86, 14.82)	6.9
Manganese uptake (Ki, mL/100 g of tissue/min) Infarct	5.3±1.4 [2.0 – 7.3]	5.4±1.4 [3.0 – 7.4]	+0.06	0.95	0.98 (0.94-0.99)	- 0.4 (-0.8, -0.3) to 0.6 (0.3, 0.7)	8.1
Hypertrophic cardiomyopathy (n=18)							
Native T1 (ms) Non fibrosis	1185 ± 35 [1104 -1237]	1188 ± 33 [1112 - 1240]	+ 2.9	0.96	0.98 (0.93-0.99)	- 15.1 (-20.7, -9.5) to 9.2 (3.6, 14.7)	2.9
30-min post Manganese T1 (ms) Non fibrosis	922± 44 [838 -994]	919± 40 [848 - 980]	-3.0	0.80	0.95 (0.81-0.98)	- 11.2 (-17.4, -4.8) to 15.1 (8.83, 21.4)	4.1
Manganese uptake (Ki, mL/100 g of tissue/min)	7.6±1.6 [4.0 – 9.9]	7.7±0.7 [7.4- 9.4]	+0.07	0.96	0.97 (0.93-0.99)	- 0.6 (-0.8, -0.1) to 0.4 (0.2, 0.7)	7.4
Dilated Cardiomyopathy (n=10)							
Native T1 (ms)	1208 ± 6 [1164 - 1252]	1206 ± 61 [1162 - 1250]	-2.7	0.92	0.99 (0.97-1.0)	-15.6 (-25.6, -6.1) to 11.4 (1.78, 20.9)	5.9
30-min post Manganese T1 (ms)	981±58 [923 - 1039]	985±61 [924 - 1046]	+5.1	0.85	0.97 (0.83-0.97)	-22.5 (-25.5, -13.2) 18.4 (1.1, 24.5)	6.3
Manganese uptake (Ki, mL/100 g of tissue/min) Non fibrosis	7.2 ± 1.5 [6.2 - 8.3]	7.4 ± 1.3 [6.4 - 8.3]	+0.2	0.81	0.95 (0.84-0.98)	- 0.9 (-1.5, -0.4) to 0.6 (0.04, 1.16)	12.5

TABLE 3.2. Intra-observer repeatability for patients with myocardial infarction (infarct), hypertrophic cardiomyopathy (non-fibrosis) or dilated cardiomyopathy. Mean± standard deviation [95% confidence interval], LCC, Lin's concordance correlation, LoA, limits of agreement, CoV, coefficient of variation.

There was no difference in mean native T1 and myocardial manganese uptake in patients with acute myocardial infarction (peri-infarct and remote) and hypertrophic cardiomyopathy (fibrosis) on repeat analysis. Similarly, there was excellent correlation and Bland-Altman plots demonstrate narrow limits of agreement (**Table 3.3**). Peri-infarct regions in patients with acute myocardial infarction and fibrotic regions in patient with hypertrophic cardiomyopathy demonstrated wider limits of agreement compared to infarct region and non-fibrotic regions in the same cohorts (**Table 3.2**).

Myocardial infarction (n=20)	**First measurement**	**Second measurement**	**Mean Difference**	**P value**	**LCC (95% CI)**	**Bland-Altman (95% LoA)**	**CoV (%)**
Native T1 (ms) Peri-infarct	1263±49 [1166-1361]	1265± 50 [1169-1358]	+2.1	0.89	0.98 (0.95 – 0.99)	-20.6 (-28.7, -12.5) to 17.0 (8.9, 25.1)	3.8
Native T1 (ms) Remote	1147 ± 36 [1071-1218]	1144 ± 38 [1078-1207]	-2.8	0.81	0.95 (0.88 – 0.98)	-20.4 (-30.1, -10.5) to 23.4 (15.7, 31.20	3.9
30 min Post Manganese T1 (ms) Peri-infarct	1009±20 [973-1058]	1010±21 [971-1041]	+1.6	0.86	0.90 (079 – 0.96)	-13.1 (-27.7, -10.5) to 22.1 (13.2, 31.0)	3.1
30 min Post Manganese T1 (ms) Remote	886 ± 37 [816 – 944]	889 ± 34 [812 – 947]	+2.2	0.83	0.94 (0.86-0.97)	-17.6 (27.8, 16.30 to 21.6 (11.1, 32.2)	4.4
Manganese uptake- (Ki, mL/100 g of tissue/min)- Peri infarct	6.7 ±1.2 [4.0-8.6]	6.5 ± 1.1 [4.1-8.6]	-0.09	0.79	0.92 (0.80-0.96)	-0.8 (-1.2, -0.40) to 1.0 (0.6, 1.4)	17.3
Manganese uptake- (Ki, mL/100 g of tissue/min)- Remote	8.6±1.2 [6.0-11]	8.7±1.3 [6.0-11.3]	+0.05	0.90	0.98 (0.96-0.99)	-0.5 (-0.6, -0.2) to 0.4 (0.2, 0.5)	15.3
Hypertrophic cardiomyopathy (n=18)							
Native T1 (ms) Fibrosis (n=11)	1332 ±91 [1219 – 1477]	1335 ± 86 [1224 – 1465]	+ 3.0	0.93	0.97 (0.92-0.98)	-11.8 (22.0, -1.6) to 19.2 (9.0, 29.3)	3.4
30 min Post Manganese T1 (ms) Fibrosis (n=11)	1083 ± 87 [1006-1261]	1086 ±90 [1010-1251]	+3.7	0.95	0.94 (0.79-0.98)	-17.7 (-36.7, -8.9) to 9.7 (0.7, 18.7)	4.3
Manganese uptake (Ki, mL/100 g of tissue/min) Fibrosis (n=11)	5.2 ±1.5 [3.2-7.3]	5.1 ± 1.2 [3.0 – 7.4]	-1.0	0.88	0.97 (0.92-0.98)	-0.3 (-0.5, -0. 2) to 0.1 (-0.5, 0.2)	14.1

Table 3.3. Intra-observer repeatability for patients with myocardial infarction and hypertrophic cardiomyopathy. Mean± standard deviation [95% confidence interval], LCC, Lin's concordance correlation, LoA, limits of agreement, CoV, coefficient of variation.

Inter-observer repeatability

Similar levels of interobserver repeatability were also seen for patients with acute myocardial infarction, hypertrophic or dilated cardiomyopathy (**Table 3.4**, **Figures 3.6, 3.7 and 3.8**). Across all cohorts, coefficient of variation was higher for myocardial manganese uptake compared to native T1. Similarly, there was excellent correlation with narrow limits of agreement in peri-infarct and remote myocardium in patients with acute myocardial infarction and fibrotic myocardium in patients with hypertrophic cardiomyopathy (**Table 3.5**).

Myocardial infarction (n=20)	**First observer**	**Second observer**	**Mean Difference**	**P value**	**LCC (95% CI)**	**Bland-Altman (95% LoA)**	**CoV (%)**
Native T1 (ms) Infarct	1395 ± 72 [1246-1501]	1390 ±74 [1222-1484]	-4.4	0.83	0.98 (0.70- 0.97)	-21.4 (-32.2, -10.5) to 28.9 (18.1, 39.80	5.2
30-min post Manganese T1 (ms) Infarct	1137±79 [996 - 1280]	1141 ± 74 [1001-1271]	+3.3	0.88	0.99 (0.97-0.99)	-23.5 (-32.5, -14.7) to 17.6 (8.7, 26.5)	6.9
Manganese uptake (Ki, mL/100 g of tissue/min) Infarct	5.3±1.4 [2.0 – 7.3]	5.2±1.3 [2.9 – 7.3]	-0.08	0.79	0.98 (0.96-0.99)	- 0.7 (-1.03, -0.4) to 0.9 (0.5, 1.2)	9.9
Hypertrophic cardiomyopathy (n=18)							
Native T1 (ms) Non fibrosis	1185 ± 35 [1104 -1237]	1189±33 [110 - 1206]	+3.9	0.88	0.97 (0.84-0.98)	-26.8 (-37.6, -16.2) to 19.1 (8.5, 27.7)	3.1
30-min post Manganese T1 (ms) Non fibrosis	922± 44 [838 -994]	917 ± 45 [844 - 975]	-4.8	0.82	0.97 (0.94-0.99)	- 11.6 (-19.8, -3.4) to 22.7 914.5, 31.0)	4.3
Manganese uptake (Ki, mL/100 g of tissue/min) Non fibrosis	7.6±1.6 [4.0 – 9.9]	7.4±1.6 [3.09 – 9.8]	-0.2	0.89	0.98 (0.96-0.99)	- 0.3 (-0.6, -1.0) to 0.7 (0.5, 0.9)	8.2
Dilated cardiomyopathy (n=10)							
Native T1 (ms)	1208 ± 60 [1164 - 1252]	1206 ± 68 [1157 - 1256]	-2.2	0.94	0.98 (0.94-0.99)	-17.7 (-31.2, -4.1) to 20.3 (6.7, 33.20	5.8
30-min post Manganese T1 (ms)	981±58 [923 -1039]	977±57 [920 - 1034]	-4.6	0.88	0.98 (0.69-0.92)	- 20.6 (-32.3, -8.9) to 12.4 90.65, 24.1)	6.5
Manganese uptake (Ki, mL/100 g of tissue/min)	7.2 ± 1.5 [6.2 - 8.3]	7.1 ± 1.3 [6.2 - 8.0]	-0.1	0.90	0.95 (0.79-0.99)	-0.8 (-1.1, -0.2) to 0.9 (0.2, 1.1)	13.2

Table 3.4. Inter-observer repeatability for patients with myocardial infarction (infarct), hypertrophic cardiomyopathy (non-fibrosis) or dilated cardiomyopathy. Mean± standard deviation [95% confidence interval], LCC, Lin's concordance correlation, LoA, limits of agreement, CoV, coefficient of variation.

Myocardial infarction (n=20)	**First observer**	**Second observer**	**Mean Difference**	**P value**	**LCC (95% CI)**	**Bland-Altman (95% LoA)**	**CoV (%)**
Native T1 (ms) Peri-infarct	1263±49 [1166-1361]	1267±50 [1169-1373]	+4.1	0.87	0.97 (0.92 – 0.99)	-33.6 (-43.7, -5.1) to 28.2 (14.9, 41.3)	4.9
Native T1 (ms) Remote	1147 ± 36 [1071-1218]	1144 ± 34 [1071 – 1209]	-2.6	0.82	0.89 (0.68- 0.97)	-19.4 (-29.3, 9.80 to 25.04 (15.6, 35.1)	3.5
30 min Post Manganese T1 (ms) Peri-infarct	1010 ± 20 [973-1058]	1015 ± 25 [971-1058]	+4.6	0.65	0.88 (0.60 – 0.96)	-28 (-36.5, -14.3) to 19.3 (13.5, 32.6)	7.1
30 min Post Manganese T1 (ms) Remote	886 ± 37 [816 – 944]	882 ± 41 [809 – 941]	-4.9	0.72	0.86 (0.55 – 0.94)	-21.4 (-26.5, -9.5) to 31.6 (22.6, 54.3)	6.4
Manganese uptake- (Ki, mL/100 g of tissue/min)- Peri infarct	6.7 ±1.2 [4.0-8.6]	6.5 ± 1.1 [3.2-8.3]	- 0.09	0.82	0.94 (0.80 – 0.98)	-0.9 (-1.37, -0.5) to 1.1 (0.6, 1.6)	17.8
Manganese uptake- (Ki, mL/100 g of tissue/min)- Remote	8.6±1.2 [6.0-11]	8.5 ±1.2 [6.3-10.2]	-0.04	0.88	0.97 (0.90 – 0.99)	-0.5 (-0.7, -.3) to 0.6 (0.4, 0.8)	16.7
Hypertrophic cardiomyopathy (n=18)							
Native T1 (ms) Fibrosis (n=11)	1332 ±91 [1219 – 1477]	1337 ± 86 [1221 – 1476]	+ 5.3	0.89	0.94 (0.90-0.98)	-24.4 (-43.7, -5.1) to 43.2 (14.9, 53.3)	6.5
30 min Post Manganese T1 (ms) Fibrosis (n=11)	1083 ± 87 [1006-1261]	1079 ± 90 [1001-1249]	-4.9	0.95	0.94 (0.79-0.98)	-18.4 (-24.3, -9.4) to 23.2 (11.5, 31.3)	7.3
Manganese uptake (Ki, mL/100 g of tissue/min) Fibrosis (n=11)	5.2 ±1.5 [3.2-7.3]	5.3 ± 1.4 [3.2 – 7.5]	+0.2	0.80	0.97 (0.92-0.99)	-0.5 (-0.8, 0.3) to 0.2 (-0.02, 0.4)	16.1

Table 3.5. Inter-observer repeatability for patients with myocardial infarction and hypertrophic cardiomyopathy. Mean± standard deviation [95% confidence interval], LCC, Lin's concordance correlation, LoA, limits of agreement, CoV, coefficient of variation.

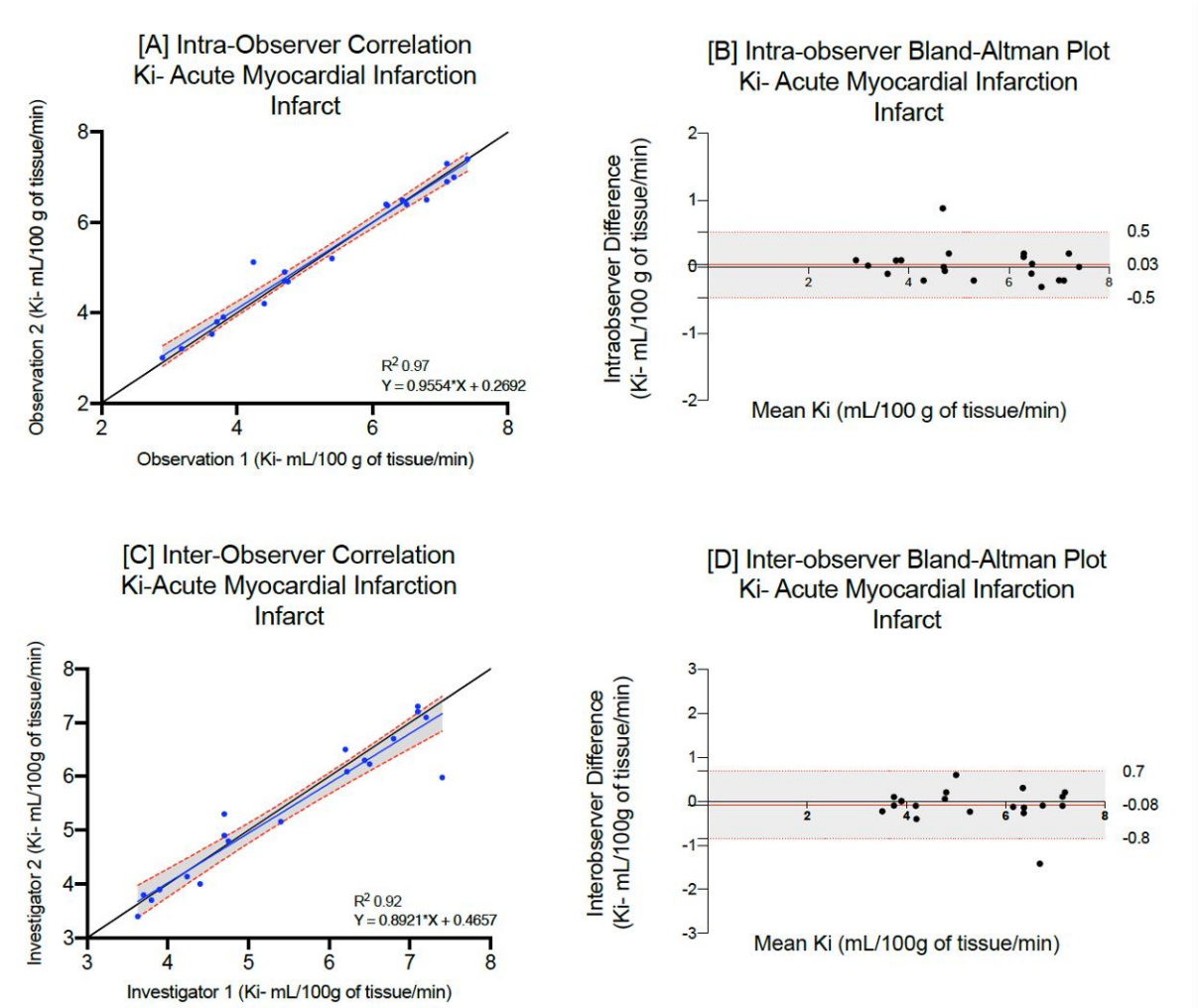

Figure 3.6. Intra-observer and Interobserver repeatability of Myocardial Manganese uptake in Acute Myocardial Infarction.

Intra-observer linear regression analysis (A) and Bland-Altman plots for myocardial manganese uptake (B) in patients with acute myocardial infarction. Inter-observer linear regression analysis (C) and Bland-Altman plots for myocardial manganese uptake (D) in patients with acute myocardial infarction.

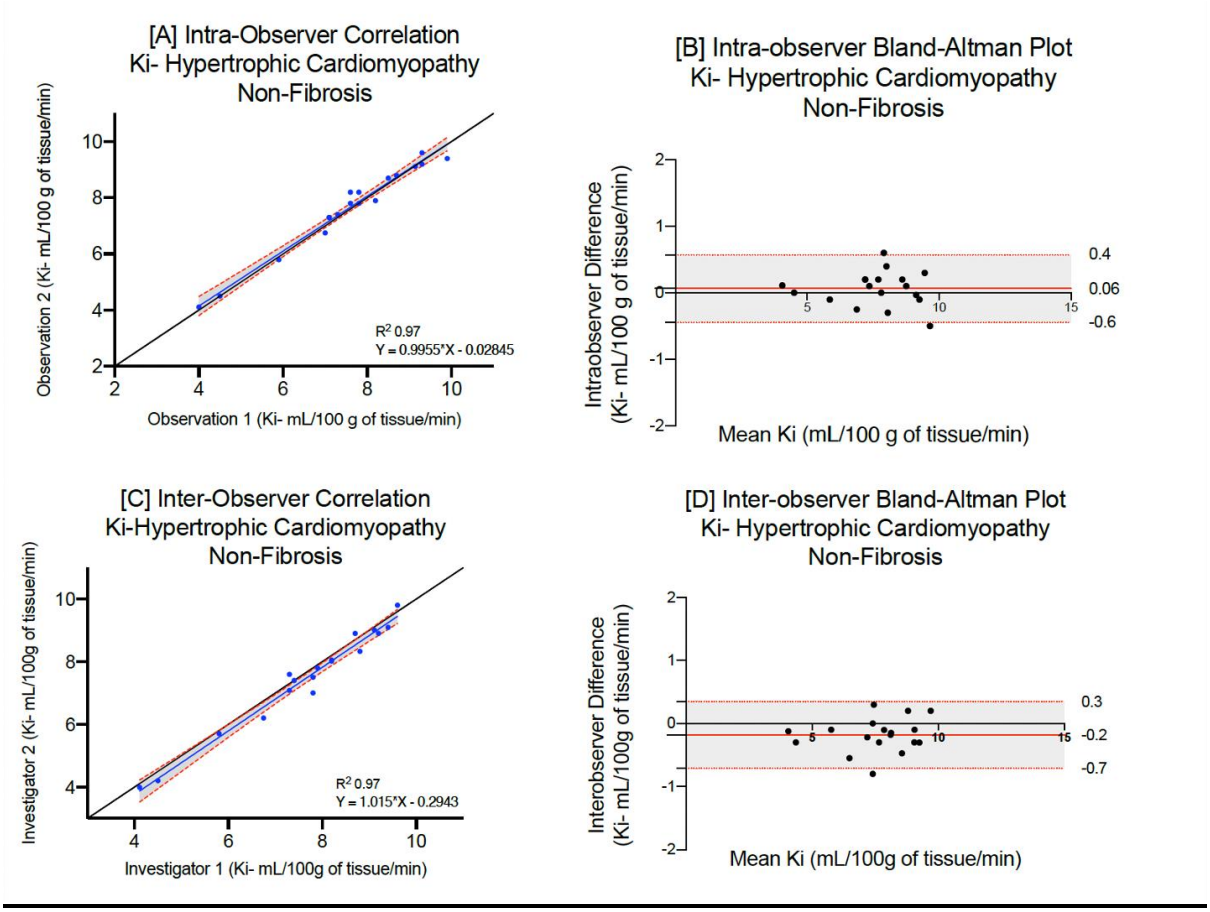

Figure 3.7. Intra-observer and Interobserver repeatability of Myocardial Manganese uptake in Hypertrophic Cardiomyopathy.

Intra-observer linear regression analysis (A) and Bland-Altman plots for myocardial manganese uptake (B) in patients with hypertrophic cardiomyopathy. Inter-observer linear regression analysis (C) and Bland-Altman plots for myocardial manganese uptake (D) in patients with hypertrophic cardiomyopathy.

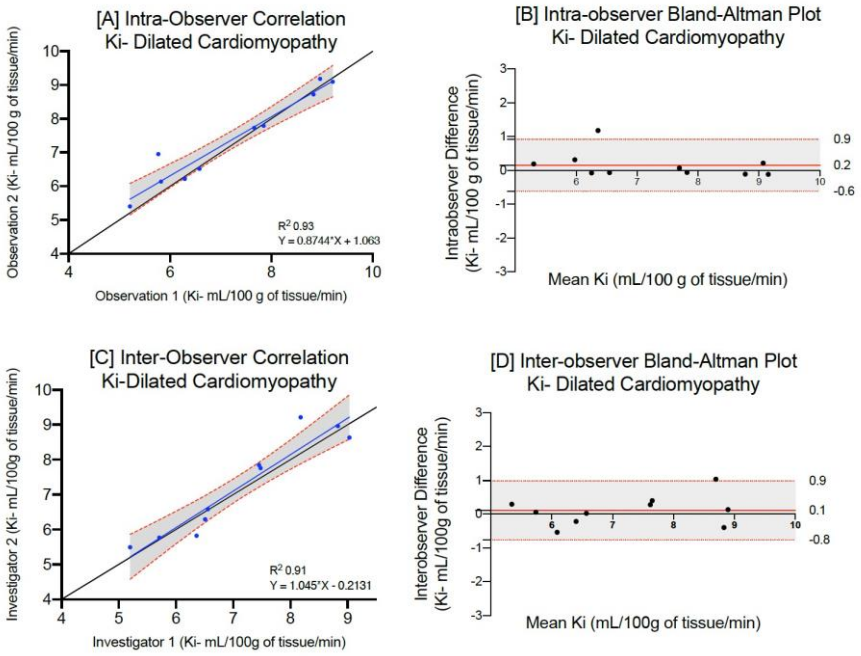

Figure 3.8. Intra-observer and Interobserver repeatability of Myocardial Manganese uptake in Dilated Cardiomyopathy.

Intra-observer linear regression analysis (A) and Bland-Altman plots for myocardial manganese uptake (B) in patients with dilated cardiomyopathy. Inter-observer linear regression analysis (C) and Bland-Altman plots for myocardial manganese uptake (D) in patients with dilated cardiomyopathy.

3.5 Discussion:

Cardiac manganese-enhanced magnetic resonance imaging holds major promise in the assessment of myocardial calcium handling. In this study of cardiac manganese-enhanced magnetic resonance imaging, we demonstrate for the first time that myocardial T1 mapping and kinetic modelling of manganese uptake is repeatable and reproducible in both healthy and diseased myocardium. We found excellent intra-observer and inter-observer repeatability as well as scan-rescan reproducibility for measures of manganese uptake in

the myocardium. This suggests that this technique is sufficiently robust for application in clinical care.

As expected, septal native T1 values for healthy volunteers and patient cohorts demonstrated less variability between intra and inter observer measurements compared to post-manganese T1 values. Previous studies have described greater variation in post-contrast T1 values with gadolinium and therefore similar effects with manganese are not unexpected (119,143–145). Contrast-enhanced T1 mapping is a function of contrast agent dispersion and volume of distribution which may differ across individuals. This can explain why post-manganese T1 values had greater variability compared to native T1, although these differences were small.

Coefficients of variation for myocardial manganese uptake in healthy volunteers and patient cohorts for both intra- and inter-observer repeatability and scan-rescan reproducibility were higher than for native and post-manganese T1. Kinetic modelling of myocardial manganese uptake is dependent on variables such as native T1, post-manganese T1 and blood pool signal. As such, variability in any of those factors will result in greater variability in myocardial manganese uptake. Furthermore, heterogeneities in cardiac perfusion, contrast agent kinetics and dispersion will also lead to greater bias and variability. Despite this, we observed very strong correlation with little variation in intra and inter-observer and inter-scan measurements of myocardial manganese uptake in healthy volunteers and patient cohorts.

Similar to previous cardiac magnetic resonance reproducibility studies (119,140,146,147), we demonstrate that intra-observer agreements for native T1 and myocardial manganese uptake were stronger than inter-observer and scan-rescan agreements for healthy volunteers and patient cohorts. However, the main differences seem to be the 95%

confidence intervals rather than the mean. Interestingly, intra-observer repeatability demonstrated broader limits of agreement in patients with dilated cardiomyopathy. This likely reflects the difficulty in defining a region of interest in the mid-septal wall in patients with dilated cardiomyopathy due to myocardial thinning. Furthermore, due to the diffuse nature of fibrosis seen in dilated cardiomyopathy, larger studies of manganese-enhanced magnetic resonance imaging would be beneficial. Despite this, there was very strong intra-observer and inter-observer correlation in T1 mapping and kinetic modelling in patients with dilated cardiomyopathy.

Compared to the other study populations and myocardial regions, peri-infarct regions in patients with acute myocardial infarction and fibrotic regions in patients with hypertrophic cardiomyopathy demonstrated broader limits of agreement and higher coefficients of variation for intra and interobserver repeatability. This likely reflects the subtle variations in discriminating peri-infarct and fibrotic regions as well as the manual delineation of endocardial and epicardial borders. Despite this, we continued to observe strong intra-observer and inter-observer correlations for such regions.

Manganese-enhanced magnetic resonance imaging has shown promise as a surrogate marker of myocardial calcium uptake in patients with ischemic and non-ischemic cardiomyopathies (84,135) demonstrating its potential for clinical application. As such, it is important to validate this technique before use in clinical practice. Current studies are underway assessing patients at risk of developing heart failure (NCT04591639). Similar to traditional imaging with gadolinium, there is variation in measurements between vendors and different T1 mapping techniques, and further work is required to ensure consistency across different platforms and scanners.

3.6 Study Limitations

Our study has some limitations. First, we were not able to perform scan-rescan measurements on patients with hypertrophic and dilated cardiomyopathy. It would be important to confirm that this technique has similar reproducibility in diseased states if it is to be used for serial scanning to assess disease progression or treatment interventions. Second, healthy volunteers were scanned using ShMOLLI T1 and patient cohorts underwent MOLLI T1 mapping. Our aim was to assess the reproducibility of manganese-enhanced magnetic resonance imaging in healthy and pathological myocardium. As such, we are not comparing patients with healthy volunteers. Furthermore, we have demonstrated that manganese-enhanced magnetic resonance imaging has strong intra- and inter-observer repeatability using either MOLLI or ShMOLLI T1 mapping. However, it is essential for future studies to assess this further. Third, performing a statistical test for defining cut-off for normal versus abnormal myocardial manganese uptake (Ki) was not in the scope of our study. This should be the focus of future work to define a normal reference range for these tracer kinetic parameters. Finally, manganese dipyridoxyl diphosphate is currently not readily or widely available for clinical use although we anticipate that this is likely to change in the near future.

3.7 Conclusion

In conclusion, although larger studies are required, our data suggest that manganese-enhanced T1 mapping and kinetic modelling is a repeatable and reproducible technique in healthy myocardium. Furthermore, this technique demonstrates high repeatability in ischaemic and non-ischaemic cardiomyopathy. However, it does require further study to assess repeatability and reproducibility in different cardiac pathologies with diffuse or

subtle fibrosis, such as patients with dilated cardiomyopathy, as well as defining normal reference ranges for these novel measures of myocardial calcium handling.

CHAPTER 4. Impaired myocardial calcium uptake in patients with diabetes mellitus: A manganese-enhanced cardiac magnetic resonance imaging study

Adapted from:

Abhishek Dattani[a]* and Shruti Joshi[b]* et al. Impaired myocardial calcium uptake in patients with diabetes mellitus: A manganese-enhanced cardiac magnetic resonance imaging study.

JACC CVI

SJ and AD contributed equally to this work

4.1 Abstract

Background

Dysregulated myocardial calcium uptake may be a key mechanism underlying the development of diabetic cardiomyopathy. Manganese-enhanced cardiac magnetic resonance imaging is a novel *in vivo* assessment of myocardial calcium uptake.

Objective: To assess myocardial calcium uptake in asymptomatic people with type 1 or 2 diabetes mellitus with normal left ventricular function.

Methods

Manganese-enhanced cardiac magnetic resonance imaging was performed in people with type 1 or type 2 diabetes and compared with control non-diabetic volunteers. Participants with concomitant cardiac disease were excluded. The rate of myocardial manganese uptake (Ki) was assessed by Patlak modelling.

Results

Compared to control volunteers (n=11), people with type 1 (n=19) and type 2 (n=30) diabetes were of similar age (median 57 [interquartile range 52-61] *versus* 52 [40-61] *versus* 61 [56-66] years, respectively) and body-mass index (25 [24-30] *versus* 26 [24-29] *versus* 29 [26-32] kg/m^2). There were no differences in left ventricular systolic and diastolic function (ejection fraction, global longitudinal strain and peak early diastolic strain rate) between groups. In comparison to control volunteers, myocardial manganese uptake was 23% and 22% lower in those with type 1 or type 2 diabetes (mean Ki 8.29±1.31, 6.43±0.77 and 6.47±0.99 mL/100 g/min respectively; P<0.001).

Conclusions

Despite apparently normal left ventricular function, there is marked impairment of myocardial calcium uptake in people with type 1 and type 2 diabetes. Altered myocardial calcium uptake occurs early before functional changes are apparent in people with

diabetes and longitudinal studies are required to assess the relationship with clinical events.

4.2 Introduction

Diabetic cardiomyopathy is a major complication of type 1 and type 2 diabetes, which can occur independently of hypertension, coronary artery disease or valvular heart disease(148). The pathophysiology is complex, involving local and systemic perturbations that precede symptom development and can eventually lead to cardiac dysfunction and heart failure (149). Identification of specific biological pathways driving progression of diabetic cardiomyopathy may unveil important targets for prevention and treatment(150). This is an urgent unmet need in cardiovascular and diabetes medicine that has been highlighted by major international cardiology and diabetes societies (151,152).

The pathophysiology of diabetic cardiomyopathy is complex and multifactorial. Amongst the many cardiac alterations observed in diabetes, dysregulated myocardial calcium handling may be a key contributor to development of diabetic cardiomyopathy and has been demonstrated in animal models (153–155). Traditional gadolinium-based contrast agents have been used in cardiac magnetic resonance imaging (MRI) for many years, but these agents remain extracellular. Manganese is a paramagnetic calcium analogue for voltage-gated L-type calcium channels on cardiac myocytes (130) and manganese-enhanced magnetic resonance imaging (MRI) of the heart provides a novel method of assessing myocardial calcium uptake *in vivo* (70). This method has been used to assess myocardial viability and calcium uptake in ischaemic and non-ischaemic cardiomyopathies (77,84,135) but no prior studies have used manganese-enhanced MRI to evaluate early perturbations in myocardial calcium handling amongst patients with diabetes mellitus and apparently normal left ventricular function.

We aimed to determine whether myocardial calcium uptake is altered in people with type 1 or type 2 diabetes and no signs, symptoms, or history of cardiac disease. We hypothesized that the rate of myocardial manganese uptake would be lower in subjects with diabetes compared with control volunteers.

4.3 Methods

4.3.1 Study design and participants

This was a prospective, two-center, case-control study performed at the National Institute for Health Research (NIHR) Leicester Biomedical Research Centre and the University of Edinburgh British Heart Foundation Centre of Research Excellence. Adults with either type 1 or type 2 diabetes were prospectively enrolled from primary care services in Leicestershire and Edinburgh, United Kingdom. Eligible participants were aged 18 to 75 years, with no prior history or symptoms of cardiovascular disease and no contraindications to MRI. Age-matched control volunteers without diabetes or known cardiac disease were recruited for comparison. The studies were approved by the United Kingdom National Research Ethics Service (references: 17/WM/0192, 20/NS/0037 and 20/WM/0304). All participants provided written informed consent prior to study entry.

4.3.2 Manganese-enhanced Magnetic Resonance Imaging

Manganese enhanced MRI was performed using 3-Tesla scanners (Skyra, Erlangen, Germany and MAGNETOM Skyrafit, Siemens Healthineers, Erlangen, Germany) with electrocardiographic gating and an 18-channel phased-array cardiac receiver coil. Participants receiving a calcium channel antagonist withheld this medication 48 h prior to scanning. All subjects had a normal electrocardiogram and underwent initial assessment of cardiac structure and function using standard cardiac MRI techniques as described previously (145). In brief, after localisers, steady-state free precession cine images were acquired in four-, three- and two-chamber views and a stack of short-axis slices was obtained covering the entire left ventricle. T1 mapping was performed pre-contrast in a mid-short-axis slice position using a modified Look-Locker inversion recovery sequence (MOLLI, Siemens MyoMaps, Erlangen, Germany). An intravenous infusion of manganese dipyridoxyl diphosphate (5 μmol/kg (0.1 mL/kg) at 1 mL/min; Exova SL Pharma,

Wilmington, DE, USA) was commenced and repeated T1 maps at the same location were performed every 2.5 min for 30 min.

4.3.3 Image analysis

Analysis was performed at an imaging core laboratory (Queen's Medical Research Institute, University of Edinburgh) offline by a single trained observer (SJ) blinded to all participant details. Cardiac chamber volumes, mass and function (including myocardial strain analysis) were assessed using Circle CVI (Circle Cardiovascular Imaging, CVI42 v5.13.5 Calgary, Canada) as described previously (156). Participants with regional wall motion abnormalities or reduced left ventricular ejection fraction were excluded. Myocardial calcium channel activity was assessed on manganese enhanced MRI T1 maps. For analysis of manganese uptake, regions of interest were drawn in the mid-ventricular infero-septal segment and the myocardial blood pool for all T1 maps from 0 to 30 min (**Figure 4.1**).

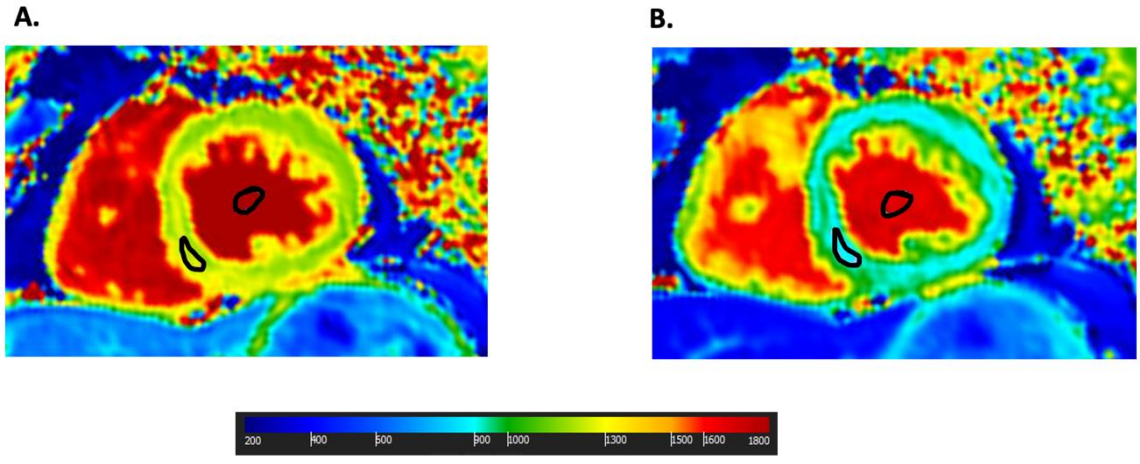

Figure 4.1. Image analysis. Example T1 maps at (A) Baseline and (B) 30 minutes in a study participant. Regions of interest were drawn at the mid infero-septal regions and left ventricular blood pool for all T1 maps from 0 to 30 min.

The primary outcome measure was myocardial manganese influx constant (Ki) calculated using Patlak modelling as described previously (77,82). In brief, a two-compartment model was used comprising a reversible compartment (arterial) and an irreversible compartment (myocardial tissue). Arterial and myocardial manganese concentrations can be derived from left ventricular blood pool and myocardial T1 values respectively. If the instantaneous myocardial tissue concentration divided by instantaneous arterial concentration is plotted against the integrated arterial concentration divided by the instantaneous arterial concentration, the data becomes linearized. The gradient of this line represents Ki.

4.3.4 Statistical analysis

Statistical analysis was performed using SPSS (Statistical Package for Social Sciences, v28.0, Chicago, IL, USA) and R studio (version 1.1.1093, Boston, USA). To detect a 15% difference in Ki between each diabetes group and controls, with a two-sided alpha level of 0.05, a minimum of 10 participants in each group would be required to achieve 80% power.

Normality was assessed using histograms and the Shapiro-Wilk test. Continuous data were expressed as mean ± standard deviation if normally distributed, or median [25-75% interquartile range] if not. Baseline characteristics were compared using analysis of variance, Kruskal-Wallis or Chi-squared test as appropriate. Imaging parameters and Ki values were compared across groups using analysis of covariance with age, sex, and body-mass index as covariates, followed by a Bonferroni *post hoc* correction. For

exploratory correlation analysis, normally distributed data were assessed using a Pearson's correlation, and non-normally distributed data were assessed using a Spearman's correlation. Statistical significance was taken as two-sided $P<0.05$.

4.4 Results

4.4.1 Study Population

Twenty-three people with type 1 diabetes, 32 with type 2 diabetes and 11 control volunteers were enrolled across the two study sites. Four participants with type 1 diabetes and two with type 2 diabetes were subsequently excluded (**Figure 4.2**). The final study population comprised of 19 patients with type 1 diabetes, 30 patients with type 2 diabetes and 11 control volunteers (**Table 4.1**). Median age was similar between groups, although people with type 2 diabetes were slightly older than those with type 1 diabetes. Sex distribution was similar across the groups and most participants were of white European ethnicity. Prevalence of hypertension and hyperlipidaemia was highest in the type 2 diabetes group, with corresponding greater use of antihypertensive and lipid-lowering therapies.

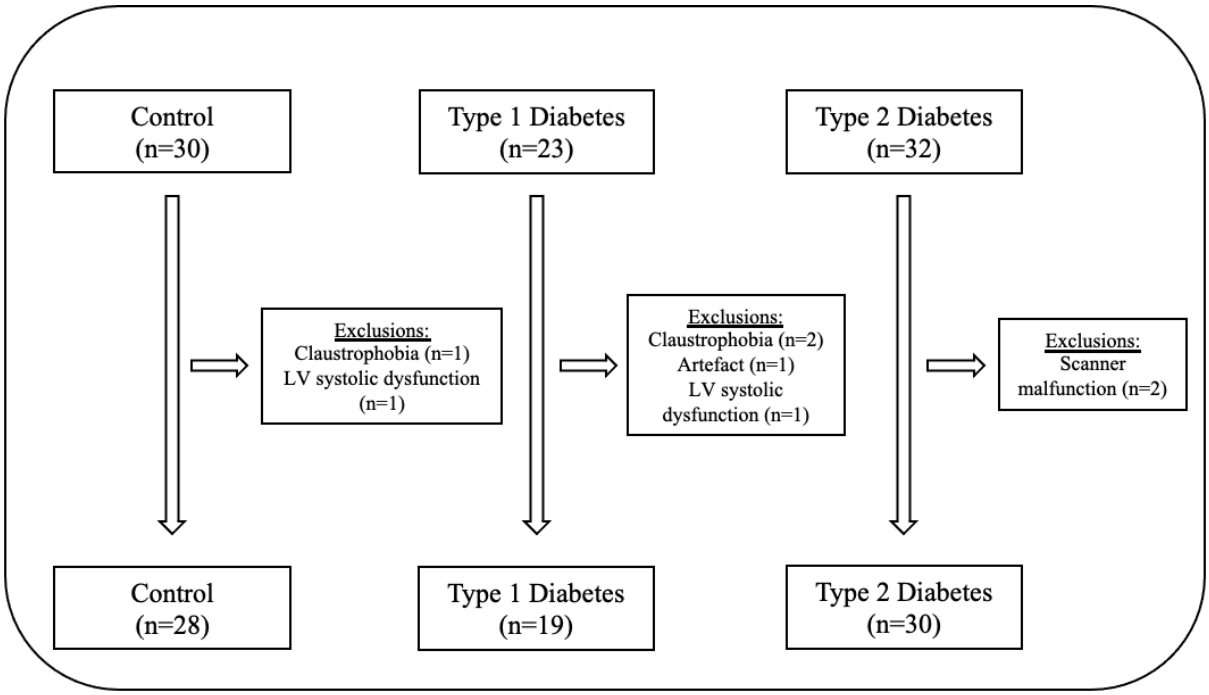

Figure 4.2: Study overview. Flow diagram of study participants showing reasons for exclusions in each group. LV = left ventricular

	Control Volunteers (n=11)	**Patients with Type 1 Diabetes Mellitus (n=19)**	**Patients with Type 2 Diabetes Mellitus (n=30)**
Age (years)	57 [52-61]	52 [40-61]	61 [56-66] †
Sex (male)	4 (36)	14 (74)	16 (53)
Ethnicity (White)	11 (100)	19 (100)	27 (90)
Height (m)	1.65 ± 0.10	1.74 ± 0.11	1.71 ± 0.10
Weight (kg)	72 ± 13	82 ± 16	85 ± 14*
Body-mass index (kg/m^2)	25 [24-30]	26 [24-29]	29 [26-32]
Systolic blood pressure (mmHg)	132 ± 15	136 ± 17	136 ± 16
Diastolic blood pressure (mmHg)	81 ± 10	80 ± 10	80 ± 10

Glycated hemoglobin (mmol/mol)	35 [30-37]	58 [48-69] *	61 [53-69] *
Glycated hemoglobin (%)	5.4 [4.9-5.5]	7.5 [6.5-8.5] *	7.7 [7.0-8.5] *
Duration of diabetes (years)	-	16 [7-29]	8 [5-16] †
Medical history			
Hypertension	2 (18)	4 (21)	18 (60) *
Hypercholesterolemia	1 (9)	9 (47) *	23 (77) *†
Medications			
ACEi/ARB	2 (18)	4 (21)	16 (53) *†
Beta blocker	1(9)	0	5 (17)
Calcium channel blocker	0	0	9 (30) *†
Thiazide-diuretic	1 (9)	0	6 (20) †
Statin	1 (9)	9 (47) *	23 (77) *†
Insulin	0	19 (100) *	7 (23) †
Sulphonylurea	0	0	5 (17)
Metformin	0	2 (11)	24 (80) *†
GLP-1 agonist	0	0	3 (10)
Gliptin	0	0	3 (10)
SGLT2i	0	0	6 (20) †

Table *4.1*: Participant characteristics. Data are presented as n (%), mean ± standard deviation or median [interquartile range]. ACEi = angiotensin converting enzyme inhibitor; ARB = angiotensin II receptor blocker; GLP-1 = glucagon-like peptide-1; SGLT2i = sodium-glucose cotransporter-2

*P<0.05 compared to control volunteers; †P<0.05 compared to patients with type 1 diabetes mellitus

4.4.2 Magnetic Resonance Imaging

Overall left ventricular volumes and mass were similar between groups (**Table 4.2**). However, mean left ventricular mass-to-volume ratio was greater in patients with type 2 diabetes than those with type 1 diabetes (*P*=0.01) and control volunteers (*P*=0.037). There were no demonstrable differences in left ventricular systolic (ejection fraction and global longitudinal strain) or diastolic function (peak early diastolic strain rate) between groups.

	Control Volunteers (n=11)	Patients with Type 1 Diabetes Mellitus (n=19)	Patients with Type 2 Diabetes Mellitus (n=30)
Left ventricular end-diastolic volume (mL)	130 ± 18	153 ± 35	131 ± 36
Left ventricular end-diastolic volume index (mL/m)	79 ± 10	88 ± 17	76 ± 18
Left ventricular end-systolic volume (mL)	44 ± 9	55 ± 14	46 ± 16
Left ventricular end-systolic volume index (mL/m)	27 ± 6	31 ± 7	28 ± 10
Left ventricular ejection fraction (%)	66 ± 5	64 ± 4	65 ± 6
Left ventricular mass (g)	96 ± 23	114 ± 26	115 ± 29
Left ventricular mass index (g/m)	58 ± 10	65 ± 11	67 ± 15
Left ventricular mass/volume (g/mL)	0.73 ± 0.10	0.75 ± 0.09	0.90 ± 0.16 *†
Left atrial maximal volume (mL)	62 ± 18	67 ± 25	64 ± 24
Left atrial maximal volume index (mL/m)	38 ± 11	38 ± 13	37 ± 13
Left ventricular global longitudinal strain (%)	18.82 ± 2.48	18.08 ± 1.95	17.65 ± 1.59

Left ventricular peak early diastolic strain rate (/s)	0.94 ± 0.27	0.92 ± 0.33	0.72 ± 0.25
Left ventricular native T1 (ms)	1233 ± 353	1235 ± 48	1237 ± 44

Table 4.2. Cardiac magnetic resonance characteristics in study participants. Data are presented as mean ± standard deviation. Global longitudinal strain values are presented as absolute values. Index values were produced using height. Between group comparisons were adjusted for age, sex and body-mass index.

*P<0.05 compared to control volunteers; †P<0.05 compared to patients with type 1 diabetes mellitus

Native (pre-contrast) T1 values were similar between study groups (**Table 4.2**). Compared to control volunteers (Ki 8.29 ± 1.31 mL/100 g of tissue/min), mean myocardial manganese uptake was lower in patients with both type 1 (Ki 6.43 ± 0.77 mL/100 g of tissue/min; P<0.001) and type 2 (Ki 6.47 ± 0.99 mL/100 g of tissue/min; P<0.001) diabetes (**Figure 4.3**). There was no difference between those with type 1 or type 2 diabetes. These findings were consistent across sexes (males: Ki 8.47± 2.16 *versus* 6.48 ± 0.79 *versus* 6.51 ± 0.68; females: 8.18 ± 0.71 *versus* 6.29 ± 0.76 *versus* 6.43 ± 1.28, respectively; all P<0.001).

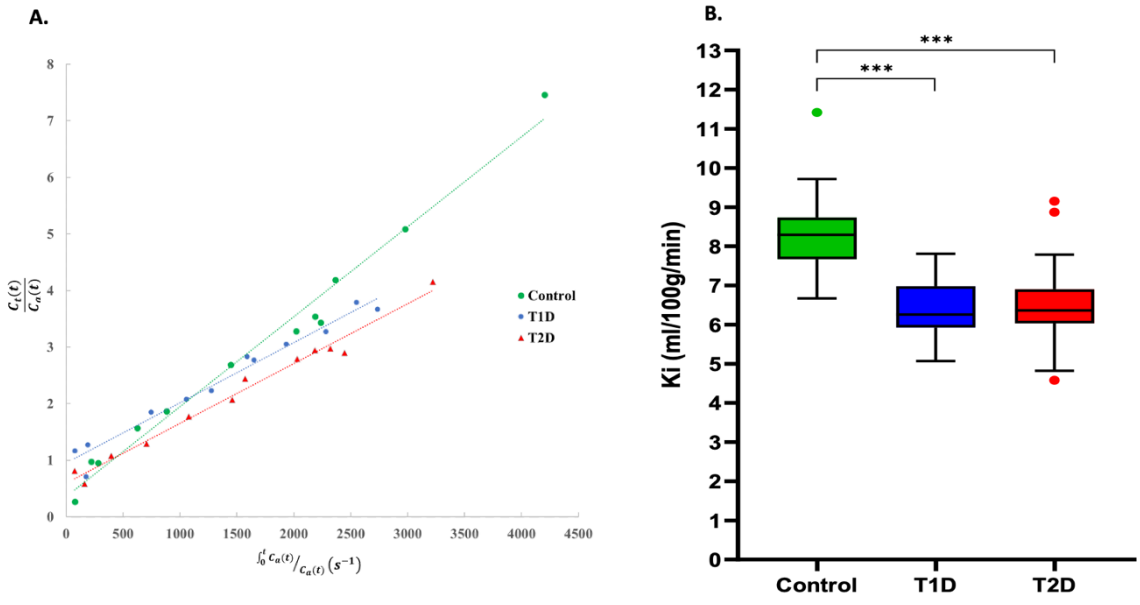

Figure 4.3. Myocardial manganese uptake in type 1 and type 2 diabetes. People with type 1 and type 2 diabetes had lower manganese uptake (Ki) compared to control volunteers. (A) Kinetic modelling depicting lower manganese uptake in participants with type 1 or type 2 diabetes compared to a healthy volunteer. (B) Box and whisker plots were generated using the Tukey method with outliers plotted individually. *** = *P*<0.001

Sensitivity analyses excluding control volunteers with hypertension or hyperlipidaemia (**Table 4.3**) showed similar and consistent findings.

	Controls (n=26)	**Patients with Type 1 Diabetes Mellitus (n=19)**	**Patients with Type 2 Diabetes Mellitus (n=28)**
Manganese influx constant (mL/100g/min)	8.29 ± 0.97	6.43 ± 0.77 *	6.47 ± 0.99 *

Table 4.3: Comparison of manganese influx constant after removal of controls with history of hypertension and hypercholesterolemia. Mean ± standard deviation. Between group comparisons are performed using ANCOVA with age, sex and body mass index as covariates. **P<0.001 compared to controls*

In exploratory analyses stratified by the presence of diabetes, there were no associations between Ki and glycated haemoglobin or diabetes duration, or with key imaging parameters such as left ventricular mass-to-volume ratio, or markers of systolic and diastolic function (**Table 4.4**).

	Controls	**Patients with Type 1 Diabetes Mellitus**	**Patients with Type 2 Diabetes Mellitus**

	Correlation coefficient	P value	Correlation coefficient	P value	Correlation coefficient	P value
Age*	-0.160	0.416	**0.594**	**0.007**	**0.434**	**0.016**
Body-mass index*	**-0.378**	**0.047**	0.112	0.647	0.322	0.082
Systolic blood pressure	-0.311	0.122	0.444	0.057	0.320	0.085
Diastolic blood pressure	-0.006	0.977	0.006	0.981	0.006	0.976
Glycated haemoglobin*	-0.649	0.115	-0.199	0.414	0.055	0.773
Left ventricular mass/volume	-0.112	0.571	0.270	0.264	0.141	0.457
Left ventricular ejection fraction	-0.118	0.549	0.053	0.828	0.257	0.170
Left ventricular global longitudinal strain	0.029	0.883	0.157	0.521	0.073	0.701
Left ventricular peak early diastolic strain rate	0.018	0.929	-0.040	0.872	-0.218	0.247

Table 4.4: Correlation of manganese influx constant with relevant baseline characteristics and key imaging parameters. *Spearman's correlation performed

4.5 Discussion

For the first time, we have demonstrated striking abnormalities of myocardial calcium uptake in asymptomatic people with type 1 or type 2 diabetes, who had no prevalent cardiovascular disease and in the absence of any apparent left ventricular systolic or diastolic dysfunction. Our *in vivo* characterisation of calcium uptake confirms results of prior animal studies suggesting altered calcium handling is a feature of the diabetic heart, which may underlie the increased propensity to develop heart failure in patients with diabetes mellitus. The manganese-enhanced MRI technique utilised provides an exciting new avenue to better understand the consequences of hyperglycaemia on the

myocardium with potential application for the early detection, prevention, and treatment of diabetic cardiomyopathy. Large scale epidemiologic studies have shown a two to five-fold excess risk of heart failure in diabetes mellitus, although this risk is slightly higher in type 1 compared with type 2 diabetes (157,158). This has led to a paradigm shift in the classification of heart failure; all individuals with diabetes are classified as being in Stage A "at risk" of heart failure and those with asymptomatic cardiac structural or functional alterations are described as having stage B heart failure (159). Cardiac abnormalities constituting stage B heart failure are only loosely described and comprise systolic or diastolic dysfunction, left ventricular hypertrophy, chamber enlargement, valvular disease or increased filling pressures (160). However, numerous other effects on cardiac structure and function are seen in diabetes, including a tendency towards smaller cardiac chamber volumes, impaired myocardial energy utilisation, coronary microvascular dysfunction, myocardial steatosis, focal and diffuse fibrosis, and now impaired calcium uptake (148). These are not included in the current classification of stage B heart failure (159), which could lead to underestimation of the prevalence of diabetic cardiomyopathy and missed opportunities for treatment. We have unmasked markedly abnormal calcium uptake in the diabetic heart in a group without any overt cardiac abnormalities and no heart failure symptoms, highlighting a putative role in development of diabetic cardiomyopathy and for myocardial manganese uptake as a biomarker for early identification of diabetic cardiomyopathy, preceding development of traditional markers of stage B heart failure. We found no associations between manganese uptake and cardiac structure or function in our cohort, possibly because no abnormalities in ejection fraction or strain were detectable when compared with control volunteers. We did not undertake myocardial perfusion imaging or assessment of myocardial energetics and steatosis, and prospective longitudinal studies of stress perfusion MRI and magnetic resonance spectroscopy are

required to study in more detail the evolution of cardiac dysfunction in diabetes and whether this is related to impaired calcium uptake.

The pathophysiology of type 1 and type 2 diabetes is distinct with type 1 diabetes a result of autoimmune destruction of pancreatic beta cells and type 2 diabetes a consequence of chronic and progressive insulin resistance with associated beta cell dysfunction (161). Nevertheless, both are complex metabolic disorders characterised by hyperglycaemia, and development of diabetic cardiomyopathy is common in both forms of diabetes mellitus. Our finding that myocardial calcium uptake is reduced to a similar extent in both type 1 and type 2 diabetes suggests a shared early mechanistic role in diabetic cardiomyopathy. This may be related to the deleterious impact of chronic hyperglycaemia on voltage gated L-type calcium channels, mediated by damage from advanced glycation end-products, which are central to cardiac myocyte contraction and relaxation and endothelial function (162–164). However, we did not find an association between Ki and glycaemic control or diabetes duration in our cohort and the precise mechanisms driving dysregulated calcium uptake warrant further investigation.

Early animal models identified intracellular myocyte uptake of manganese ions via voltage gated L-type calcium channels (165,166). Subsequent work using manganese chloride-based contrast media confirmed its ability to assess myocardial calcium uptake *in vivo* in humans (167,168). With administration of manganese dipyridoxyl diphosphate contrast, progressive shortening of T1 relaxation times are observed in myocardium with intact calcium handling, due to avid uptake by voltage gated L-type calcium channels (70). Therefore, lower manganese influx indicates impaired intracellular calcium uptake and myocardial calcium handling.

Accumulating evidence from recent studies using manganese-enhanced MRI have shown dysregulated calcium uptake in patients with established non-ischaemic cardiomyopathies (84). In a small study of 20 healthy controls with 10 patients with severe non-ischemic

dilated cardiomyopathy, lower myocardial manganese uptake was observed in those with dilated cardiomyopathy and this correlated with left ventricular ejection fraction. However, abnormalities in manganese uptake are also evident in patients with hypertrophic cardiomyopathy, preserved left ventricular ejection fraction and no myocardial fibrosis (84) as well as patients who have recovered from takotsubo cardiomyopathy and have a normal left ventricular ejection fraction (77). As such, reduced myocardial manganese uptake is evident across a spectrum of cardiomyopathies, is variably associated with conventional measures of left ventricular function and may be a consequence of different underlying pathophysiological alterations in calcium handling. Nevertheless, prevailing studies indicate it is a pathological phenomenon with consistent reductions in patients with cardiovascular disease and we have now demonstrated it occurs in patients with diabetes before the development of any apparent left ventricular dysfunction. Ideally, we would have liked to have followed up the current cohort of patients to see if they developed left ventricular systolic dysfunction, but this would clearly have required extended long-term follow up. Longitudinal studies with serial follow-up imaging are now required to evaluate the association between reduced manganese uptake and the downstream development of heart failure. Reversal of dysregulated myocardial calcium uptake may be a target for future prevention and treatment of diabetic cardiomyopathy. For example, in pre-clinical models, glucagon-like peptide 1 activates cyclic adenosine monophosphate-dependent protein kinase A leading to increased activity of the L-type calcium channel (169). This could indicate a future role of glucagon-like peptide 1 receptor agonists in diabetic cardiomyopathy, though the impact of these drugs on heart failure requires more evidence (170). Sodium glucose co-transporter 2 inhibitors have inhibitory effects on the sodium-hydrogen exchanger 1 which could lead to reduced intracellular sodium and thereby preventing intracellular calcium overload (171). The impact of these agents on calcium handling in patients with symptomatic heart failure with and without type 2 diabetes is

currently being undertaken (DAPA-MEMRI trial; NCT04591639). Novel interventions targeting myocardial calcium uptake in diabetes, particularly before the onset of overt symptomatic heart failure, represents an exciting avenue of investigation and could be assessed with manganese-enhanced MRI as a marker of treatment response.

4.6 Study Limitations

Our study had a case-control cross-sectional design with a modest sample size comprising of a predominantly Caucasian cohort, without longitudinal follow up. We did include two control volunteers who were receiving lipid and blood pressure lowering medications. This may have impacted on the magnitude of our findings, but our results were consistent in sensitivity analyses when these subjects were excluded (**Table 4.3**). We also acknowledge that there are some assumptions and limitations of Patlak modelling. For example, it is assumed that there is irreversible trapping of the manganese contrast within the intracellular compartment. Although we have demonstrated alterations in myocardial calcium handling in diabetes, we are unable to identify specific biological pathways underpinning these abnormalities. Laboratory studies using molecular approaches are needed to describe the pathobiology of impaired calcium handling in diabetes. Finally, manganese-based contrast agents are not currently available for clinical use as they were voluntarily withdrawn for market reasons. This limits its current potential for widespread use although this is expected to change with commercially available preparations likely being made available soon (74).

4.7 Conclusion

Asymptomatic patients with type 1 or type 2 diabetes with apparently normal cardiac function have marked impairment in myocardial calcium uptake. This suggests that the

diabetic heart has a particular problem with calcium uptake despite apparently normal systolic and diastolic function. This impairment of calcium uptake may in part contribute to and underlie the propensity to develop diabetic cardiomyopathy but this remains to be established in prospective longitudinal studies. Myocardial manganese-enhanced MRI represents a promising novel imaging biomarker to improve our understanding of the impact of hyperglycaemia on the myocardium and may have potential to guide targeted therapeutic interventions in patients with diabetic cardiomyopathy.

CHAPTER 5

Manganese-Enhanced Magnetic Resonance Imaging in Diabetic Cardiomyopathy

Adapted from:

Manganese-Enhanced Magnetic Resonance Imaging in Diabetic Cardiomyopathy . Joshi SS et al (In preparation for submission to JACC)

5.1 ABSTRACT

Aim

To investigate myocardial calcium handling using manganese-enhanced magnetic resonance imaging in patients with type 2 diabetes in the presence and absence of heart failure with reduced ejection fraction.

Methods

In a prospective case-control study, 14 healthy volunteers, 24 patients with type 2 diabetes with normal left ventricular function (early stages of diabetic cardiomyopathy), 20 patients with heart failure with reduced ejection fraction, and 20 patients with both heart failure with reduced ejection fraction and type 2 diabetes (late stages of diabetic cardiomyopathy) underwent cardiac manganese-enhanced magnetic resonance imaging.

Results

Mean myocardial manganese uptake was 8.3±1.3 mL/100 g of tissue/min in healthy volunteers, falling to 6.5±0.9 mL/100g of tissue/min in patients with type 2 diabetes and lowest in patients with heart failure (4.5±1.0 mL/100g of tissue/min). Patients in late stages of diabetic cardiomyopathy had lower myocardial manganese uptake compared to patients in early stages of diabetic cardiomyopathy (4.9±0.7 versus 6.5±0.9, $p<0.001$). Furthermore, patients with both type 2 diabetes and heart failure had suppressed myocardial manganese uptake compared to patients with heart failure without type 2 diabetes (4.9±0.8 versus 5.7±1.1 mL/100g of tissue/min, $p=0.01$). On multivariable analysis, type 2 diabetes and left ventricular ejection fraction were the independent predictors of myocardial manganese uptake in patients with heart failure, after adjusting for age, sex, ischaemic heart disease, hypertension, and hyperlipidaemia.

Conclusions

Patients with either heart failure or type 2 diabetes have impaired myocardial calcium handling, and these effects appear to be additive. Type 2 diabetes and impaired left ventricular systolic dysfunction an independent predictor for abnormal myocardial calcium handling, and this may play an important role in the pathogenesis of diabetic cardiomyopathy.

5.2 INTRODUCTION

The current worldwide prevalence of type 2 diabetes is 463 million, 9.3% of the world population, and this is expected to rise to 693 million by 2045 (172). It can cause a range of microvascular and macrovascular complications and is associated with multiorgan damage (173). People with diabetes have over twice the risk of developing heart failure, and patients with both heart failure and diabetes have a four-fold increased risk of dying than those without diabetes (174). Furthermore, even after adjusting for commonly associated risk factors, such as age, sex, coronary artery disease, hypertension and dyslipidaemia, diabetes still confers a two-fold added risk for the development of heart failure (175). Large studies involving multifactorial risk factor management in people with diabetes have failed to show a reduction in the incidence of heart failure in this cohort (175). As such, heart failure has emerged as a major cause of death in the setting of diabetes mellitus. This has led to the recognition of diabetic cardiomyopathy as a separate clinical entity which is defined as the presence of abnormal myocardial structure and function in the absence of atherosclerosis, hypertension and valvular heart disease (176). Early stages of diabetic cardiomyopathy (stages A and B) are usually characterised by a lack of clinical symptoms and secondary complications but later stages (stages C and D) coexist with symptoms and other complications, such as coronary artery disease and hypertension (148).

The pathophysiology of diabetic cardiomyopathy is incompletely understood and various mechanisms have been proposed including dysregulated myocardial energetics, mitochondrial function, and myocardial calcium handling (54). There is strong pre-clinical evidence suggesting reduced calcium transients and smaller endoplasmic reticulum calcium stores occur in subjects with diabetes (177). However, this hypothesis has not previously been investigated in human subjects. A better understanding of these

underlying abnormalities may aid early diagnosis and may provide an opportunity to test pharmacological interventions that may slow disease progression and improve patient outcomes.

Manganese-enhanced magnetic resonance imaging offers a novel non-invasive imaging method to quantify myocardial calcium handling. Like gadolinium, manganese is paramagnetic and causes shortening of T1 relaxation of water protons, providing contrast in tissues where it accumulates (71). Furthermore, it is a calcium analogue and is taken up by the tissues, such as the heart, pancreas, kidney, liver and brain, that have functional L-type voltage gated calcium channels and sodium-hydrogen exchangers (71). In this study, we hypothesised that abnormal myocardial calcium handling would be apparent in patients with either type 2 diabetes or heart failure with reduced ejection fraction, and this would be exacerbated in the presence of both conditions.

5.3 RESEARCH DESIGN AND METHODS

5.3.1 Study Design

We conducted a prospective observational study (NCT04591639) in accordance with the Declaration of Helsinki, a favourable ethical opinion from the research ethics committee (20/NS/0037) and the written informed consent of all participants.

5.3.2 Study Participants

People with a confirmed diagnosis of heart failure with left ventricular ejection fraction <50%, aged ≥18 years were identified and approached through the Edinburgh Heart Centre, NHS Lothian, Edinburgh, United Kingdom. We specifically recruited 20 people with both heart failure and type 2 diabetes and 20 people with heart failure without type 2 diabetes. People with type 2 diabetes with normal ejection fraction (early stages of diabetic cardiomyopathy, n=24) were recruited from Edinburgh Centre for Endocrinology and Diabetes, NHS Lothian, UK and Glenfield hospital, Leicester, UK. Healthy volunteers (n=14) were recruited via advertisement with inclusion criteria of age ≥ 18 years, and no known clinically significant medical condition. Exclusion criteria for all study participants included renal failure (estimated glomerular filtration rate <30 mL/min/1.73 m^2), an inability to consent, contraindications to magnetic resonance imaging, and pregnancy or breast-feeding.

All participants had an assessment of clinical haematology and biochemistry including full blood count, liver and renal function, and glycated haemoglobin.

5.3.3 Echocardiography

All patients with heart failure underwent transthoracic echocardiography to ensure that their ejection fraction was <50% prior to magnetic resonance imaging. Transthoracic echocardiography was performed using a dedicated echocardiogram machine (Affiniti 70, Philips, Amsterdam, Netherlands) at the Edinburgh Clinical Research Facility by a British Society of Echocardiography-accredited cardiac sonographer. Research transthoracic echocardiograms were undertaken by this sonographer according to the British Society of Echocardiography guidelines. Left ventricular ejection fraction was calculated using the Simpson's biplane method

5.3.4 Magnetic Resonance Imaging

Magnetic resonance imaging was performed using 3 T scanners (MAGNETOM Skyrafit, Siemens Healthineers, Erlangen, Germany and Siemens Skyra, Erlangen, Germany) with electrocardiographic gating and an 18-channel phased-array cardiac receiver coil. Manganese-enhanced magnetic resonance imaging was performed using intravenous manganese dipyridoxyl diphosphate (5 μmol/kg (0.1 mL/kg) at 1 mL/min; Exova SL Pharma, Wilmington, Delaware, USA) administered over 10 minutes. Localizers, half-Fourier single-shot turbo spin-echo (HASTE) and standard breath-hold cine sequences of the heart were followed by T1 mapping sequences of the heart. Cardiac T1 mapping was performed in a mid-short-axis slice position prior to contrast using a breath-held modified Look-Locker inversion recovery acquisition and every 2.5 min for 30 min after commencing the intravenous manganese dipyridoxyl diphosphate infusion. Septal and left ventricular blood pool T1 values were compared.

5.3.5 Image Analysis

Image analysis was performed at an imaging core lab (Queen's Medical Research Institute, University of Edinburgh) offline and blinded to all participant details. Cardiac chamber volumes, mass and function (including myocardial strain analysis) were assessed using Circle CVI (Circle Cardiovascular Imaging, CVI42 v5.13.5 Calgary, Canada). Endocardial and epicardial borders were defined on the short-axis cine images for volumetric and wall motion measurements. For serial T1-mapping before and after MnDPDP infusion, regions of interest were drawn within the mid-ventricular inferoseptal segment and the left ventricular blood pool for all the T1 maps from 0 to 30 minutes.

5.3.6 Manganese Kinetic Modelling

Patlak et al were the first to provide a graphical analysis of unidirectionality of transfer and of the influx constant, using brain uptake data (81). The multi-timepoint approach produces information about the exchange rate of the compartments that rapidly and reversibly exchange with plasma. Moreover, this can be used to assess the rate constant of any type of irreversible process within any organ system. The Patlak two-compartment model was used in this study to measure the rate of myocardial manganese uptake. This assumes the influx of manganese ions from a reversible (v_e, extracellular and vascular space) into a largely irreversible (v_i, intracellular and cardiomyocyte) compartment. This apparent unidirectional influx constant (Ki) for the transfer of manganese from plasma to irreversible compartments v_i, can be measured, using the equation below:

$$\frac{C_t(t)}{C_a(t)} = Ki\frac{\int_0^t C_a(\tau)d\tau}{C_a(t)} + v_e$$

where C_t and C_a are the manganese concentration in the myocardium and blood pool (arterial input function) respectively. This formula is equivalent to the Patlak model and describes that if a contrast medium is irreversibly trapped in the tissue within the imaging period, the instantaneous tissue concentration (myocardial T1) divided by the

instantaneous arterial concentration (blood pool T1) plotted against the integrated arterial concentration divided by the instantaneous arterial concentration, will result in linearisation of the data.

5.3.7 Statistical Analysis

All statistical analyses were performed with R Studio (RStudio, Boston, USA). Categorical baseline variables were presented as number (%) and compared using a Chi-squared test. Continuous data were assessed for normality using the Shapiro test and presented as mean ± standard deviation or median [interquartile range]. Myocardial manganese uptake measurements were compared using analysis of variance (ANOVA) and Tukey's HSD (honestly significant difference) post-hoc test. Values were compared using paired or unpaired Student's *t*-tests, Wilcoxon or Mann-Whitney tests and Kruskal-Wallis tests as appropriate. Correlation analyses between myocardial manganese uptake and other parameters were performed using Spearman's rank correlation coefficient. Statistical significance was taken as two-sided $p<0.05$. Backward stepwise linear regression was performed to investigate the predictors of myocardial calcium handling and included age, sex, type 2 diabetes, left ventricular ejection fraction, ischaemic heart disease, hypertension and hyperlipidaemia.

5.4 RESULTS

5.4.1 Study Population

We recruited 78 participants: 14 healthy volunteers, 24 people with type 2 diabetes with normal left ventricular function (early stages of diabetic cardiomyopathy), 20 people with heart failure without type 2 diabetes, and 20 people with heart failure and type 2 diabetes (**Figure 5.1**, **Table 5.1**).

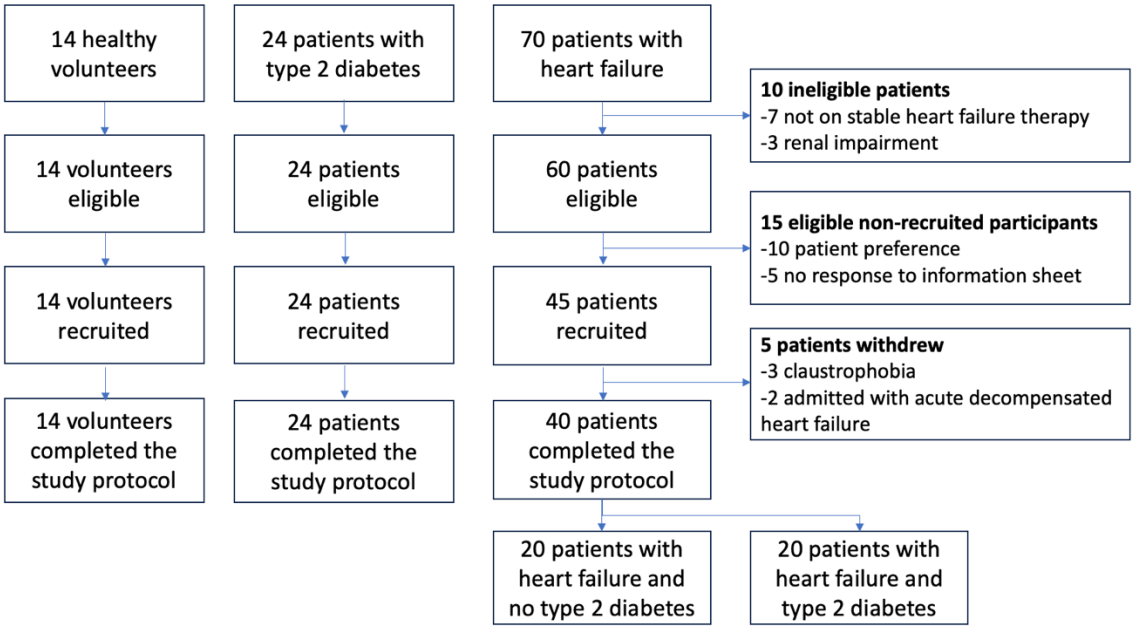

Figure 5.1. Consort Diagram

	Healthy volunteers	Patients with type 2 diabetes and no known cardiovascular disease	Patients with heart failure without type 2 diabetes	Patients with heart failure and type 2 diabetes	P value (ANOVA)
Number	14	24	20	20	
Age (years)	58±6*	64±6	65±10	68±7	0.004
Sex (Men:Women)	10:4	14:10	16:4	13:7	0.16
Body-mass index (kg/m^2)	25.6±3.3**	29.8±4.4	30.9±6.3	28.3±4.2	0.03
Glycated Haemoglobin (mmol/mol)	34.4±3.7***	63.5±20.5	40.6±2.9***	59.6±15.0	<0.001
Ischaemic heart disease	-	-	7 (35%)	11 (55%)	0.2
Hypertension	2 (14%)‡	17 (71%)	10 (50%)	12 (60%)	0.004
Hypercholesterolaemia	1 (7%)‡‡	19 (79%)	10 (50%)	16 (80%)	<0.001
Medications					
Beta Blockers	-	-	16 (80%)	17 (87%)	0.68
Angiotensin-converting enzyme inhibitors or Angiotensin II receptor blockers	-	-	7 (35%)	8 (40%)	0.95
Sacubitril/Valsartan	-	-	13 (65%)	12 (60%)	0.95
Mineralocorticoid Receptor Antagonists	-	-	16 (80%)	16 (80%)	0.09
Sodium-glucose Cotransporter-2 inhibitors	-	-	10 (50%)	9 (47%)	0.09
Cardiac Magnetic Resonance					
Indexed End Diastolic Volume(mL/m^2)	71.4±8.6†	65.3±14.5†	91.0±33.7	100.4±33.6	<0.001
Indexed End Systolic Volume(mL/m^2)	24.9±4.4††	23.8±7.7††	62.8±32.1	67.6±33.9	<0.001

Indexed Left Ventricular Mass (g/m^2)	52±8.9[$]	58.4±9.6[$]	75.5±21.02	76.9±17.9	<0.001
Indexed Left Atrial Volume (mL/m^2)	32.4±10.5	32.4±10.2	36.4±20.3	39.5 ±18.7	0.4
Ejection Fraction (%)	64.9±4.3[^]	65.6±5.8[^]	33.7±11.5	35.4±12.2	<0.001
Native T1 values (ms)	1232.1±33.2[§]	1236.0±43.6[§]	1257.4±53.1	1315.1±51.4	<0.001

Table 5.1. Clinical and Imaging Characteristics of the Study Populations

n (%); mean ± standard deviation.
Chi-square test used to analyse categorical data and analysis of variance (ANOVA) test used to analyse numerical data.

*Healthy volunteers were younger than patients with heart failure (p=0.002)

**Healthy volunteers had lower body-mass index compared to the other study participants (p=0.03)

**Patients with type 2 diabetes had higher glycated haemoglobin values compared to participants without type 2 diabetes (p<0.001)

‡Healthy volunteers had a lower incidence of hypertension compared to the other study cohorts (p=0.004)

‡‡Healthy volunteers had a lower incidence of hyperlipidaemia compared to the other study cohorts (p<0.001)

†Patients with heart failure had higher end diastolic volume compared to participants with preserved ejection fraction (p=0.01 for healthy volunteers and p=0.001 for patients with type 2 diabetes with preserved ejection fraction)

††Patients with heart failure had higher end systolic volume compared to participants with preserved ejection fraction (p<0.001 for both healthy volunteers and patients with type 2 diabetes with preserved ejection fraction)

$Patients with heart failure had higher left ventricular mass compared to participants with preserved ejection fraction (p<0.001 for both healthy volunteers and patients with type 2 diabetes with preserved ejection fraction)

^Patients with heart failure had lower ejection fraction compared to participants with preserved ejection fraction (p<0.001 for both healthy volunteers and patients with type 2 diabetes with preserved ejection fraction)

§Patients with heart failure had higher native T1 values compared to participants with preserved ejection fraction (p=0.002 for healthy volunteers and p=0.0006 for patients with

type 2 diabetes). Patients with both heart failure and type 2 diabetes had higher native T1 values compared to patients with heart failure without type 2 diabetes (p=0.001)

5.4.2 Influence of heart failure on myocardial calcium handling

Healthy volunteers were younger than patients with heart failure but patients with type 2 diabetes were well matched for age and sex with patients with heart failure (**Table 5.1**). As anticipated, patients with heart failure had higher indexed left ventricular end diastolic and systolic volumes, indexed left ventricular mass and native T1 values and lower left ventricular ejection fraction compared to healthy volunteers and patients with type 2 diabetes who had normal left ventricular function (**Table 5.1**).

Myocardial manganese uptake was lower in patients with heart failure (n=40) compared to participants with normal left ventricular ejection fraction and no heart failure (n=38; 5.3±1.0 versus 7.3±1.4 mL/100g of tissue/min, p<0.001; **Figure 5.2**).

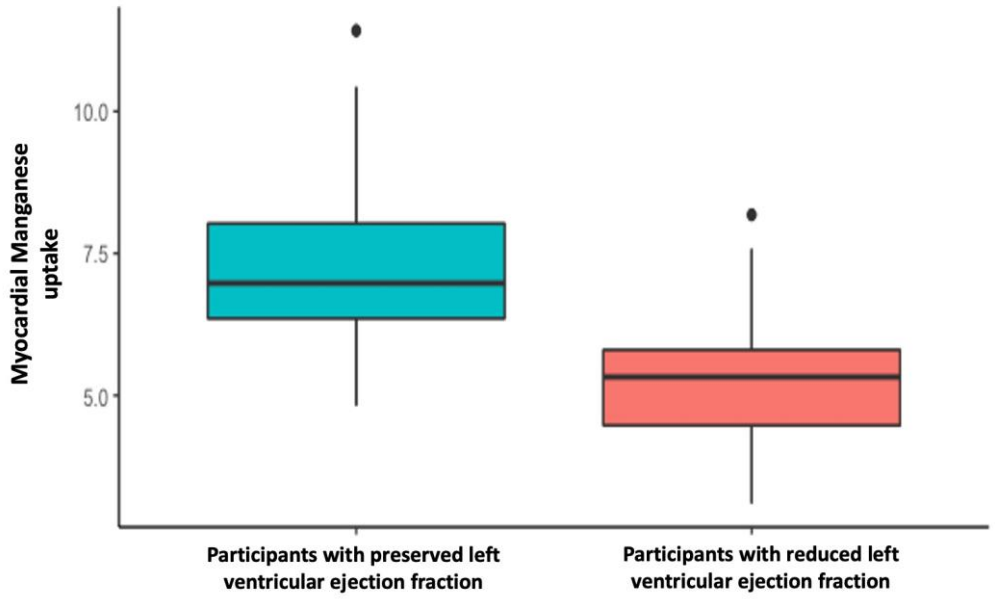

Figure 5.2. Influence of heart failure on myocardial calcium handling. Myocardial manganese uptake was lower in patients with heart failure with reduced ejection fraction (n=40) (5.3±1.0 mL/100g of tissue/min) versus participants with normal ejection fraction (healthy volunteers and patients with type 2 diabetes with normal ejection fraction, n=38) (7.3±1.4 mL/100g of tissue/min), p<0.001

5.4.3 Influence of type 2 diabetes on myocardial calcium handling

Twenty-four patients in early stages (stages A/B) of diabetic cardiomyopathy with early asymptomatic alterations in the myocardial structure but no clinical or imaging features of heart failure were compared to twenty patients in late stages (stages C/D) of diabetic cardiomyopathy with structural heart disease and symptomatic heart failure. Patients in early and late stages of diabetic cardiomyopathy were well matched for age, sex and other co-morbidities (**Table 5.1**). In contrast to those with late-stage diabetic cardiomyopathy, patients in early stages of diabetic cardiomyopathy had normal left ventricular ejection fraction, volume, and mass (**Table 5.1**).

Myocardial manganese uptake was lower in patients with later stages of diabetic cardiomyopathy (n=20) compared to those with early stages of diabetic cardiomyopathy (n=24; 4.9±0.7 versus 6.5±0.9 mL/100 g of tissue/min, p<0.001, Figure 3). Similarly, myocardial manganese uptake was lower in all subjects with diabetes with or without heart failure (n=44) compared to healthy volunteers or patients with heart failure in the absence of diabetes (n=34; 5.8±1.2 versus 6.8±1.8, p=0.007, **Figure 5.3**).

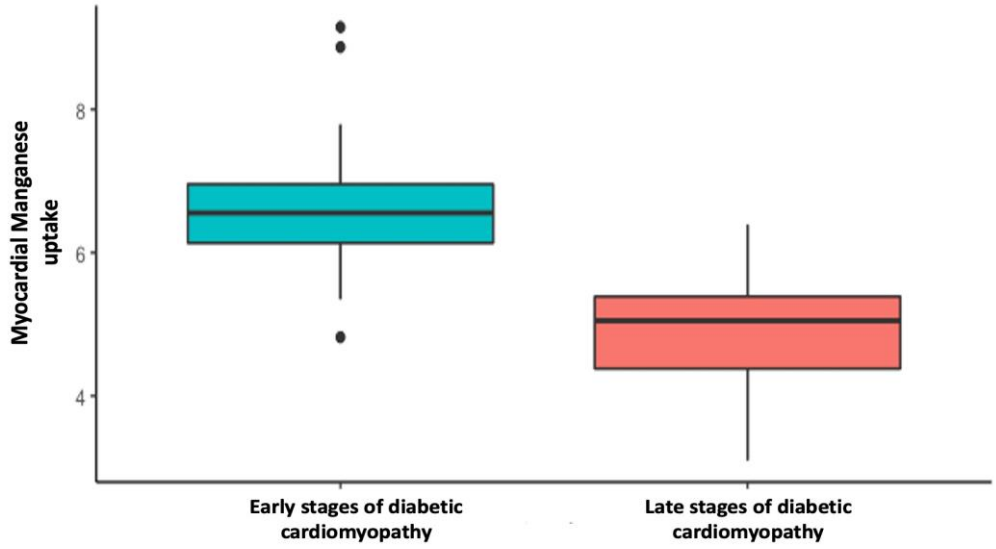

Figure 5.3. Influence of type 2 diabetes on myocardial calcium handling. Myocardial manganese uptake was lower in late stages of diabetic cardiomyopathy (patients with type 2 diabetes with reduced ejection fraction, n=20) (4.9±0.7 mL/100g of tissue/min) versus patients in early stages of diabetic cardiomyopathy (patients with type 2 diabetes with normal ejection fraction, n=24) (6.5±0.9 mL/100g of tissue/min), p<0.001

5.4.4 Influence of heart failure and type 2 diabetes on myocardial calcium handling

Patients with heart failure with and without type 2 diabetes were well matched for age, sex and other co-morbidities, such as ischaemic heart disease, hypertension and hyperlipidaemia (**Table 5.1**). Heart failure therapy and baseline imaging parameters were also similar between the two groups (**Table 5.1**).

Myocardial manganese uptake was lower in participants with both type 2 diabetes and heart failure compared to patients with heart failure without type 2 diabetes (4.9±0.8 versus 5.7±1.1 mL/100g of tissue/min, p=0.01, **Figures 5.4 and 5.5**).

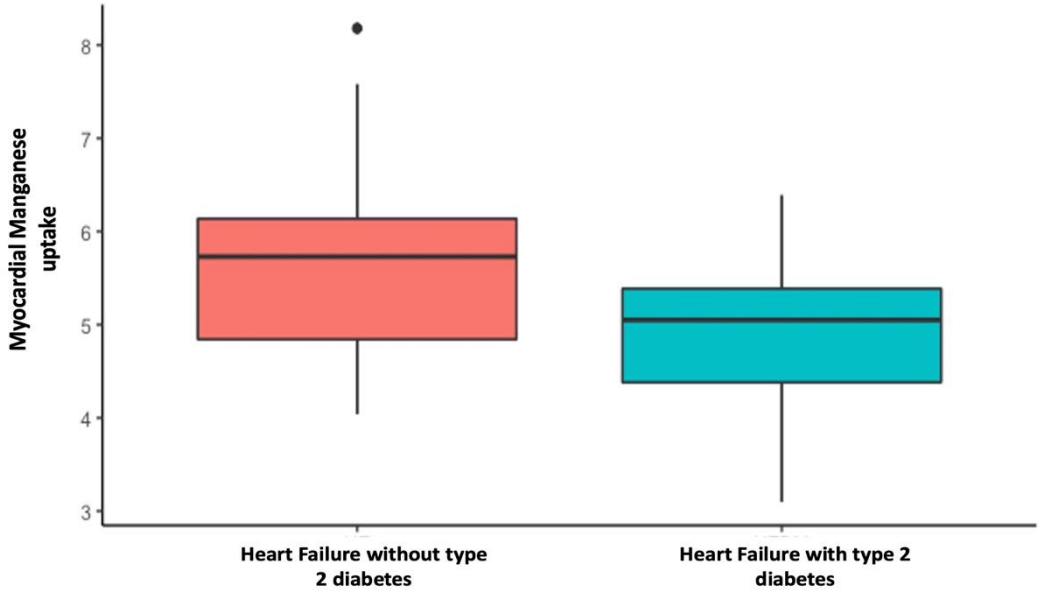

Figure 5.4. Influence of heart failure and type 2 diabetes on myocardial calcium handling. Myocardial manganese uptake was lower in patients with both heart failure and type 2 diabetes (n=20) (4.9±0.8 mL/100g of tissue/min) versus patients with heart failure without type 2 diabetes (n=20) (5.7±1.1 mL/100g of tissue/min), p=0.01

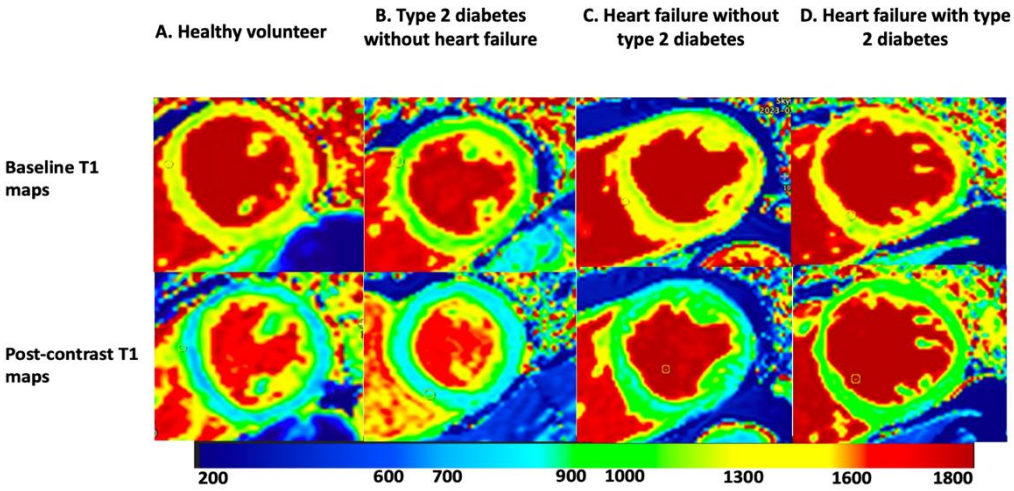

Figure 5.5. Example T1 maps in the study population. Myocardium (at mid left ventricular level) at baseline (top panel) and 30 min after manganese contrast infusion (bottom panel) in (A) healthy volunteer (B) individual with type 2 diabetes mellitus with normal left ventricular function, (C) individual with heart failure without type 2 diabetes and (D) individual with both heart failure and type 2 diabetes. Colours are assigned to different T1 values on a pixel-by-pixel basis. The colour scale shows T1 values corresponding to the different colours. Note the differences in the appearance of myocardium in different study participants. The areas with reduced enhancement post contrast represent reduced manganese uptake.

5.4.5 Correlation and Multivariate analysis

Myocardial manganese uptake correlated with left ventricular ejection fraction in patients with heart failure (r=0.61, p<0.001) but not in patients with type 2 diabetes with normal left ventricular function (r=0.27, p=0.19) or healthy volunteers (r=-0.23, p=0.46). There were no correlations between myocardial manganese uptake and age, sex or body-mass index in any of the participant cohorts. Furthermore, in patients with both type 2 diabetes and heart failure, we did not find any correlation between glycated haemoglobin and myocardial manganese uptake (rho=-0.16, p=0.52). On multivariable analysis, type 2 diabetes (r^2 (IQR): 0.16 (-0.79-1.11), p=0.01) and left ventricular ejection fraction (r^2 (IQR): 0.37 (-0.87-1.61), p<0.001) were the only predictors of myocardial manganese uptake, after adjusting for age, sex, ischaemic heart disease, hypertension, and hyperlipidaemia, in patients with heart failure.

5.5 DISCUSSION

We have demonstrated differential myocardial manganese uptake in different stages of diabetic cardiomyopathy and in patients with heart failure with or without type 2 diabetes. This highlights the importance of abnormal myocardial calcium handling in the pathophysiology of heart failure and diabetic cardiomyopathy. This is particularly pertinent for the detection of the early subclinical stages of diabetic cardiomyopathy. Our findings have a number of important potential implications and clinical applications.

In this study, we have confirmed our previous finding of reduced myocardial manganese uptake, and by inference, abnormal myocardial calcium handling in patients with left ventricular systolic dysfunction (84). This suggests that manganese-enhanced magnetic resonance imaging is a robust technique and can be potentially used as a biomarker for diagnosis, risk stratification, disease progression and response to treatment in patients with left ventricular systolic dysfunction. It also highlights the importance of calcium metabolism in myocardial cellular physiology although our findings are restricted to describing associations rather than inferring causality. Is the alterations in myocardial calcium handling a cause or a consequence of heart failure? This will require further evaluation, including interventional studies to demonstrate whether response to heart failure medications improve myocardial manganese uptake and calcium handling.

We have recently shown reduced myocardial manganese uptake in early stages of diabetic cardiomyopathy compared with healthy volunteers (78) and we have here confirmed this. In addition, we now demonstrate further reductions in myocardial manganese uptake in later stages of diabetic cardiomyopathy. This finding suggests that this abnormality precedes the onset of heart failure and could suggest that, at least for diabetic cardiomyopathy, there may be a causal association. Furthermore, we have now

shown that manganese uptake is further suppressed in patients with both heart failure and type 2 diabetes. This exacerbation of abnormal calcium handling could help explain the worser outcomes associated with diabetes in patients with heart failure (36,178,179). Indeed, systolic dysfunction is accompanied by a dramatic decrease of cellular calcium transients in diabetic mice and this reduction in calcium release is thought to underlie the mechanism of systolic dysfunction in diabetic mice (180) and are in keeping with our findings in the clinic.

If our findings are correct and that there is a causal association, what are the potential mechanisms and cellular pathways? Calcium plays a central role in cardiac contraction. During myocardial contraction, calcium ions enter the cardiac myocytes predominantly through the voltage-gated L-type calcium channels where they trigger further calcium release from sarcoendoplasmic reticulum stores through surface ryanodine receptors. This process results in a ten-fold increase in intracellular calcium concentrations, triggering cross-bridge formation between myofilaments that drives myocardial contraction (181,182). In diastole, calcium is actively transported back into the sarcoplasmic reticulum by sarcoplasmic reticulum calcium ATPase (SERCA2a), in addition to passage into the extracellular space via the sodium/calcium exchangers and uptake into mitochondria (182). Sorrentino et al demonstrated enhanced spontaneous calcium release from sarcoplasmic reticulum and reduced cytoplasmic calcium clearance in diabetic mice and similarly Belke et al demonstrated that a reduced decay rate of calcium transients in diabetic myocytes (183,184). Furthermore, while sodium/calcium exchanger dysfunction, sarcoplasmic reticulum Calcium-ATPase (SERCA2a) depletion and reduced sarcolemmal calcium binding are the primary factors responsible for the development of early diabetic cardiomyopathy, factors responsible for late stages of diabetic cardiomyopathy include ryanodine receptor (RYR2) depletion, a decline in the number of L-type calcium channels

and a reduction in the sarcoplasmic reticulum calcium stores (185). This may explain our findings of reduced myocardial manganese uptake and profound myocardial calcium mishandling in patients in later stages of diabetic cardiomyopathy.

5.6 STUDY LIMITATIONS

We acknowledge that our study has limitations. Firstly, the study population size is modest and large multicentre studies are needed to demonstrate the clinical utility and generalisability of our findings. Secondly, there are no currently available preparations of manganese-based contrast media available for widespread clinical use. However, this is likely to change with future commercially available preparations anticipated next year. Finally, we have not assessed the reproducibility or time course of manganese-enhanced magnetic resonance imaging with repeated serial measurements. However, we have previously demonstrated very good reproducibility of our technique (186), and need to undertake future longitudinal cohort studies of patients with heart failure to determine whether it can indeed track disease progression.

5.7 CONCLUSION

In conclusion, we have conducted the first observational study investigating myocardial calcium handling in different stages of diabetic cardiomyopathy and in patients with heart failure with or without type 2 diabetes using manganese enhanced magnetic resonance imaging. We have demonstrated that myocardial manganese uptake is highly supressed in both heart failure and diabetes, and these effects are additive. These findings have provided novel insights into the pathophysiology of diabetic cardiomyopathy, and could

help with its risk stratification and facilitate identification of novel therapeutic approaches targeted towards myocardial calcium homeostasis in diabetes.

Chapter 6. Non-invasive imaging of functional pancreatic islet beta-cell mass in people with type 1 diabetes mellitus

Adapted from:

Joshi SS, Singh T, Kershaw LE, Gibb FW, Dweck MR, Williams M, Idris I, Semple S, Forbes S, Newby DE, Reynolds RM. Non-invasive imaging of functional pancreatic islet beta-cell mass in people with type 1 diabetes mellitus. Diabet Med. 2023 Oct;40(10):e15111. doi: 10.1111/dme.15111. Epub 2023 Apr 21. PMID: 37035965.

6.1 ABSTRACT

Objectives

To investigate whether manganese-enhanced magnetic resonance imaging can assess the functional pancreatic beta-cell mass in people with type 1 diabetes mellitus.

Methods

In a prospective case-control study, 20 people with type 1 diabetes mellitus (10 with low (≥50 pmol/L) and 10 with very low (<50 pmol/L) C-peptide concentrations) and 15 healthy volunteers underwent manganese-enhanced magnetic resonance imaging of the pancreas following an oral glucose load. Scan-rescan reproducibility was performed in 10 participants.

Results

Mean pancreatic manganese uptake was 31±6 mL/100 g of tissue/min in healthy volunteers (median 32 [interquartile range 23-36] years, 6 women), falling to 23±4 and 13±5 mL/100 g of tissue/min ($p \leq 0.002$ for both) in people with type1 diabetes mellitus (52 [44-61] years, 6 women) and low or very low plasma C-peptide concentrations respectively. Pancreatic manganese uptake correlated strongly with plasma C-peptide concentrations in people with type1 diabetes mellitus ($r=0.73$, $p=0.02 \times 10^{-2}$) but not in healthy volunteers ($r=-0.05$, $p=0.88$). There were no correlations between manganese uptake and age, body-mass index or glycated haemoglobin. There was strong intra-observer (mean difference: 0.31 (limits of agreement -1.42 to 2.05) mL/100 g of tissue/min; intra-class correlation, ICC=0.99), inter-observer (-1.23 (-5.74 to 3.27) mL/100 g of tissue/min; ICC=0.85) and scan-rescan (-0.72 (-2.99 to 1.61) mL/100 g of tissue/min; ICC=0.96) agreement for pancreatic manganese uptake.

Conclusions

Manganese-enhanced magnetic resonance imaging provides a reproducible non-invasive imaging technique to assess the functional beta-cell mass in people with type1 diabetes mellitus. This holds major promise for the investigation of diabetes, monitoring disease progression and assessment of novel immunomodulatory interventions.

6.2 INTRODUCTION

Type 1 diabetes mellitus is characterised by autoimmune destruction of pancreatic beta-cells resulting in insulin deficiency (21). The destruction of beta-cells precedes the clinical manifestation of the disease and impaired insulin secretion can be detected several years prior to the onset of hyperglycaemia (187). Beta-cell mass is reduced by 80-90% at the time of diagnosis (21,23) and the degree of beta-cell dysfunction often exceeds beta-cell loss (188), indicating additional functional impairment in insulin secretion. Both beta-cell mass and function further decline over time, but are not always reflected in plasma C-peptide concentrations(189,190). It is now recognized that there are micro-secretors of insulin and that preservation of insulin secretion in these cases is associated with several physiological advantages, such as reduction in hypoglycaemic episodes, improved quality of life and reduced hospitalisations(191,192) . This provides a rationale for novel therapeutic strategies aimed at restoring or at least preventing further loss of beta-cell mass in type 1 diabetes mellitus.

Evaluation of novel immunomodulatory therapies to prevent beta-cell destruction requires reliable methods to measure beta-cell function. Although plasma C-peptide concentrations can be measured with high sensitivity assays, it does not reflect the functional numbers of beta cells present(93). Therefore, novel methods to evaluate functional beta cell mass would be invaluable for understanding the pathophysiology of type 1 diabetes mellitus, tracking disease progression and treatment response in combination with plasma C-peptide concentrations. For effective *in vivo* beta-cell imaging, contrast media need to be sufficiently selective for beta-cells, provide a stable high-intensity signal, and reflect the functional state of beta-cells (193). An example includes the use of gadolinium-based zinc sensitive agents which exploit the fact that zinc ions are secreted along with insulin from the pancreatic beta cells. Translation of this approach into human subjects has yet to be

established (194). A new promising approach is manganese-enhanced magnetic resonance imaging.

All irreversibly chelated contrast media provide contrast enhancement when they enter the extracellular space. They do not cross over into the intracellular space and therefore are unable to provide intracellular contrast. Initially developed for staging hepatobiliary cancers, mangafodipir is a partially chelated form of manganese that is bound to dipyridoxyl diphosphate and circulates within a protein bound complex. After intravenous administration, mangafodipir releases manganese ions into plasma by dephosphorylation and transmetallation with zinc thereby allowing rapid intracellular manganese uptake and renal clearance. This approach mitigates the toxicity seen with non-chelated forms of manganese-based contrast media(69). Manganese has paramagnetic properties which shorten T1 relaxation and free dissociated manganese ions are taken up into pancreatic beta-cells during insulin secretion via voltage-gated calcium channels, serving as an intracellular contrast agent(195). Mn^{2+} and Ca^{2+} ions compete during insulin secretion, thereby leading to pancreatic enhancement with manganese contrast in a way dependent on beta cell function. Therefore, lower manganese uptake is seen in diabetic mice versus non-diabetic mice. The specificity of this technique for pancreatic beta cells has also been demonstrated in various pre-clinical studies using pharmacological treatments like nifedipine, tolbutamide and diazoxide, shown to selectively activate or inactivate the voltage gated calcium channels in the pancreatic beta cells(90,196).

In this proof-of-concept study, we investigated whether manganese-enhanced magnetic resonance imaging can be used as a non-invasive and reproducible measure of pancreatic beta-cell function in people with type 1 diabetes mellitus. Specifically, we hypothesised that pancreatic manganese uptake as assessed by T1 mapping will be

reduced in people with type 1 diabetes mellitus and that this will be proportional to plasma C-peptide concentrations.

6.3 RESEARCH DESIGN AND METHODS

6.3.1 Study Design

We conducted a prospective proof-of-concept investigational study (NCT05298735) in accordance with the Declaration of Helsinki, a favourable ethical opinion from the research ethics committee (20/WM/0304) and the written informed consent of all participants.

6.3.2 Study Participants

People with a confirmed diagnosis of type 1 diabetes mellitus, aged ≥18 years were identified and approached through the Edinburgh Centre for Endocrinology and Diabetes, Royal Infirmary of Edinburgh, Edinburgh, UK. We specifically recruited 10 people with low (>50 pmol/L) and 10 people with very low (<50 pmol/L) plasma C-peptide concentrations. We had baseline C-peptide concentrations available for all patients from the clinic, which was used to screen participants for the study. Stimulated C-peptide concentrations were measured after a standardised oral glucose load (Fortisip Compact) in all participants, on the day of their scan. Healthy volunteers were recruited via advertisement with inclusion criteria of age ≥ 18 years, no regular medication, and no known clinically significant medical condition. Exclusion criteria for all study participants included renal failure (estimated glomerular filtration rate <30 mL/min/1.73 m^2), an inability to consent, contraindications to magnetic resonance imaging, symptoms suggestive of coronavirus disease 2019 (COVID-19), and pregnancy or breast-feeding. All participants had an

assessment of clinical haematology and biochemistry including full blood count, liver and renal function, glycated haemoglobin and plasma C-peptide. Plasma C-peptide concentrations were measured using an immunoassay (ARCHITECT C-peptide assay, Abbott, USA). Internal assay validation demonstrated a coefficient of variation of 7% at 7 pmol/L and of 15% at 4 pmol/L.

6.3.3 Magnetic Resonance Imaging

Subjects fasted from midnight and, on the following morning, were given a standardized glucose load (125 mL of Fortisip compact, 2.4Kcal/mL (Nutricia, United Kingdom) supplement drink) (197) half an hour prior to their imaging to stimulate pancreatic beta-cell insulin secretion. People with type 1 diabetes mellitus withheld any quick-acting insulin prior to the scan.

Magnetic resonance imaging was performed using a 3T scanner (MAGNETOM Skyrafit, Siemens Healthineers, Erlangen, Germany) with a dedicated 30-channel body matrix coil. Manganese-enhanced magnetic resonance imaging was performed using intravenous manganese dipyridoxyl diphosphate (5 μmol/kg (0.1 mL/kg) at 1 mL/min; Exova SL Pharma, Wilmington, Delaware, USA) administered over 10 minutes. Localizers, half-Fourier single-shot turbo spin-echo (HASTE) and standard breath-hold cine sequences of the heart were followed by T1 mapping sequences of the pancreas. Pancreatic T1 mapping was performed prior to contrast using a breath-held modified Look-Locker inversion recovery acquisition and every 2.5 min for 30 min after commencing the intravenous manganese dipyridoxyl diphosphate infusion(142). Pancreas and left ventricular blood pool T1 values were compared. T1 values represent the time constant for longitudinal relaxation time which is measured in milliseconds and is a standard measure for magnetic resonance imaging.

6.3.4 Image Analysis

Magnetic resonance images were analysed offline using Circle CVI (Circle Cardiovascular Imaging, CVI42 v5.13.5, Calgary Canada). Quantitative analysis of manganese accumulation was performed by measuring T1 relaxation time in the region of interest drawn within the head, body and tail of the pancreas and compared with the left ventricular blood pool. T1 maps were generated using commercially available software (CVI42, Circle cardiovascular imaging, Calgary Canada) and applying a three-parameter non-linear curve fitting as described previously (140). Analysis was performed by experienced observers (SJ, TS).

6.3.5 Manganese Kinetic Modelling

Patlak et al were the first to provide a graphical analysis of unidirectionality of transfer and of the influx constant, using brain uptake data(81). The multi-timepoint approach produces information about the exchange rate of the compartments that rapidly and reversibly exchange with plasma. Moreover, this can be used to assess the rate constant of any type of irreversible process within any organ system. The Patlak two-compartment model was used in this study to measure the rate of pancreatic manganese uptake. This assumes the influx of manganese ions from a reversible (v_e, extracellular and vascular space) into a largely irreversible compartment (v_i, pancreatic beta cells during the imaging period). This apparent unidirectional influx constant (Ki) for the transfer of manganese from plasma to irreversible compartments v_i, can be measured, using the equation below:

$$\frac{C_t(t)}{C_a(t)} = Ki\frac{\int_0^t C_a(\tau)d\tau}{C_a(t)} + v_e$$

where C_t and C_a are the manganese concentration in pancreatic tissue and blood pool (arterial input function) respectively. This formula is equivalent to the Patlak model and describes that if a contrast medium is irreversibly trapped in the tissue within the imaging period, the instantaneous tissue concentration (pancreatic T1) divided by the instantaneous arterial concentration (blood pool T1) plotted against the integrated arterial concentration divided by the instantaneous arterial concentration, will result in linearisation of the data.

6.3.6 Intra-observer and Inter-observer Repeatability and Scan-rescan Reproducibility

To assess intra-observer repeatability, images from ten participants were analysed by the same observer (SJ) at two different time points, at least 8-12 weeks apart and in random order to minimize recall bias. Similarly, repeated measurements were made in ten participants by two independent observers (SJ and TS) to assess inter-observer repeatability. Ten participants also underwent repeat manganese-enhanced magnetic resonance imaging to assess scan-rescan reproducibility.

6.3.7 Statistical Analysis

All statistical analyses were performed with R Studio (RStudio, Boston, USA). Categorical baseline variables were presented as number (%) and compared using a Chi-squared test. Continuous data were assessed for normality using the Shapiro test and presented as mean ± standard deviation or median [interquartile range]. Pancreatic manganese uptake measurements were compared using analysis of variance (ANOVA) and Tukey's HSD (honestly significant difference) post-hoc test. Values were compared using paired or unpaired Student's *t*-tests, Wilcoxon or Mann-Whitney tests and Kruskal-Wallis tests as appropriate. Correlation analyses between pancreatic manganese uptake and other

parameters were performed using Spearman's rank correlation coefficient. Statistical significance was taken as two-sided $p<0.05$. Reproducibility and repeatability analyses were carried out using intra-class correlation coefficient (ICC) and Bland Altmann analysis. A positive or negative correlation coefficient with a value of 1.0 considered as perfect correlation, between 0.9-1.0 very strong, between 0.70-0.90 strong, between 0.5-0.6 moderate and 0.1-0.4 weak.

6.4 RESULTS

6.4.1 Study Population

We recruited 38 participants: 23 people with type 1 diabetes mellitus and 15 healthy volunteers. Three participants were withdrawn because of incomplete data acquisition due to claustrophobia (n=2) and poor image quality due to body habitus (n=1). People with type 1 diabetes mellitus were on average 20-25 years older than the healthy volunteers (**Table 6.1**). However, there were no correlations between pancreatic manganese uptake and age in either people with type 1 diabetes mellitus or healthy volunteers.

	Healthy volunteers	People with type 1 diabetes mellitus and low plasma C-peptide concentrations	People with type 1 diabetes mellitus and very low plasma C-peptide concentrations
Number of participants	**15**	**10**	**10**
Age (years)	**32 [22-36]**	**59 [40-70]**	**51 [46-56]**
Sex (Men:Women)	**9:6**	**7:3**	**7:3**
Baseline Plasma C-peptide concentration (pmol/L)	**794 [399-1,591]**	**186 [124-387]**	**32 [0-61]**
Body-mass index (kg/m^2)	**24.5 [23.3-27.9]**	**26.0 [21.3-28.2]**	**27.4 [25.0-30.5]**
Duration of diabetes mellitus (years)	**N/A**	**9 [5-17]**	**25 [10-31]**

Table 6.1. Baseline characteristics of study participants. n (%), median [interquartile range]

6.4.2 Pancreatic Magnetic Resonance Imaging

The native (pre-contrast) pancreatic T1 values for people with type 1 diabetes mellitus were higher than those in healthy volunteers (950 [880-1,000] versus 820 [770-830] ms respectively, $p<0.01x10^{-2}$). During manganese dipyridoxyl diphosphate infusion, pancreatic T1 values demonstrated a rapid initial reduction followed by a gradual and sustained reduction. Median T1 values 30 minutes after manganese dipyridoxyl diphosphate infusion were higher in people with type 1 diabetes mellitus compared to healthy volunteers (595 [520-635] versus 435 [415-430] ms respectively, $p=0.14x10^{-3}$).

Compared to the healthy volunteers, participants with type 1 diabetes mellitus had visibly lower pancreatic enhancement 30 minutes after manganese contrast infusion. Moreover, participants with very low plasma C-peptide concentrations had lower pancreatic enhancement compared with participants with low plasma C-peptide concentrations (**Figure 6.1**). There were no regional differences in enhancement within the pancreatic tissue (head versus body versus tail).

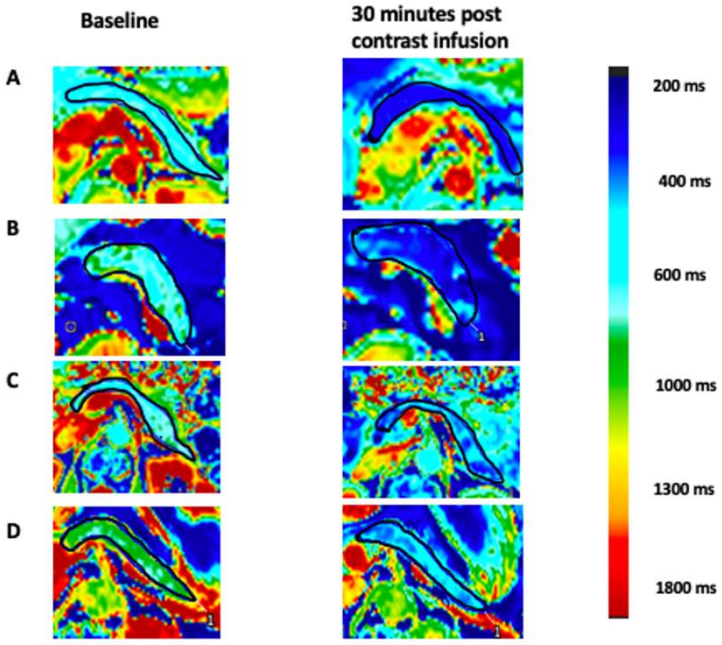

Figure 6.1. Example pancreatic T1 maps in study participants.

Pancreas at baseline (left-hand column) and 30 min after manganese contrast infusion (right-hand column) in (A) healthy volunteer (plasma C-peptide concentration >500 pmol/L; Ki 35 mL/100 g of tissue/min), (B) individual with type 1 diabetes mellitus and low C-peptide concentration (362 pmol/L; Ki 27 mL/100 g of tissue/min), (C) individual with type 1 diabetes mellitus and very low C-peptide concentration (0 pmol/L; Ki 5 mL/100 g of tissue/min) and (D) individual with type 1 diabetes mellitus and very low C-peptide concentration (32 mol/L; Ki 15 mL/100 g of tissue/min). Colours are assigned to different T1 values on a pixel-by-pixel basis. The colour scale shows T1 values corresponding to the different colours. T1 values represent the time constant for longitudinal relaxation time which is measured in milliseconds and is a standard measure for magnetic resonance imaging.

Note the differences in the appearance of pancreas in participants with different C-peptide concentrations. The areas with reduced enhancement post contrast represent reduced manganese uptake and likely areas of beta-cell loss.

Kinetic modelling demonstrated a lower rate of pancreatic manganese uptake in participants with type 1 diabetes mellitus compared with healthy volunteers (**Figure 6.2).** Mean pancreatic manganese uptake (Ki) was 31±6 mL/100 g of tissue/min in healthy volunteers falling to 23±4 and 13±5 mL/100 g of tissue/min in people with type 1 diabetes mellitus with low and very low C-peptide concentrations respectively ($p \leq 0.02 \times 10^{-1}$ for both versus healthy volunteers; **Figure 6.3**).

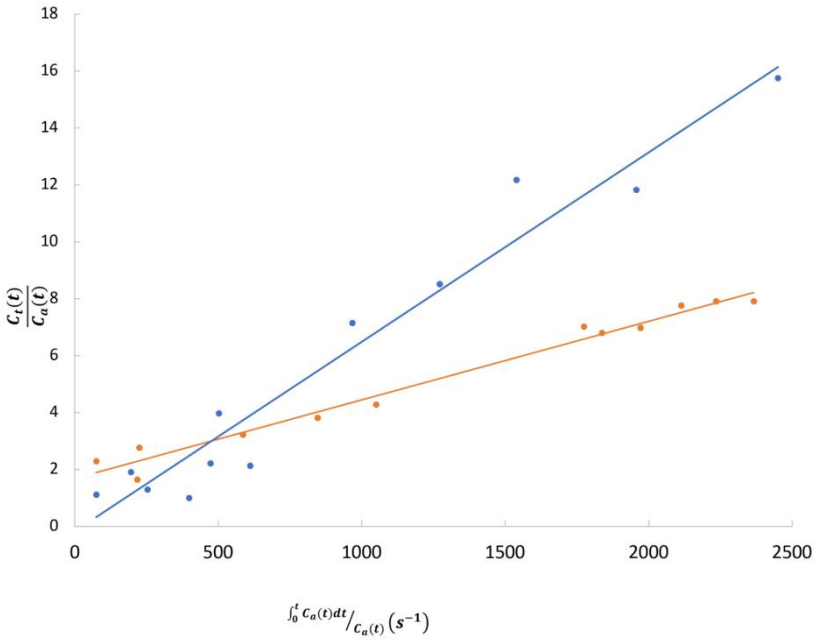

Figure 6.2. Patlak (Kinetic modelling) plots for a healthy volunteer (blue) and a participant with type 1 diabetes mellitus (orange). The gradient of the fitted straight line is equal to Ki, the manganese uptake constant. C_t= Manganese concentration in the pancreas, C_a=arterial Manganese concentration and t=time.

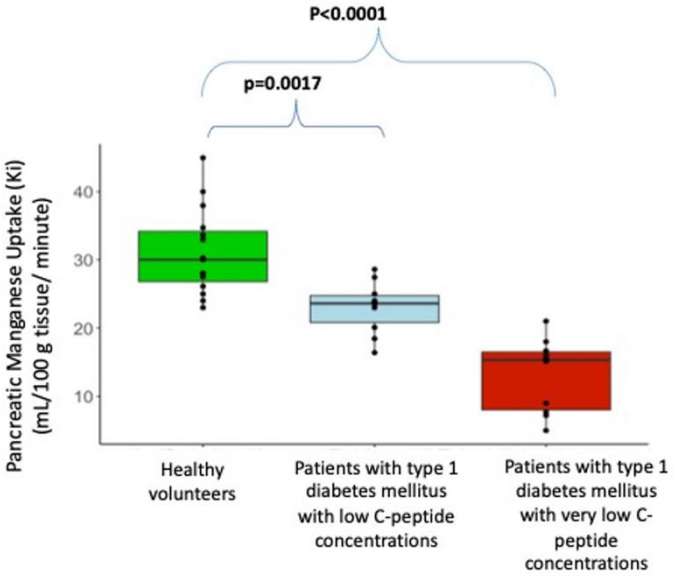

Figure 6.3. Pancreatic manganese uptake (Ki) in participant cohorts. Mean Ki was higher in healthy volunteers (31 ± 6 mL/100 g of tissue/min) compared to people with type 1 diabetes mellitus and low (23 ± 4 mL/ 100 g of tissue/min) or very low (13 ± 5 mL/ 100 g of tissue/min) plasma C-peptide concentrations.
ANOVA with Tukey's post hoc test p≤0.002 for both versus healthy volunteers.

Pancreatic manganese uptake was directly proportional to both baseline plasma C-peptide and stimulated C-peptide concentrations in people with type 1 diabetes mellitus (r=0.73, $p=2.0x10^{-4}$ and r=0.71, $p=0.07x10^{-1}$ respectively) but not in healthy volunteers (r=-0.05, p=0.88; **Figure 6.4**). There were no correlations between age and pancreatic Ki for either people with type 1 diabetes mellitus (r=-0.03, p=0.89) or healthy volunteers (r=0.31, p=0.25). Similarly, there were no correlations between the pancreas Ki and body-mass index or glycated haemoglobin for people with type 1 diabetes mellitus.

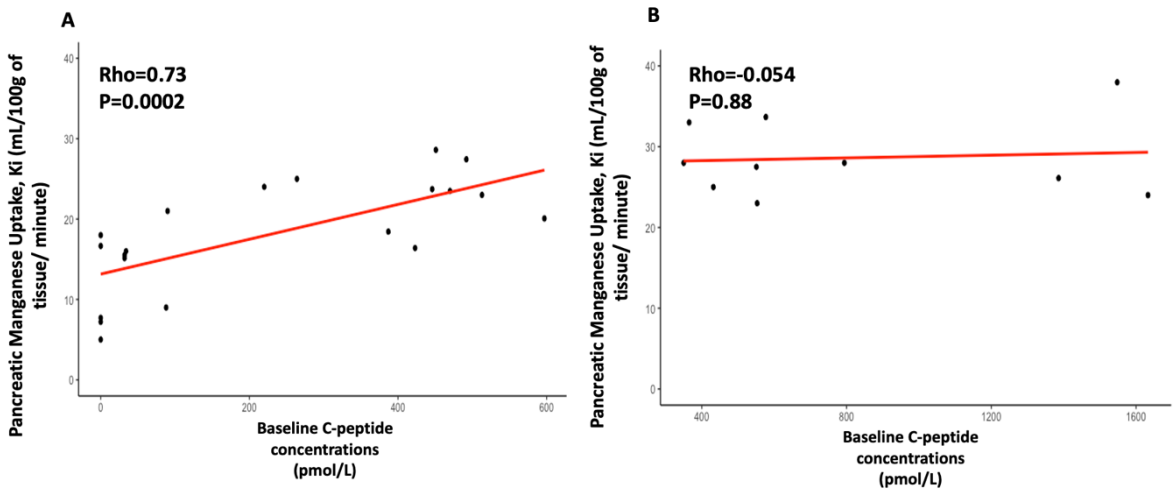

Figure 6.4. Correlation analysis. Correlations between pancreatic manganese uptake and baseline plasma C-peptide concentrations in participants with type 1 diabetes mellitus (panel A) and healthy volunteers (panel B).

6.4.3 Repeatability and Reproducibility

Intra-observer Repeatability

There were no differences in repeated measurements of pancreatic native T1 values (833 [778-848] versus 824 [765-843] ms, p=0.65), post-contrast T1 values (437 [426-436] versus 435 [419-451] ms, p=0.84) and pancreatic manganese uptake (Ki, 30 [29-34] versus 28 [26-33] mL/100 g of tissue/min, p=0.63). There were strong correlations between the paired pancreatic native T1 values (mean difference: -12.01 (limits of agreement: -10.81 to 34.82) ms, ICC=0.93), post-contrast T1 values (mean difference: -2.52 (limits of agreement: -31.43 to 26.41) ms, ICC=0.87) and pancreatic manganese uptake (mean difference 0.31 (limits of agreement -1.42 to 2.05) mL/100 g of tissue/min; ICC=0.99).

Inter-observer Repeatability

There were no differences in repeated measurements of pancreatic native T1 values (833 [778-848] versus 818 [763-837] ms, p=0.47), post-contrast T1 values (438 [427-452] versus 435 [414-450] ms, p=0.66) and pancreatic manganese uptake (30 [28-34] versus 33 [29-35] mL/100 g tissue/min, p =0.82). There were strong correlations and good limits of agreement between the paired pancreatic native T1 values (mean difference: 25.50 (limits of agreement 0.98 to 50) ms; ICC= 0.83), post-contrast T1 values (mean difference: 11.32 (limits of agreement: -10.52 to 33.11) ms; ICC=0.80) and pancreatic manganese uptake, Ki (mean difference -1.23 (limits of agreement -5.74 to 3.27) mL/100 g of tissue/min; ICC=0.85).

Scan-rescan Reproducibility

Repeated scans were performed 88 [62-124] days apart. There were no differences between native T1 (801 [785-826] versus 806 [757-823] ms, p=0.70), post-contrast T1 (441 [426-441] versus 446 [415-456] ms, p=0.88) values and pancreatic manganese uptake (30 [28-34] versus 28 [24-31] mL/100 g of tissue/min, p=0.15) values. There were strong correlations between the scan-rescan pancreatic native T1 values (mean difference: -3.5 (limits of agreement -47.1 to 40) ms; ICC=0.84), post-contrast T1 values (mean difference: 2.10 (limits of agreement: -23.90 to 28.11) ms; ICC=0.88) and pancreatic manganese uptake (mean difference: -0.72 (limits of agreement: -2.99 to 1.61) mL/100 g of tissue/min; ICC=0.96).

6.5 DISCUSSION

This is the first prospective clinical study investigating manganese-enhanced magnetic resonance imaging of the pancreas in people with type 1 diabetes mellitus. We have shown that pancreatic manganese uptake is markedly reduced in people with type 1 diabetes mellitus and that this reduction is directly proportional to plasma C-peptide

concentrations. This technique represents a non-invasive method of quantifying *in vivo* human pancreatic beta-cell function and mass with implications for the diagnosis, monitoring of disease progression and assessment of treatment efficacy.

As an analogue of calcium, manganese is readily taken up into cells that use calcium-dependent processes including hepatic, cardiac and pancreatic cells. Active insulin secretion is highly dependent on intracellular fluxes of calcium. It is therefore unsurprising that manganese-enhanced magnetic resonance imaging markedly decreases the T1 values of pancreatic beta cells (198). There have been previous animal and human studies in diabetes suggesting manganese-based contrast media have the potential for detecting differences in beta cell mass and function (89,199). There is also strong pre-clinical evidence to suggest that enhancement in the pancreatic signal after manganese-based contrast media is predominantly due to the uptake of manganese by the pancreatic beta-cells, especially after glucose-stimulation. Several animal studies support our findings that manganese uptake in the pancreas is specific to beta cells as opposed to exocrine cells or other islet cell populations using agents that target beta cell function including tolbutamide, streptozotocin and diazoxide. Streptozotocin specifically targets pancreatic beta cells, entering through a GLUT2 transporter, causing beta cell necrosis(85). Tolbutamide and diazoxide target beta cell adenosine tri-phosphate sensitive potassium channels (K_{ATP}), but not exocrine pancreas cells, and therefore selectively activate or inactivate beta cell voltage gated calcium channels, respectively(86). There is a significant decrease in pancreatic manganese uptake in streptozotocin treated mice compared to the non-diabetic mice. The increase in pancreatic manganese uptake can also be inhibited in mice treated with diazoxide. Diazoxide opens beta cell K_{ATP} channels and inhibits calcium ions influx even in the presence of glucose(87). These data indicate that reduction in pancreatic manganese uptake is secondary to reduced beta cell uptake as seen with diazoxide or

beta cell destruction as seen with streptozotocin. Conversely, pancreatic manganese uptake is increased in mice treated with tolbutamide which promotes beta cell calcium ion influx through voltage gated calcium channels(88). Given the results from these pre-clinical studies, it is very likely that pancreatic enhancement seen with mangafodipir is predominantly due to the manganese uptake in beta cells (89,91,196,199).
For the first time, we provide the proof-of-concept that manganese-enhanced magnetic resonance imaging can be applied in people with type 1 diabetes mellitus to assess beta-cell function non-invasively.

We have demonstrated that there is a marked suppression of manganese uptake in people with type 1 diabetes mellitus and especially in those with very low plasma C-peptide concentrations. Indeed, there was a proportional reduction in pancreatic manganese uptake with progressive falls in plasma C-peptide concentrations. This is consistent with the loss of beta-cell function and reduced endogenous calcium-dependent insulin secretion. Interestingly, we also identified differential patchy uptake of manganese visually in pancreas in people with type 1 diabetes compared with healthy volunteers and this enhancement was lowest in participants with lower C-peptide concentrations, suggesting that we can potentially estimate the functional beta cell mass using this technique. Our findings are also in keeping with results from pre-clinical studies exploring manganese enhanced magnetic resonance imaging of the pancreas in rodent models of diabetes(90,200). In the murine model of streptozotocin-induced pancreatic beta-cell destruction, Meyer et al reported a 79% reduction in pancreatic manganese uptake which correlated with a 73% loss in beta cell mass (200). Similarly, Antkoviak et al observed a streptozotocin dose-dependent reduction in pancreatic manganese uptake in a murine model(199). In a retrospective analysis of abdominal manganese-enhanced magnetic resonance imaging, Botsikas et al found lower enhancement of pancreatic signal in people

with type 2 diabetes(89). This is likely in keeping with 20-30% reduction in pancreatic beta-cell mass that is observed in people with type 2 diabetes. However, this imaging had been performed for other indications, had not been optimized for analysis of the pancreas, and was conducted in the absence of a standardized glucose load(89).

Our novel imaging method has several important strengths. First, unlike other techniques used for pancreatic beta-cell imaging, this method does not require isolation or labelling of islet cells(201,202). Second, this technique is non-invasive, does not involve radiation and has excellent observer repeatability and scan-rescan reproducibility. This would make it an ideal modality for repeated pancreatic imaging which may be required to monitor disease progression as well as response to immunomodulator drugs in clinical trials for type 1 diabetes mellitus. Third, manganese-enhanced magnetic resonance imaging can assess beta-cell function dynamically in response to a standardized glucose load and provide a visual assessment of the functional beta cell mass. This could help describe the pattern of beta-cell loss in the natural history of type 1 diabetes mellitus and in differentiating between different causes of pancreatic insufficiency. This is particularly relevant in the context of diagnostic trials in type 1 diabetes mellitus (such as The Environmental Determinants of Diabetes in the Young (TEDDY) study, NCT00279318) that require invasive pancreatic biopsies which can cause complications and are susceptible to sampling error (203). Moreover, in the last two decades, pancreas pathology in type 1 diabetes mellitus has been better characterised and different disease endotypes have been recognised. Recent studies have demonstrated the presence of ‘insulitis’, pathological changes in islet cells in pre-clinical stages of type 1 diabetes mellitus(204). This imaging technique could further contribute to valuable information regarding pre-clinical stages of type 1 diabetes mellitus. Finally, although blood biomarkers are widely used in clinical practice, there are several important limitations of plasma C-peptide

concentrations. The correlation between plasma C-peptide concentrations and beta-cell mass is imperfect and has limitations. The presence of anti-insulin antibodies that bind both pro-insulin and C-peptide can give falsely high C-peptide concentrations and there is evidence from *in vivo* studies that plasma C-peptide concentrations do not correlate with beta-cell mass in humans(93). Similarly, plasma C-peptide concentrations are challenging to interpret in patients with chronic kidney disease and in the presence of anti-insulin antibodies that bind both pro-insulin and C-peptide. This study is likely to inform future studies tracking disease progression with manganese enhanced magnetic resonance imaging. This imaging modality may aid drug development by allowing clinicians to track response to novel disease modifying therapies in the future. Future studies could incorporate dynamic C-peptide testing during the scan as well as assessing measures of insulin sensitivity. Further studies are also needed to investigate the optimal oral glucose load to best assess pancreatic manganese uptake and assessment of functional beta cell mass.

6.6 STUDY LIMITATIONS

We acknowledge that our study has certain limitations. This was a proof-of-concept study and we observed substantial differences in pancreatic manganese uptake between people with type 1 diabetes mellitus and healthy volunteers. We acknowledge that the patient cohorts and healthy volunteers were not well matched for age, although there was no association between age and pancreatic manganese uptake in either the healthy volunteers or people with type 1 diabetes mellitus. Secondly, this study comprised of a modest sample size and therefore these findings should be further validated in future studies involving larger cohorts. Finally, there are no currently available preparations of

manganese-based contrast medium for widespread clinical use. However, this is likely to change with commercially available preparations anticipated soon(74,205).

6.7 CONCLUSION

We have demonstrated, for the first time, that manganese-enhanced magnetic resonance imaging can provide a non-invasive imaging technique to assess the functional beta-cell mass in people with type 1 diabetes mellitus. This has important implications for the investigation of the pathophysiology of diabetes, the monitoring of disease progression and the assessment of novel beta-cell preserving therapeutic interventions.

CHAPTER 7. Conclusions

7.1 Summary of the findings

Although gadolinium-based magnetic resonance imaging is one of the key imaging modalities used for tissue characterisation and to assess cardiac function in clinical medicine, it has certain limitations. It can only serve as a marker of the intravascular and extracellular space and does not provide direct information with regards to tissue viability. In contrast, manganese-based magnetic resonance imaging can provide intracellular contrast for calcium-dependent processes, including cardiomyocyte and pancreatic beta cell calcium handling, and can assess tissue functionality and viability (71).

In this thesis, we have demonstrated excellent intra-observer and inter-observer repeatability and scan-rescan reproducibility of manganese-enhanced magnetic resonance imaging in healthy and diseased myocardium. We then showed impaired myocardial manganese uptake in asymptomatic patients with normal left ventricular systolic function and type 2 diabetes. This finding provides significant insights into the pathophysiology of early diabetic cardiomyopathy.

We also confirmed our previous finding of reduced myocardial manganese uptake, and by inference, abnormal myocardial calcium handling in patients with left ventricular systolic dysfunction. In the same study, we also found that there is a further reduction in myocardial manganese uptake in later stages of diabetic cardiomyopathy. In addition, we also demonstrated that manganese uptake is deeply suppressed in patients with both heart failure and type 2 diabetes compared to patients with heart failure without type 2 diabetes.

Finally, we determined that manganese-enhanced magnetic resonance imaging provides a reproducible non-invasive imaging technique to assess the functional beta-cell mass in people with type 1 diabetes.

7.1.1 Repeatability and Reproducibility of Cardiac Manganese-Enhanced Magnetic Resonance Imaging

Recent clinical studies have established the beneficial role of manganese-enhanced magnetic resonance imaging assessing myocardial calcium handling in various cardiomyopathies (76,77,84). However, repeatability and reproducibility of cardiac manganese-enhanced magnetic resonance imaging has not been previously evaluated and is an essential next step for its future application.

In this study, we demonstrated that myocardial T1 mapping and kinetic modelling of manganese uptake is repeatable and reproducible in both healthy and diseased myocardium. We showed excellent intra-observer and inter-observer repeatability as well as scan-rescan reproducibility for cardiac manganese-enhanced magnetic resonance imaging. These findings suggest that this novel imaging technique is an accurate and reproducible measure of myocardial calcium handling and is sufficiently robust for clinical application.

7.1.2 Manganese-enhanced Magnetic Resonance Imaging in Asymptomatic Patients with Type 1 and Type 2 Diabetes

The pathophysiology of diabetic cardiomyopathy is complex and may involve myocardial calcium mishandling which has been demonstrated in animal models but this has not been

tested in human studies previously. Manganese-enhanced magnetic resonance imaging is an excellent non-invasive method to assess the myocardial calcium handling.

In this study, we demonstrated striking reductions in myocardial manganese uptake in patients with type 1 and type 2 diabetes, who had no prevalent cardiac disease and in the absence of any apparent left ventricular systolic or diastolic dysfunction. Abnormal calcium handling is therefore an early pathologic feature of the diabetic heart, reduced to a similar extent in both type 1 and type 2 diabetes. This may be related to the deleterious impact of chronic hyperglycaemia on voltage-gated L-type calcium channels, mediated by damage from advanced glycation end products, which are central to cardiac myocyte contraction and relaxation and endothelial function. Manganese-enhanced magnetic resonance imaging, therefore, represents a promising novel approach to further our understanding of the earlier stages of diabetic cardiomyopathy and may have potential to guide targeted therapeutic interventions in patients with diabetic cardiomyopathy.

7.1.3 Manganese-enhanced Magnetic Resonance Imaging in Diabetic Cardiomyopathy

People with diabetes have over twice the risk of developing heart failure, and patients with both heart failure and diabetes have a four-fold increased risk of dying than those without diabetes. Large studies involving multifactorial risk factor management in people with diabetes have failed to show a reduction in the incidence of heart failure in this cohort and therefore, heart failure has emerged as a major cause of death in the setting of diabetes mellitus (36). This has led to the recognition of diabetic cardiomyopathy as a separate clinical entity which is defined as the presence of abnormal myocardial structure and function in the absence of atherosclerosis, hypertension and valvular heart disease. The

pathophysiology of diabetic cardiomyopathy is incompletely understood but there is strong pre-clinical evidence suggesting reduced calcium transients and smaller endoplasmic reticulum calcium stores occur in diabetic subjects. However, this hypothesis has not been tested in a clinical setting previously.

In this study, we demonstrated that myocardial manganese uptake is highly supressed in the late stages of diabetic cardiomyopathy. Furthermore, patients with heart failure with type 2 diabetes have a profoundly depressed myocardial manganese uptake compared to patients with heart failure without type 2 diabetes. These findings have provided novel insights into the pathophysiology of diabetic cardiomyopathy, and could help with its risk stratification and facilitate identification of novel therapeutic approaches targeted towards myocardial calcium homeostasis in diabetes.

7.1.4 Non-invasive Imaging of Functional Pancreatic Islet Beta-cell Mass in People with Type 1 Diabetes Mellitus

Type 1 diabetes mellitus is characterised by autoimmune destruction of pancreatic beta-cells resulting in insulin deficiency. Pancreatic beta cell mass is reduced by 80-90% at the time of diagnosis and the degree of beta-cell dysfunction often exceeds beta-cell loss, indicating additional functional impairment in insulin secretion. It is now recognised that there are micro-secretors of insulin and that preservation of insulin secretion in these cases is associated with several physiological advantages (21–23). This provides a rationale for novel therapeutic strategies aimed at restoring or preventing further beta-cell loss. However, evaluation of novel immunomodulatory therapies to prevent beta-cell destruction requires reliable methods to measure beta-cell mass and function which are currently unavailable.

In this study, we demonstrated that manganese-enhanced magnetic resonance imaging provides a reproducible non-invasive imaging technique to assess the functional beta-cell mass in people with type1 diabetes mellitus. This holds major promise for the investigation of diabetes, monitoring disease progression and assessment of novel immunomodulatory interventions.

7.2 Clinical perspectives

In the era of precision medicine, there is increasing emphasis on tailoring the right therapies for the right patients and optimising secondary prevention in early and subclinical stages of non-ischaemic cardiomyopathy and other conditions. Tissue characterisation using manganese-enhanced magnetic resonance imaging could play an important role in a number of aspects of clinical medicine.

7.2.1 Screening

The ability to detect abnormal tissue calcium handling using manganese-enhanced magnetic resonance imaging may enable early diagnosis and prognostication of various conditions. This could be of particular benefit in subclinical detection of conditions like diabetic cardiomyopathy and pancreatic beta-cell dysfunction in type 1 diabetes. This may allow identification of patients most likely to benefit from treatment targeted at the prevention as well as amelioration of disease.

This is relevant in the setting of type 1 diabetes as this imaging technique could facilitate the recognition of pancreatic beta-cell dysfunction in patients at risk of developing type 1 diabetes (such as those with family history of type 1 diabetes). Novel therapeutic strategies to prevent further destruction of pancreatic beta cells could potentially be directed at these patients in order to preserve the functional pancreatic beta cell mass. Similarly, early stages of diabetic cardiomyopathy may be more amenable to interventions to prevent the development of later stage disease and avoid heart failure. This is particularly important given the poor prognosis associated with the development of heart failure in patients with diabetes.

7.2.2 Diagnostics

Beyond screening, manganese-enhanced magnetic resonance imaging also has the potential to differentiate between reversible and irreversible causes of heart failure and to aid diagnosis of uncertain or subclinical cardiomyopathy. This could be of particular relevance in reversible and non-reversible myocardial ischaemia, various genetic cardiomyopathies and other conditions like athlete's heart. Furthermore, diagnosing underlying cardiomyopathy prior to overt left ventricular dysfunction, will aid early detection and treatment, which can have an impact on patient outcomes. Further studies will provide more information on the diagnostic ability of manganese-enhanced magnetic resonance in a range of cardiomyopathies.

7.2.3 Therapeutics

Manganese-enhanced magnetic resonance imaging can identify viable myocardium within the peri-infarct region after an ischaemic insult (70,206) and could be used as a method to assess novel treatments to reduce infarct size, especially within the penumbra of the infarct. This could include interventions targeting reperfusion injury where assessments of myocardial viability will be important.

Myocardial manganese uptake can be used as a surrogate measure of successful delivery and function of implanted stem cells (injected myocyte stem cells take up manganese when contracting) as demonstrated following human amniotic mesenchymal stem cell delivery in a porcine model of acute myocardial infarction (207). Early studies have suggested a benefit from stem cell therapy following acute myocardial infarction. However, more recent blinded randomised trials have produced mixed results and potential mechanisms of benefit remain uncertain (208). Future studies could use manganese-

enhanced magnetic resonance imaging to assess cell retention, cell viability and treatment response to stem cell therapies, providing a comprehensive assessment of the response to stem cell therapy after acute myocardial infarction.

7.2.4 Prognostication

Manganese-enhanced magnetic resonance imaging offers an opportunity to assess intracellular calcium handling which we have been unable to quantify in the past using conventional imaging techniques such as gadolinium-enhanced magnetic resonance imaging. Late gadolinium enhancement is associated with poor prognosis in a variety of conditions including ischaemic or non-ischaemic cardiomyopathy. However, the significance of abnormal myocardial calcium handling in predicting patient outcomes has yet to be established. Large studies are needed to assess whether manganese-enhanced magnetic resonance imaging can provide useful prognostic information.

7.3 Future Directions

The use of manganese-enhanced magnetic resonance imaging to study calcium handling in the other cardiac conditions and other organs is warranted. To that end, we have proposed and secured funding for three further clinical studies exploring the role of calcium handling in myocarditis, aortic stenosis and in acute and chronic kidney disease.

7.3.1 Imaging Protocol Optimisation

In the studies presented in this thesis, magnetic resonance imaging has been performed using prolonged imaging protocols in order to enable the description of manganese uptake kinetics. However, this approach is time consuming and optimisation is required for wider clinical use. Therefore, the next step would be to use this imaging technique in large muti-centre studies and applying the kinetic modelling used in these studies to large datasets. With its application to larger datasets, we may be able to streamline and tailor manganese imaging further to allow imaging at fewer time points, thereby enabling imaging protocols to be shortened. This is crucial to establish the clinical utility of this promising new imaging technique.

7.3.2 Manganese-enhanced Magnetic Resonance Imaging in Myocarditis

We have previously demonstrated that manganese-enhanced magnetic resonance imaging can detect myocardial calcium mishandling in reversible heart failure (84). We have also shown ongoing subclinical myocardial dysfunction despite resolution of left ventricular ejection fraction and regional wall motion abnormalities (83). Therefore, it would be of interest to investigate whether manganese-enhanced magnetic resonance imaging can detect myocardial calcium handling in myocarditis, a reversible pathology. More

importantly, it will also be important to determine whether this can predict functional recovery after convalescence. One in twenty patients with acute myocarditis will go on to develop heart failure (209) and the earlier detection of abnormal myocardial calcium handling may help guide earlier treatment to prevent or to reduce left ventricular systolic dysfunction and thereby improve outcomes.

We will therefore explore the role of manganese-enhanced magnetic resonance imaging in patients with acute myocarditis and during convalescence (NCT04623788). These responses will be compared with age and sex matched healthy volunteers. 20 patients with acute myocarditis and 20 age and sex-matched healthy volunteers will be recruited. All patients will undergo 2 magnetic resonance scans (gadolinium and manganese-enhanced) at least 48 hours apart at baseline. Patients will undergo repeat manganese-enhanced magnetic resonance imaging at 3-6 months. Healthy volunteers will undergo a single manganese-enhanced magnetic resonance imaging scan at baseline. We hypothesise that there will be marked alterations in myocardial manganese uptake during the acute phase of myocarditis. We also anticipate that manganese uptake will recover following clinical recovery.

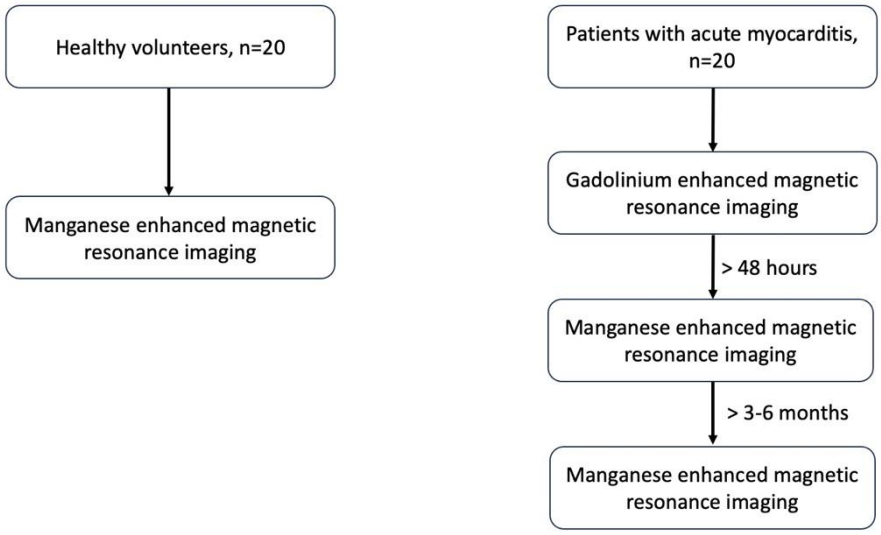

Figure 7.1. Manganese-enhanced Magnetic Resonance Imaging in Myocarditis

7.3.3 Manganese-enhanced Magnetic Resonance Imaging in Aortic Stenosis

Severe aortic stenosis causes cardiac remodelling, with a poor prognosis without intervention once symptoms develop (210). Traditionally, the focus of evaluation has been limited to the aortic valve, but it is recognised that the myocardial response to pressure overload is equally important in disease progression. In pre-clinical models, dysregulated myocardial calcium handling has been implicated in the development of heart failure in aortic stenosis, but this has not been studied *in vivo*. This will be investigated in a prospective case control study which will be performed by our collaborators in Leicester, United Kingdom. Patients with severe aortic stenosis will undergo manganese-enhanced magnetic resonance imaging at baseline and 6-12 months following aortic valve replacement, and compared to healthy volunteers. Exclusion criteria will include other severe valve disease, cardiomyopathy, diabetes, arrhythmia, glomerular filtration rate <30 mL/min/1.73 m^2 or contraindications to manganese-enhanced magnetic resonance imaging.

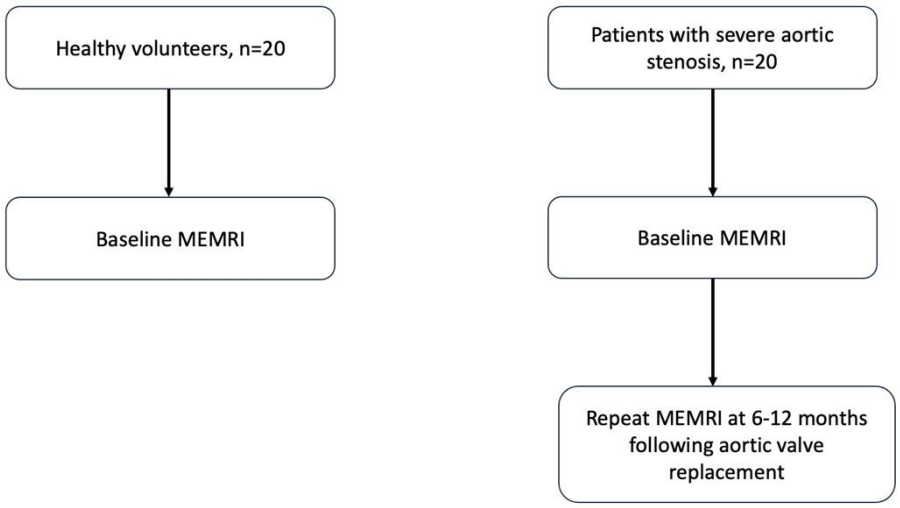

Figure 7.2. Manganese-enhanced magnetic resonance imaging in aortic stenosis.
MEMRI – manganese-enhanced magnetic resonance imaging.

7.3.3 MEMRI-Kidney Studies

Acute kidney injury is both common and costly. Although patients who suffer an episode of acute kidney injury may recover, many will go on to develop chronic kidney disease and cardiovascular disease (211). Currently, there are no reliable biomarkers that identify these patients. Such biomarkers would not only allow evidence-based risk reduction strategies to be implemented early (such as angiotensin-converting enzyme inhibitors), but they might also act as short- and medium-term endpoints in clinical trials of novel therapies targeting the transition from acute kidney injury to chronic kidney disease. Building on previous work in a range of cardiovascular diseases, these studies will explore the potential of manganese-enhanced magnetic resonance imaging to act as a biomarker of acute kidney injury and its renal and cardiovascular complications. We hypothesise that patients presenting with acute kidney injury will have suppressed manganese uptake in both the kidneys and the heart. This will improve in those who recover fully but remain

suppressed in those who develop, or who are at-risk of developing, chronic kidney disease or cardiovascular disease.

Patients presenting with acute kidney injury; age- and sex-matched patients with chronic kidney disease; age-, sex- and cardiovascular risk factor-matched control subjects; (n=20 /group) will be recruited to these studies. Patients admitted with acute kidney injury will undergo manganese-enhanced magnetic resonance imaging at presentation and then again at 3-6 months. Following interval imaging of all subjects with acute kidney injury, we will recruit control subjects and subjects with chronic kidney disease. Renal and myocardial manganese uptake will be measured serially during and for 60 minutes after intravenous infusion of manganese contrast agent. Additionally, all subjects will undergo gold-standard assessments of three independent cardiovascular risk factors: 24-hour blood pressure, arterial stiffness, and endothelial dysfunction (Figure 7.3) . The rate of manganese uptake in the kidney (cortex and medulla) and myocardium will be the primary endpoint for these studies.

These studies will be the first to assess manganese-enhanced magnetic resonance imaging of the kidney and heart in any kidney disease, specifically, acute kidney injury, chronic kidney disease, and the transition of acute kidney injury to chronic kidney disease and cardiovascular disease. They will provide an opportunity to better understand the clinical potential of manganese-based contrast media, describe the real-time effect of ischaemia on calcium handing in the kidney and heart, better understand the mechanisms and pathways associated with the acute kidney injury to chronic kidney disease continuum, and potentially develop a diagnostic or disease activity biomarker. Manganese-enhanced magnetic resonance imaging has major future potential in a range of cardiovascular and kidney diseases including as a tool to identify those with chronic kidney

disease who progress fastest to cardiovascular disease and kidney failure, identifying rejection in the transplanted kidney, or as a short- and medium-term endpoint in clinical trials of novel therapies for acute kidney injury, chronic kidney disease, and cardiovascular disease.

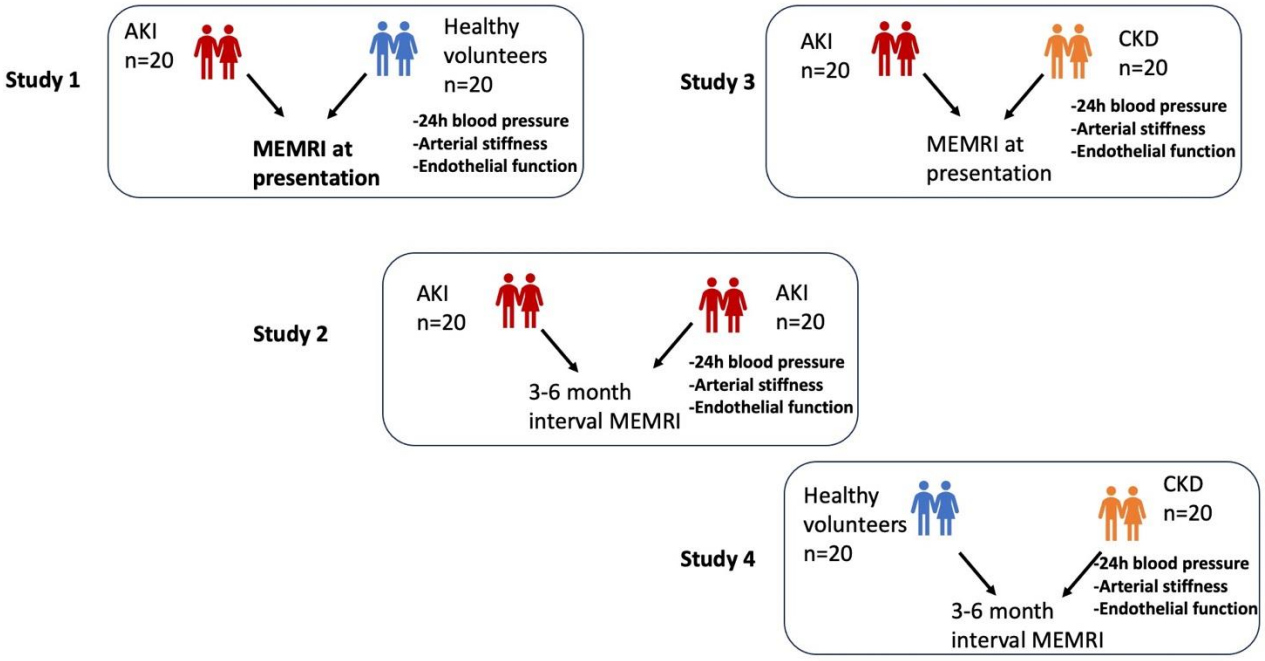

Figure 7.3. The Kidney MEMRI studies. AKI – acute kidney injury, CKD – chronic kidney disease, MEMRI – manganese-enhanced magnetic resonance imaging

7.3.4 Concluding Remarks

Manganese-enhanced magnetic resonance imaging is a safe, non-invasive, reproducible biomarker of tissue calcium handling and its utility has been established in a range of clinical conditions. Recent studies using manganese-enhanced magnetic resonance imaging have provided valuable insights into the pathophysiology of various cardiomyopathies. However, there are no currently available preparations of manganese-based contrast media for widespread clinical use but this is likely to change soon with

commercially available preparations anticipated soon. Moreover, the next step in further development of manganese-enhanced magnetic resonance imaging would be to use this imaging modality in large multi-centre studies. This would be essential for its further assessment in a wider clinical population and imaging protocol optimisation for clinical use. Future studies will not only explore the role of manganese-enhanced magnetic resonance imaging in various cardiac conditions but also in extra-cardiac conditions like pancreatic and renal dysfunction.

Publications during PhD

1) **Joshi SS** and Andrews JPM, Tzolos E, Syed MB, Cuthbert H, Crica LE, Lozano N, Raftis JB, Bruce L, Poland CA, Duffin R, Fokkens PHB, Boere AJF, Laseman DLAC, Megson IL, Whitefield PD, Ziegler K, Tammireddy S, Okwelogu E, Hadjidemetriou M, Bussy C, Cassee FR, Newby DE, Kostaleros K and Miller MR. First-in-human controlled inhalation of thin graphene oxide nanosheets to study acute cardiorespiratory responses. Nature Nanotechnology (Provisionally accepted for publication).

2) **Joshi SS** and Lembo M, Geers J, Bing R, Carnevale L, Pawade TA, Doris MK, Tzolos E, Grodecki K, Cadet S, Craig N, Singh T, Slomka PJ, White A, Guala A, Rodriguez-Palomares R, Ruiz-Munoz A, Dux-Santoy L, Teixido-Tura G, Galian-Gay L, Williams MW, Newby DE, Kwak S, Lee S, Powers A, Clavel MA, Dey D, Dweck MR. Quantitative computed tomography angiography for the evaluation of valvular fibrocalcific volume in aortic stenosis. JACC Cardiovasc Imaging (Accepted with minor revisions).

3) Henriksen PA, Hall P, MacPherson IR, **Joshi SS**, Singh T, Maclean M, Lewis S, Rodriguez A, Fletcher A, Everett RJ, Stavert H, Broom A, Eddie L, Primrose L, McVicars H, McKay P, Borley A, Rowntree C, Lord S, Collins G, Radford J, Guppy A, Williams MC, Japp A, Payne JR, Newby DE, Mills NL, Oikonomidou O, Lang NN. Multicenter, Prospective, Randomized Controlled Trial of High-Sensitivity Cardiac Troponin I-Guided Combination Angiotensin Receptor Blockade and Beta-Blocker Therapy to Prevent Anthracycline Cardiotoxicity: The Cardiac CARE Trial. Circulation. 2023; in press. doi: 10.1161/CIRCULATIONAHA.123.064274.

4) Singh T, **Joshi SS**, Kershaw LE, Baker AH, McCann GP, Dawson DK, Dweck MR, Semple SI, Newby DE. Manganese Enhanced Magnetic Resonance Imaging in Takotsubo Syndrome. Circulation. 2022;146:1823-1835. doi: 0.1161/CIRCULATIONAHA.122.060375

5) **Joshi SS** and Dattani A (joint first authors), Yeo JL, Singh A, Brady EM, Parke KS, Arnold JR, Singh T, Kershaw LE, Spath NB, Reynolds RM, Forbes S, Gibb FW, Semple SI, Dweck MR, Newby DE, McCann GP, Gulsin GS. Impaired Myocardial Calcium Uptake in Patients with Diabetes Mellitus: A Manganese-Enhanced Cardiac Magnetic Resonance Study. JACC Cardiovasc Imaging. 2023; in press. doi: 10.1016/j.jcmg.2023.05.009.

6) **Joshi SS**, Singh T, Newby DE, Singh J. Sodium-glucose co-transporter 2 inhibitor therapy: mechanisms of action in heart failure. Heart 2021;107:1032-8. doi: 10.1136/heartjnl-2020-318060.

7) Joshi SS, Miller MR, Newby DE. Air pollution and cardiovascular disease: the Paul Wood Lecture, British Cardiovascular Society 2021. Heart. 2022;108:1267-1273. doi: 10.1136/heartjnl-2021-319844.

8) **Joshi SS**, Singh T, Singh J, Newby DE. Response to: Correspondence on “Sodium-glucose co-transporter 2 inhibitor therapy: mechanisms of action in heart failure” by Yalta et al. Heart 2021;107:1922-1923. doi: 10.1136/heartjnl-2021-320174.

9) **Joshi SS**, Stankovic I, Demirkiran A, Haugaa K, Maurovich-Horvat P, Popescu BA, Cosyns B, Edvardsen T, Petersen SE, Carvalho RF, Cameli M, Dweck MR. EACVI survey on burnout amongst cardiac imaging specialists during the 2019 coronavirus disease pandemic. Eur Heart J Cardiovasc Imaging. 2022;23:441-446. doi: 10.1093/ehjci/jeac002

10) Singh T, Kite TA, **Joshi SS**, Spath NB, Kershaw L, Baker A, Jordan H, Gulsin GS, Williams MC, van Beek EJR, Arnold JR, Semple SIK, Moss AJ, Newby DE, Dweck M, McCann GP. MRI and CT coronary angiography in survivors of COVID-19. Heart. 2022;108:46-53. doi: 10.1136/heartjnl-2021-319926.

11) Fletcher AJ, Tew YY, Tzolos E, **Joshi SS**, Kaczynski J, Nash J, Debono S, Lembo M, Kwiecinski J, Bing R, Syed MBJ, Doris MK, van Beek EJR, Moss AJ, Jenkins WS, Walker NL, Joshi NV, Pawade TA, Adamson PD, Whiteley WN, Wardlaw JM, Slomka PJ, Williams MC, Newby DE, Dweck MR. Thoracic Aortic 18F-Sodium Fluoride Activity and Ischemic Stroke in Patients with Established Cardiovascular Disease. JACC Cardiovasc Imaging. 2022;15:1274-1288. doi: 10.1016/j.jcmg.2021.12.013.

12) Sandeman D, Syed MBJ, Kimenai DM, Lee KK, Anand A, **Joshi SS**, Dinnel L, Wenham PR, Campbell K, Jarvie M, Galloway D, Anderson M, Roy B, Andrews JPM, Strachan FE, Ferry AV, Chapman AR, Elsby S, Francis M, Cargill R, Shah ASV, Mills NL. Implementation of an early rule-out pathway for myocardial infarction using a high-sensitivity cardiac troponin T assay. Open Heart. 2021;8:e001769. doi: 10.1136/openhrt-2021-001769.

13) Tsampasian V, Baral R, Chattopadhyay R, Debski M, **Joshi SS**, Reinhold J, Dweck MR, Garg P, Vassiliou VS. The Role of SGLT2 inhibitors in Heart Failure: A systematic Review and Meta-Analysis. Cardiol Res Pract. 2021:9927533. doi: 10.1155/2021/9927533.

14) Kwak S, Everett RJ, Treibel TA, Yang S, Hwang D, Ko T, Williams MC, Bing R, Singh T, **Joshi SS**, Lee H, Lee W, Kim YJ, Chin CWL, Fukui M, Al Musa T, Rigolli M, Singh A, Tastet L, Dobson LE, Wiesemann S, Ferreira VM, Captur G, Lee S, Schulz-Menger J, Schelbert EB, Clavel MA, Park SJ, Rheude T, Hadamitzky M, Gerber BL, Newby DE, Myerson SG, Pibarot P, Cavalcante JL, McCann GP, Greenwood JP, Moon JC, Dweck MR, Lee SP. Markers of Myocardial Damage Predict Mortality in Patients with Aortic Stenosis. J Am Coll Cardiol. 2021;78:545-558. doi: 10.1016/j.jacc.2021.05.047.

15) Singh T, **Joshi SS**, Kershaw L, Semple S, Dweck MR, Newby DE. Manganese Enhanced Magnetic Resonance Imaging of the Heart. J Magn Reson Imaging. 2023;57:1011-1028. doi: 10.1002/jmri.28499.

16) **Joshi SS**, Soliman-Aboumarie H, Cameli M, Michalski B, Manka R, Haugaa K, Demirkiran A, Podlesnikar T, Jurcut R, Muraru D, Badano LP, Dweck MR. EACVI Survey on the Multi-modality Imaging Assessment of the Right Heart . Eur Heart J Cardiovasc Imaging. 2022;23:1417-1422. doi: 10.1093/ehjci/jeac183.

17) Bennett M, **Joshi SS**, Denvir M. Factors affecting the cost and availability of travel insurance for patients with cardiac disease: a web-based case control study. J R Coll Physicians Edinb. 2020;50:233-240.

18) Lee KK, Bing R, Kiang J, Bashir S, Spath N, Stelzle D, Mortimer K, Bularga A, Doudesis D, **Joshi SS**, Strachan F, Gumy S, Adair-Rohani H, Attia EF, Chung MH, Miller MR, Newby DE, Mills NL, McAllister DA, Shah ASV. Adverse health effects associated with

household air pollution: a systematic review, metanalysis, and burden estimation study. Lancet Glob Health. 2020;8:e1427-e1434. doi: 10.1016/S2214-109X(20)30343-0

19) **Joshi SS**. RCPE Symposioum – Cardiology. J R Coll Physicians Edinb. 2020;50:90-91. doi: 10.4997/JRCPE.2020.123.

20) **Joshi SS**, Kadavath S, Mandoli GE, Gimelli A, Gulati M, Thamman R, Lundberg G, Mehran R, Mulvagh SL, Sade LE, Shivalkar B, Shaw LJ, Hristova K, Dweck MR, Almeida AG, Julia G. Women in Cardiovascular Imaging: A Call for Action to Address Ongoing Challenges. Eur Heart J Cardiovasc Imaging. 2023; in press. 10.1093/ehjci/jead158.

21) **Joshi SS**, Singh T, Kershaw LE, Gibb FW, Dweck MR, Williams M, Idris I, Semple S, Forbes S, Newby DE, Reynolds RM. Non-invasive imaging of functional pancreatic islet beta-cell mass in people with type 1 diabetes mellitus. Diabet Med. 2023;40:e15111. doi: 10.1111/dme.15111.

22) Sade LE, **Joshi SS**, Cameli M, Cosyns B, Delgado V, Donal E, Edvardsen T, Carvalho RF, Manka R, Podlesnikar T, Popescu BA, Hanzevacki JS, Sitges M, Dweck MR. Current Clinical Use of Speckle Tracking Strain Imaging: Insights from a Worldwide Survey from the European Association of Cardiovascular Imaging-EACVI. Eur Heart J Cardiovasc Imaging. 2023; in press. doi: 10.1093/ehjci/jead170.

Presentations during PhD

Oral

1) **Myocardial fibrosis activity in ischaemic and non-ischaemic cardiomyopathy. Late Breaking Clinical Trial.** EACVI Congress. **May 2023**.

2) **Fibrocalcific Score Assessment in Aortic Stenosis. Young Investigator Award Finalist.** British Society of Cardiovascular Imaging meeting. **September 2023.**

3) **Dysregulated myocardial calcium handling may be a driver of heart failure in Type 1 and Type 2 diabetes.** American Heart Association Conference. Chicago, United States of America. **November 2022**.

4) **Non-invasive imaging of functional pancreatic islet beta-cell mass in people with type 1 diabetes mellitus. Roger Wadsworth prize session finalist.** Scottish Cardiovascular forum meeting. **February 2023.**

5) **Non-invasive imaging of functional pancreatic islet beta-cell mass in people with type 1 diabetes mellitus. Early career researcher presentation winner.** CVS symposium. **June 2022**.

6) **Manganese Enhanced Magnetic Resonance Imaging in Cardiometabolic Disorders.** NRS Symposium. Glasgow, United Kingdom. **October 2022.**

Poster

1) **Quantitative computed tomography angiography for the evaluation of valvular fibrocalcific volume in aortic stenosis**. British Cardiovascular Society conference. **June 2023**.

2) Myocardial Fibrosis Activity in Heart Failure. European Society of Cardiology Congress. **August 2023**.

3) **Manganese Enhanced Magnetic Resonance Imaging in Type 1 and Type 2 Diabetes**. **Joshi SS**, Singh T, Kershaw LE, Spath N, Dattani A, Gulsin GS, Semple

SI, Williams MC, Gibb FW, Forbes S, Reynolds RM, McCann GP, Dweck MR, Newby DE. European Society of Cardiology Congress. Barcelona, Spain. **August 2022**.

4) **Non-Invasive Imaging of Pancreatic Islet Beta-Cell Function in People with Type 1 Diabetes. Joshi SS,** Singh T, Kershaw LE, Gibb FW, Dweck MR, Williams MC, Semple S, Forbes S, Reynolds RM and Newby DE. European Society of Endocrinology Conference. Milan, Italy. **May 2022.**

References

1. Sattar N, Gill JMR, Alazawi W. Improving prevention strategies for cardiometabolic disease. Nat Med [Internet]. 2020 Mar 9;26(3):320–5. Available from: https://www.nature.com/articles/s41591-020-0786-7
2. Miranda JJ, Barrientos-Gutiérrez T, Corvalan C, Hyder AA, Lazo-Porras M, Oni T, et al. Understanding the rise of cardiometabolic diseases in low- and middle-income countries. Nat Med [Internet]. 2019 Nov 7;25(11):1667–79. Available from: https://www.nature.com/articles/s41591-019-0644-7
3. Ndisang JF, Rastogi S. Cardiometabolic Diseases and Related Complications: Current Status and Future Perspective. Biomed Res Int [Internet]. 2013;2013:1–3. Available from: http://www.hindawi.com/journals/bmri/2013/467682/
4. WHO - Diabetes Mellitus. Available from: https://www.who.int/health-topics/diabetes#tab=tab_1
5. Karamanou M. Milestones in the history of diabetes mellitus: The main contributors. World J Diabetes [Internet]. 2016;7(1):1. Available from: http://www.wjgnet.com/1948-9358/full/v7/i1/1.htm
6. International Diabetes Federation reports. Available from: https://diabetesatlas.org/
7. Cho NH, Shaw JE, Karuranga S, Huang Y, da Rocha Fernandes JD, Ohlrogge AW, et al. IDF Diabetes Atlas: Global estimates of diabetes prevalence for 2017 and projections for 2045. Diabetes Res Clin Pract [Internet]. 2018 Apr;138:271–81. Available from: https://linkinghub.elsevier.com/retrieve/pii/S0168822718302031
8. Diabetes - WHO. Available from: https://www.who.int/news-room/fact-sheets/detail/diabetes#:~:text=In 2019%2C diabetes was the,of cardiovascular deaths (1).
9. 2. Classification and Diagnosis of Diabetes: Standards of Medical Care in Diabetes—2021. Diabetes Care [Internet]. 2021 Jan 1;44(Supplement_1):S15–33.

Available from: https://diabetesjournals.org/care/article/44/Supplement_1/S15/30859/2-Classification-and-Diagnosis-of-Diabetes

10. Diabetes UK statistics. Available from: https://www.diabetes.org.uk/professionals/position-statements-reports/statistics
11. Galicia-Garcia U, Benito-Vicente A, Jebari S, Larrea-Sebal A, Siddiqi H, Uribe KB, et al. Pathophysiology of Type 2 Diabetes Mellitus. Int J Mol Sci [Internet]. 2020 Aug 30;21(17):6275. Available from: https://www.mdpi.com/1422-0067/21/17/6275
12. Kahn SE, Cooper ME, Del Prato S. Pathophysiology and treatment of type 2 diabetes: perspectives on the past, present, and future. Lancet [Internet]. 2014 Mar;383(9922):1068–83. Available from: https://linkinghub.elsevier.com/retrieve/pii/S0140673613621546
13. Farmaki P, Damaskos C, Garmpis N, Garmpi A, Savvanis S, Diamantis E. Complications of the Type 2 Diabetes Mellitus. Curr Cardiol Rev [Internet]. 2021 Jul;16(4):249–51. Available from: https://www.eurekaselect.com/189582/article
14. 2. Classification and Diagnosis of Diabetes: Standards of Medical Care in Diabetes—2022. Diabetes Care [Internet]. 2022 Jan 1;45(Supplement_1):S17–38. Available from: https://diabetesjournals.org/care/article/45/Supplement_1/S17/138925/2-Classification-and-Diagnosis-of-Diabetes
15. Mobasseri M, Shirmohammadi M, Amiri T, Vahed N, Hosseini Fard H, Ghojazadeh M. Prevalence and incidence of type 1 diabetes in the world: a systematic review and meta-analysis. Heal Promot Perspect [Internet]. 2020 Mar 30;10(2):98–115. Available from: http://hpp.tbzmed.ac.ir/Article/hpp-31920
16. JDRF Type 1 diabetes facts. Available from: https://jdrf.org.uk/knowledge-support/about-type-1-diabetes/

17. Burrack AL, Martinov T, Fife BT. T Cell-Mediated Beta Cell Destruction: Autoimmunity and Alloimmunity in the Context of Type 1 Diabetes. Front Endocrinol (Lausanne) [Internet]. 2017 Dec 5;8. Available from: http://journal.frontiersin.org/article/10.3389/fendo.2017.00343/full

18. Chase HP, Voss MA, Butler-Simon N, Hoops S, O'Brien D, Dobersen MJ. Diagnosis of pre-type I diabetes. J Pediatr [Internet]. 1987 Dec;111(6):807–12. Available from: https://linkinghub.elsevier.com/retrieve/pii/S0022347687801920

19. Ginsberg-Fellner F. Triad of Markers for Identifying Children at High Risk of Developing Insulin-Dependent Diabetes Mellitus. JAMA J Am Med Assoc [Internet]. 1985 Sep 20;254(11):1469. Available from: http://jama.jamanetwork.com/article.aspx?doi=10.1001/jama.1985.03360110059024

20. Beer SF, Heaton DA, Alberti KGMM, Pyke DA, Leslie RDG. Impaired glucose tolerance precedes but does not predict insulin-dependent diabetes mellitus: a study of identical twins. Diabetologia [Internet]. 1990 Aug;33(8):497–502. Available from: http://link.springer.com/10.1007/BF00405112

21. Gepts W. Pathologic Anatomy of the Pancreas in Juvenile Diabetes Mellitus. Diabetes [Internet]. 1965 Oct 1;14(10):619–33. Available from: http://diabetes.diabetesjournals.org/cgi/doi/10.2337/diab.14.10.619

22. Pipeleers D, Ling Z. Pancreatic beta cells in insulin-dependent diabetes. Diabetes / Metab Rev [Internet]. 1992 Oct;8(3):209–27. Available from: http://doi.wiley.com/10.1002/dmr.5610080303

23. Butler AE, Galasso R, Meier JJ, Basu R, Rizza RA, Butler PC. Modestly increased beta cell apoptosis but no increased beta cell replication in recent-onset type 1 diabetic patients who died of diabetic ketoacidosis. Diabetologia [Internet]. 2007 Oct 1;50(11):2323–31. Available from: http://link.springer.com/10.1007/s00125-007-0794-x

24. Oram RA, Jones AG, Besser REJ, Knight BA, Shields BM, Brown RJ, et al. The majority of patients with long-duration type 1 diabetes are insulin microsecretors and have functioning beta cells. Diabetologia [Internet]. 2014 Jan 12;57(1):187–91. Available from: http://link.springer.com/10.1007/s00125-013-3067-x

25. Diabetes UK statistics. Available from: https://www.diabetes.org.uk/professionals/position-statements-reports/statistics#:~:text=Our data shows that more,by 148%2C591 from 2020-2021.

26. Leon BM. Diabetes and cardiovascular disease: Epidemiology, biological mechanisms, treatment recommendations and future research. World J Diabetes [Internet]. 2015;6(13):1246. Available from: http://www.wjgnet.com/1948-9358/full/v6/i13/1246.htm

27. Grundy SM, Benjamin IJ, Burke GL, Chait A, Eckel RH, Howard B V., et al. Diabetes and Cardiovascular Disease. Circulation [Internet]. 1999 Sep 7;100(10):1134–46. Available from: https://www.ahajournals.org/doi/10.1161/01.CIR.100.10.1134

28. Einarson TR, Acs A, Ludwig C, Panton UH. Prevalence of cardiovascular disease in type 2 diabetes: a systematic literature review of scientific evidence from across the world in 2007–2017. Cardiovasc Diabetol [Internet]. 2018 Dec 8;17(1):83. Available from: https://cardiab.biomedcentral.com/articles/10.1186/s12933-018-0728-6

29. Rana JS, Dunning A, Achenbach S, Al-Mallah M, Budoff MJ, Cademartiri F, et al. Differences in Prevalence, Extent, Severity, and Prognosis of Coronary Artery Disease Among Patients With and Without Diabetes Undergoing Coronary Computed Tomography Angiography. Diabetes Care [Internet]. 2012 Aug 1;35(8):1787–94. Available from: https://diabetesjournals.org/care/article/35/8/1787/29813/Differences-in-Prevalence-Extent-Severity-and

30. Kaur R, Kaur M, Singh J. Endothelial dysfunction and platelet hyperactivity in type 2

diabetes mellitus: molecular insights and therapeutic strategies. Cardiovasc Diabetol [Internet]. 2018 Dec 31;17(1):121. Available from: https://cardiab.biomedcentral.com/articles/10.1186/s12933-018-0763-3

31. Sugiyama T, Yamamoto E, Bryniarski K, Xing L, Fracassi F, Lee H, et al. Coronary Plaque Characteristics in Patients With Diabetes Mellitus Who Presented With Acute Coronary Syndromes. J Am Heart Assoc [Internet]. 2018 Jul 17;7(14). Available from: https://www.ahajournals.org/doi/10.1161/JAHA.118.009245
32. Association of the magnitude of weight loss and changes in physical fitness with long-term cardiovascular disease outcomes in overweight or obese people with type 2 diabetes: a post-hoc analysis of the Look AHEAD randomised clinical trial. Lancet Diabetes Endocrinol [Internet]. 2016 Nov;4(11):913–21. Available from: https://linkinghub.elsevier.com/retrieve/pii/S2213858716301620
33. Chen R, Ovbiagele B, Feng W. Diabetes and Stroke: Epidemiology, Pathophysiology, Pharmaceuticals and Outcomes. Am J Med Sci [Internet]. 2016 Apr;351(4):380–6. Available from: https://linkinghub.elsevier.com/retrieve/pii/S0002962915379337
34. Fowler P. The UK Prospective Diabetes study. Lancet [Internet]. 1998 Dec;352(9144):1933. Available from: https://linkinghub.elsevier.com/retrieve/pii/S0140673605604242
35. NHS. National Diabetes Audit 2016-17. Available from: https://digital.nhs.uk/data-and-information/publications/statistical/national-diabetes-audit/national-diabetes-audit-report-1-findings-and-recommendations-2016-17
36. Kenny HC, Abel ED. Heart Failure in Type 2 Diabetes Mellitus. Circ Res [Internet]. 2019 Jan 4;124(1):121–41. Available from: https://www.ahajournals.org/doi/10.1161/CIRCRESAHA.118.311371
37. Kannel WB. Diabetes and cardiovascular disease. The Framingham study. JAMA J

Am Med Assoc [Internet]. 1979 May 11;241(19):2035–8. Available from: http://jama.ama-assn.org/cgi/doi/10.1001/jama.241.19.2035

38. Aronow WS, Ahn C. Incidence of Heart Failure in 2,737 Older Persons With and Without Diabetes Mellitus. Chest [Internet]. 1999 Mar;115(3):867–8. Available from: https://linkinghub.elsevier.com/retrieve/pii/S001236921635663X

39. MacDonald MR, Petrie MC, Hawkins NM, Petrie JR, Fisher M, McKelvie R, et al. Diabetes, left ventricular systolic dysfunction, and chronic heart failure. Eur Heart J [Internet]. 2008 May;29(10):1224–40. Available from: https://academic.oup.com/eurheartj/article-lookup/doi/10.1093/eurheartj/ehn156

40. Udell JA, Cavender MA, Bhatt DL, Chatterjee S, Farkouh ME, Scirica BM. Glucose-lowering drugs or strategies and cardiovascular outcomes in patients with or at risk for type 2 diabetes: a meta-analysis of randomised controlled trials. Lancet Diabetes Endocrinol [Internet]. 2015 May;3(5):356–66. Available from: https://linkinghub.elsevier.com/retrieve/pii/S2213858715000443

41. Scirica BM, Bhatt DL, Braunwald E, Steg PG, Davidson J, Hirshberg B, et al. Saxagliptin and Cardiovascular Outcomes in Patients with Type 2 Diabetes Mellitus. N Engl J Med [Internet]. 2013 Oct 3;369(14):1317–26. Available from: http://www.nejm.org/doi/10.1056/NEJMoa1307684

42. Cosmi F, Shen L, Magnoli M, Abraham WT, Anand IS, Cleland JG, et al. Treatment with insulin is associated with worse outcome in patients with chronic heart failure and diabetes. Eur J Heart Fail [Internet]. 2018 May;20(5):888–95. Available from: http://doi.wiley.com/10.1002/ejhf.1146

43. Joshi SS, Singh T, Newby DE, Singh J. Sodium-glucose co-transporter 2 inhibitor therapy: mechanisms of action in heart failure. Heart [Internet]. 2021 Feb 26;heartjnl-2020-318060. Available from: https://heart.bmj.com/lookup/doi/10.1136/heartjnl-2020-318060

44. Jia G, Hill MA, Sowers JR. Diabetic Cardiomyopathy. Circ Res [Internet]. 2018 Feb 16;122(4):624–38. Available from: https://www.ahajournals.org/doi/10.1161/CIRCRESAHA.117.311586

45. Kannel WB, Hjortland M, Castelli WP. Role of diabetes in congestive heart failure: The Framingham study. Am J Cardiol [Internet]. 1974 Jul;34(1):29–34. Available from: https://linkinghub.elsevier.com/retrieve/pii/0002914974900897

46. Wilkens S. <scp>ATP</scp> Synthesis, Chemistry of. In: Wiley Encyclopedia of Chemical Biology [Internet]. Wiley; 2008. p. 0–0. Available from: https://onlinelibrary.wiley.com/doi/10.1002/9780470048672.wecb648

47. Gray S, Kim JK. New insights into insulin resistance in the diabetic heart. Trends Endocrinol Metab [Internet]. 2011 Oct;22(10):394–403. Available from: https://linkinghub.elsevier.com/retrieve/pii/S1043276011000737

48. Wei S, Binbin L, Yuan W, Zhong Z, Donghai L, Caihua H. β-Hydroxybutyrate in Cardiovascular Diseases : A Minor Metabolite of Great Expectations. Front Mol Biosci [Internet]. 2022 Jun 13;9. Available from: https://www.frontiersin.org/articles/10.3389/fmolb.2022.823602/full

49. Ranjbarvaziri S, Kooiker KB, Ellenberger M, Fajardo G, Zhao M, Vander Roest AS, et al. Altered Cardiac Energetics and Mitochondrial Dysfunction in Hypertrophic Cardiomyopathy. Circulation [Internet]. 2021 Nov 23;144(21):1714–31. Available from: https://www.ahajournals.org/doi/10.1161/CIRCULATIONAHA.121.053575

50. Ramesh P, Yeo JL, Brady EM, McCann GP. Role of inflammation in diabetic cardiomyopathy. Ther Adv Endocrinol Metab [Internet]. 2022 Jan 15;13:204201882210835. Available from: http://journals.sagepub.com/doi/10.1177/20420188221083530

51. Kuethe F, Sigusch H, Bornstein S, Hilbig K, Kamvissi V, Figulla H. Apoptosis in Patients with Dilated Cardiomyopathy and Diabetes: A Feature of Diabetic

Cardiomyopathy? Horm Metab Res [Internet]. 2007 Sep;39(9):672–6. Available from: http://www.thieme-connect.de/DOI/DOI?10.1055/s-2007-985823

52. Chen Y, Hua Y, Li X, Arslan IM, Zhang W, Meng G. Distinct Types of Cell Death and the Implication in Diabetic Cardiomyopathy. Front Pharmacol [Internet]. 2020 Feb 7;11. Available from: https://www.frontiersin.org/article/10.3389/fphar.2020.00042/full

53. Batista JPT, Faria AOV de, Ribeiro TFS, Simões e Silva AC. The Role of Renin–Angiotensin System in Diabetic Cardiomyopathy: A Narrative Review. Life [Internet]. 2023 Jul 21;13(7):1598. Available from: https://www.mdpi.com/2075-1729/13/7/1598

54. Jia G, Hill MA, Sowers JR. Diabetic Cardiomyopathy: An Update of Mechanisms Contributing to This Clinical Entity. Circ Res [Internet]. 2018 Feb 16;122(4):624–38. Available from: http://www.ncbi.nlm.nih.gov/pubmed/29449364

55. Khalid M, Petroianu G, Adem A. Advanced Glycation End Products and Diabetes Mellitus: Mechanisms and Perspectives. Biomolecules [Internet]. 2022 Apr 4;12(4):542. Available from: https://www.mdpi.com/2218-273X/12/4/542

56. Hartog JWL, Voors AA, Bakker SJL, Smit AJ, van Veldhuisen DJ. Advanced glycation end-products (AGEs) and heart failure: Pathophysiology and clinical implications. Eur J Heart Fail [Internet]. 2007 Dec 11;9(12):1146–55. Available from: https://onlinelibrary.wiley.com/doi/10.1016/j.ejheart.2007.09.009

57. Muir WW, Hamlin RL. Myocardial Contractility: Historical and Contemporary Considerations. Front Physiol [Internet]. 2020 Mar 31;11. Available from: https://www.frontiersin.org/article/10.3389/fphys.2020.00222/full

58. Lacombe VA, Viatchenko-Karpinski S, Terentyev D, Sridhar A, Emani S, Bonagura JD, et al. Mechanisms of impaired calcium handling underlying subclinical diastolic dysfunction in diabetes. Am J Physiol Integr Comp Physiol [Internet]. 2007 Nov;293(5):R1787–97. Available from: https://www.physiology.org/doi/10.1152/ajpregu.00059.2007

59. Fan W. Epidemiology in diabetes mellitus and cardiovascular disease. Cardiovasc Endocrinol [Internet]. 2017 Mar;6(1):8–16. Available from: https://journals.lww.com/01626549-201703000-00004

60. Kodama S, Fujihara K, Horikawa C, Sato T, Iwanaga M, Yamada T, et al. Diabetes mellitus and risk of new-onset and recurrent heart failure: a systematic review and meta-analysis. ESC Hear Fail [Internet]. 2020 Oct 29;7(5):2146–74. Available from: https://onlinelibrary.wiley.com/doi/10.1002/ehf2.12782

61. Suh J, Lee HI, Lee M, Song K, Choi HS, Kwon A, et al. Insulin Requirement and Complications Associated With Serum C-Peptide Decline in Patients With Type 1 Diabetes Mellitus During 15 Years After Diagnosis. Front Endocrinol (Lausanne) [Internet]. 2022 Apr 19;13. Available from: https://www.frontiersin.org/articles/10.3389/fendo.2022.869204/full

62. Pugliese A. Insulitis in the pathogenesis of type 1 diabetes. Pediatr Diabetes [Internet]. 2016 Jul 13;17(S22):31–6. Available from: https://onlinelibrary.wiley.com/doi/10.1111/pedi.12388

63. Jafri MS. Models of Excitation–Contraction Coupling in Cardiac Ventricular Myocytes. In 2012. p. 309–35. Available from: https://link.springer.com/10.1007/978-1-61779-965-5_14

64. Fu Z, Gilbert ER, Liu D. Regulation of insulin synthesis and secretion and pancreatic Beta-cell dysfunction in diabetes. Curr Diabetes Rev [Internet]. 2013 Jan 1;9(1):25–53. Available from: http://www.ncbi.nlm.nih.gov/pubmed/22974359

65. Klec C, Ziomek G, Pichler M, Malli R, Graier WF. Calcium Signaling in ß-cell Physiology and Pathology: A Revisit. Int J Mol Sci [Internet]. 2019 Dec 4;20(24):6110. Available from: https://www.mdpi.com/1422-0067/20/24/6110

66. Rorsman P, Ashcroft FM. Pancreatic β-Cell Electrical Activity and Insulin Secretion: Of Mice and Men. Physiol Rev [Internet]. 2018 Jan 1;98(1):117–214. Available from:

https://www.physiology.org/doi/10.1152/physrev.00008.2017

67. Aschner JL, Aschner M. Nutritional aspects of manganese homeostasis. Mol Aspects Med [Internet]. 2005 Aug;26(4–5):353–62. Available from: https://linkinghub.elsevier.com/retrieve/pii/S0098299705000385

68. Chen P. Manganese metabolism in humans. Front Biosci [Internet]. 2018;23(9):4665. Available from: https://imrpress.com/journal/FBL/23/9/10.2741/4665

69. Singh T, Joshi S, Kershaw LE, Dweck MR, Semple SI, Newby DE. <scp>Manganese-Enhanced</scp> Magnetic Resonance Imaging of the Heart. J Magn Reson Imaging [Internet]. 2022 Oct 31; Available from: https://onlinelibrary.wiley.com/doi/10.1002/jmri.28499

70. Spath NB, Thompson G, Baker AH, Dweck MR, Newby DE, Semple SIK. Manganese-enhanced MRI of the myocardium. Heart [Internet]. 2019 Nov;105(22):1695–700. Available from: http://www.ncbi.nlm.nih.gov/pubmed/31337670

71. Singh T, Joshi S, Kershaw LE, Dweck MR, Semple SI, Newby DE. <scp>Manganese-Enhanced</scp> Magnetic Resonance Imaging of the Heart. J Magn Reson Imaging [Internet]. 2023 Apr;57(4):1011–28. Available from: https://onlinelibrary.wiley.com/doi/10.1002/jmri.28499

72. Fernandes JL, Storey P, da Silva JA, de Figueiredo GS, Kalaf JM, Coelho OR. Preliminary assessment of cardiac short term safety and efficacy of manganese chloride for cardiovascular magnetic resonance in humans. J Cardiovasc Magn Reson [Internet]. 2011 Dec 14;13(1):6. Available from: https://jcmr-online.biomedcentral.com/articles/10.1186/1532-429X-13-6

73. Storey P, Danias PG, Post M, Li W, Seoane PR, Harnish PP, et al. Preliminary Evaluation of EVP 1001-1. Invest Radiol [Internet]. 2003 Oct;38(10):642–52.

Available from: https://journals.lww.com/00004424-200310000-00005

74. IC Targets [Internet]. Available from: https://ictargets.com/what-we-do/#mri

75. Wang X, Xu L, Ren Z, Fan M, Zhang J, Qi H, et al. A novel manganese chelated macromolecular MRI contrast agent based on O-carboxymethyl chitosan derivatives. Colloids Surfaces B Biointerfaces [Internet]. 2019 Nov;183:110452. Available from: https://linkinghub.elsevier.com/retrieve/pii/S092777651930596X

76. Spath N, Spath N, Papanastastiou G, Singh T, Gulsin G, Baker A, et al. MANGANESE-ENHANCED T1MAPPING IN NON-ISCHAEMIC CARDIOMYOPATHY. J Am Coll Cardiol [Internet]. 2020 Mar;75(11):1761. Available from: https://linkinghub.elsevier.com/retrieve/pii/S0735109720323883

77. Singh T, Joshi S, Kershaw LE, Baker AH, McCann GP, Dawson DK, et al. Manganese-Enhanced Magnetic Resonance Imaging in Takotsubo Syndrome. Circulation [Internet]. 2022 Dec 13;146(24):1823–35. Available from: https://www.ahajournals.org/doi/10.1161/CIRCULATIONAHA.122.060375

78. Dattani A, Joshi S, Yeo JL, Singh A, Brady EM, Parke KS, et al. Impaired Myocardial Calcium Uptake in Patients With Diabetes Mellitus. JACC Cardiovasc Imaging [Internet]. 2023 Jun; Available from: https://linkinghub.elsevier.com/retrieve/pii/S1936878X23002309

79. Andruska KM, Racette BA. Neuromythology of Manganism. Curr Epidemiol Reports [Internet]. 2015 Jun 7;2(2):143–8. Available from: http://link.springer.com/10.1007/s40471-015-0040-x

80. Taylor AJ, Salerno M, Dharmakumar R, Jerosch-Herold M. T1 Mapping. JACC Cardiovasc Imaging [Internet]. 2016 Jan;9(1):67–81. Available from: https://linkinghub.elsevier.com/retrieve/pii/S1936878X15008670

81. Patlak CS, Blasberg RG, Fenstermacher JD. Graphical Evaluation of Blood-to-Brain Transfer Constants from Multiple-Time Uptake Data. J Cereb Blood Flow Metab

[Internet]. 1983 Mar 29;3(1):1–7. Available from: http://journals.sagepub.com/doi/10.1038/jcbfm.1983.1

82. Skjold A, Kristoffersen A, Vangberg TR, Haraldseth O, Jynge P, Larsson HB. An apparent unidirectional influx constant for manganese as a measure of myocardial calcium channel activity. J Magn Reson Imaging [Internet]. 2006 Nov;24(5):1047–55. Available from: https://onlinelibrary.wiley.com/doi/10.1002/jmri.20736

83. Spath NB, Lilburn DML, Gray GA, Le Page LM, Papanastasiou G, Lennen RJ, et al. Manganese-Enhanced T 1 Mapping in the Myocardium of Normal and Infarcted Hearts. Contrast Media Mol Imaging [Internet]. 2018 Oct 25;2018:1–13. Available from: https://www.hindawi.com/journals/cmmi/2018/9641527/

84. Spath NB, Singh T, Papanastasiou G, Kershaw L, Baker AH, Janiczek RL, et al. Manganese-enhanced magnetic resonance imaging in dilated cardiomyopathy and hypertrophic cardiomyopathy. Eur Heart J Cardiovasc Imaging [Internet]. 2020 Nov 17; Available from: http://www.ncbi.nlm.nih.gov/pubmed/33200175

85. Szkudelski T. The mechanism of alloxan and streptozotocin action in B cells of the rat pancreas. Physiol Res [Internet]. 2001;50(6):537–46. Available from: http://www.ncbi.nlm.nih.gov/pubmed/11829314

86. Hernández-Sánchez C, Wood TL, LeRoith D. Developmental and Tissue-Specific Sulfonylurea Receptor Gene Expression. Endocrinology [Internet]. 1997 Feb 1;138(2):705–11. Available from: https://academic.oup.com/endo/article/138/2/705/2987361

87. Gomis A, Valdeolmillos M. Regulation by tolbutamide and diazoxide of the electrical activity in mouse pancreatic β -cells recorded in vivo. Br J Pharmacol [Internet]. 1998 Feb;123(3):443–8. Available from: http://doi.wiley.com/10.1038/sj.bjp.0701628

88. Yang S-N, Berggren P-O. The Role of Voltage-Gated Calcium Channels in Pancreatic β-Cell Physiology and Pathophysiology. Endocr Rev [Internet]. 2006 Oct

1;27(6):621–76. Available from: https://academic.oup.com/edrv/article/27/6/621/2355181

89. Botsikas D, Terraz S, Vinet L, Lamprianou S, Becker CD, Bosco D, et al. Pancreatic magnetic resonance imaging after manganese injection distinguishes type 2 diabetic and normoglycemic patients. Islets [Internet]. 4(3):243–8. Available from: http://www.ncbi.nlm.nih.gov/pubmed/22722479

90. Antkowiak PF, Stevens BK, Nunemaker CS, McDuffie M, Epstein FH. Manganese-enhanced magnetic resonance imaging detects declining pancreatic β-cell mass in a cyclophosphamide-accelerated mouse model of type 1 diabetes. Diabetes [Internet]. 2013 Jan;62(1):44–8. Available from: http://www.ncbi.nlm.nih.gov/pubmed/22933107

91. Rorsman P, Berggren PO, Hellman B. Manganese accumulation in pancreatic β -cells and its stimulation by glucose. Biochem J [Internet]. 1982 Feb 15;202(2):435–44. Available from: https://portlandpress.com/biochemj/article/202/2/435/13790/Manganese-accumulation-in-pancreatic-cells-and-its

92. Schultess J, van Duren C, Martens M, Costa M, Llop T, Martí T, et al. Diagnostic performance of the ARCHITECT C-Peptide immunoassay. Clin Chem Lab Med [Internet]. 2009 Jan 1;47(7). Available from: https://www.degruyter.com/document/doi/10.1515/CCLM.2009.185/html

93. Larsen MO, Rolin B, Wilken M, Carr RD, Gotfredsen CF. Measurements of Insulin Secretory Capacity and Glucose Tolerance to Predict Pancreatic -Cell Mass In Vivo in the Nicotinamide/Streptozotocin Gottingen Minipig, a Model of Moderate Insulin Deficiency and Diabetes. Diabetes [Internet]. 2003 Jan 1;52(1):118–23. Available from: http://diabetes.diabetesjournals.org/cgi/doi/10.2337/diabetes.52.1.118

94. NICE, NG17, 2015. Available from: https://www.nice.org.uk/guidance/ng17

95. NICE, NG28, 2015. Available from: https://www.nice.org.uk/guidance/ng28

96. Marwick TH. Ejection Fraction Pros and Cons. J Am Coll Cardiol [Internet]. 2018 Nov;72(19):2360–79. Available from: https://linkinghub.elsevier.com/retrieve/pii/S0735109718383542

97. Lang RM, Badano LP, Mor-Avi V, Afilalo J, Armstrong A, Ernande L, et al. Recommendations for Cardiac Chamber Quantification by Echocardiography in Adults: An Update from the American Society of Echocardiography and the European Association of Cardiovascular Imaging. Eur Hear J – Cardiovasc Imaging [Internet]. 2015 Mar;16(3):233–71. Available from: https://academic.oup.com/ehjcimaging/article-lookup/doi/10.1093/ehjci/jev014

98. Klaeboe LG, Edvardsen T. Echocardiographic assessment of left ventricular systolic function. J Echocardiogr [Internet]. 2019 Mar 2;17(1):10–6. Available from: http://link.springer.com/10.1007/s12574-018-0405-5

99. Malik SB, Chen N, Parker RA, Hsu JY. Transthoracic Echocardiography: Pitfalls and Limitations as Delineated at Cardiac CT and MR Imaging. RadioGraphics [Internet]. 2017 Mar;37(2):383–406. Available from: http://pubs.rsna.org/doi/10.1148/rg.2017160105

100. Wharton G, Steeds R, Allen J, Phillips H, Jones R, Kanagala P, et al. A minimum dataset for a standard adult transthoracic echocardiogram: a guideline protocol from the British Society of Echocardiography. Echo Res Pract [Internet]. 2015 Mar 1;2(1):G9–24. Available from: https://echo.biomedcentral.com/articles/10.1530/ERP-14-0079

101. Kosaraju A, Goyal A, Grigorova Y, Makaryus AN. Left Ventricular Ejection Fraction [Internet]. StatPearls. 2023. Available from: http://www.ncbi.nlm.nih.gov/pubmed/25559473

102. Grover VPB, Tognarelli JM, Crossey MME, Cox IJ, Taylor-Robinson SD, McPhail

MJW. Magnetic Resonance Imaging: Principles and Techniques: Lessons for Clinicians. J Clin Exp Hepatol [Internet]. 2015 Sep;5(3):246–55. Available from: https://linkinghub.elsevier.com/retrieve/pii/S0973688315004156

103. Aherne E, Chow K, Carr J. Cardiac T 1 mapping: Techniques and applications. J Magn Reson Imaging [Internet]. 2020 May 23;51(5):1336–56. Available from: https://onlinelibrary.wiley.com/doi/10.1002/jmri.26866

104. Burt JR, Zimmerman SL, Kamel IR, Halushka M, Bluemke DA. Myocardial T1 Mapping: Techniques and Potential Applications. RadioGraphics [Internet]. 2014 Mar;34(2):377–95. Available from: http://pubs.rsna.org/doi/10.1148/rg.342125121

105. Radenkovic D, Weingärtner S, Ricketts L, Moon JC, Captur G. T1 mapping in cardiac MRI. Heart Fail Rev [Internet]. 2017 Jul 16;22(4):415–30. Available from: http://link.springer.com/10.1007/s10741-017-9627-2

106. Child N, Suna G, Dabir D, Yap M-L, Rogers T, Kathirgamanathan M, et al. Comparison of MOLLI, shMOLLLI, and SASHA in discrimination between health and disease and relationship with histologically derived collagen volume fraction. Eur Hear J - Cardiovasc Imaging [Internet]. 2018 Jul 1;19(7):768–76. Available from: https://academic.oup.com/ehjcimaging/article/19/7/768/4725042

107. Chin CWL, Semple S, Malley T, White AC, Mirsadraee S, Weale PJ, et al. Optimization and comparison of myocardial T1 techniques at 3T in patients with aortic stenosis. Eur Hear J - Cardiovasc Imaging [Internet]. 2014 May;15(5):556–65. Available from: https://academic.oup.com/ehjcimaging/article-lookup/doi/10.1093/ehjci/jet245

108. Bluemke DA, Kronmal RA, Lima JAC, Liu K, Olson J, Burke GL, et al. The Relationship of Left Ventricular Mass and Geometry to Incident Cardiovascular Events. J Am Coll Cardiol [Internet]. 2008 Dec;52(25):2148–55. Available from: https://linkinghub.elsevier.com/retrieve/pii/S0735109708032312

109. Gjesdal O, Almeida ALC, Hopp E, Beitnes JO, Lunde K, Smith H, et al. Long axis strain by MRI and echocardiography in a postmyocardial infarct population. J Magn Reson Imaging [Internet]. 2014 Nov 8;40(5):1247–51. Available from: https://onlinelibrary.wiley.com/doi/10.1002/jmri.24485
110. Pohost GM, Hung L, Doyle M. Clinical Use of Cardiovascular Magnetic Resonance. Circulation [Internet]. 2003 Aug 12;108(6):647–53. Available from: https://www.ahajournals.org/doi/10.1161/01.CIR.0000083233.86078.3E
111. BOTTINI P, CARR A, PRISANT L, FLICKINGER F, ALLISON J, GOTTDIENER J. Magnetic resonance imaging compared to echocardiography to assess left ventricular mass in the hypertensive patient. Am J Hypertens [Internet]. 1995 Mar;8(3):221–8. Available from: https://academic.oup.com/ajh/article-lookup/doi/10.1016/0895-7061(94)00178-E
112. Katz J, Milliken MC, Stray-Gundersen J, Buja LM, Parkey RW, Mitchell JH, et al. Estimation of human myocardial mass with MR imaging. Radiology [Internet]. 1988 Nov;169(2):495–8. Available from: http://pubs.rsna.org/doi/10.1148/radiology.169.2.2971985
113. Shapiro EP, Rogers WJ, Beyar R, Soulen RL, Zerhouni EA, Lima JA, et al. Determination of left ventricular mass by magnetic resonance imaging in hearts deformed by acute infarction. Circulation [Internet]. 1989 Mar;79(3):706–11. Available from: https://www.ahajournals.org/doi/10.1161/01.CIR.79.3.706
114. Myerson SG, Bellenger NG, Pennell DJ. Assessment of Left Ventricular Mass by Cardiovascular Magnetic Resonance. Hypertension [Internet]. 2002 Mar;39(3):750–5. Available from: https://www.ahajournals.org/doi/10.1161/hy0302.104674
115. Bellenger N, Davies LC, Francis J, Coats A, Pennell D. Reduction in Sample Size for Studies of Remodeling in Heart Failure by the Use of Cardiovascular Magnetic Resonance. J Cardiovasc Magn Reson [Internet]. 2000 Nov 1;2(4):271–8. Available

from:
http://www.informaworld.com/openurl?genre=article&doi=10.3109/10976640009148691&magic=crossref%7C%7CD404A21C5BB053405B1A640AFFD44AE3

116. Semelka RC, Tomei E, Wagner S, Mayo J, Kondo C, Suzuki J, et al. Normal left ventricular dimensions and function: interstudy reproducibility of measurements with cine MR imaging. Radiology [Internet]. 1990 Mar;174(3):763–8. Available from: http://pubs.rsna.org/doi/10.1148/radiology.174.3.2305059
117. Matheijssen NAA, Baur LHB, Reiber JHC, van der Velde EA, van Dijkman PRM, van der Geest RJ, et al. Assessment of left ventricular volume and mass by cine magnetic resonance imaging in patients with anterior myocardial infarction intra-observer and inter-observer variability on contour detection. Int J Card Imaging [Internet]. 1996 Mar;12(1):11–9. Available from: http://link.springer.com/10.1007/BF01798113
118. Grothues F, Smith GC, Moon JC., Bellenger NG, Collins P, Klein HU, et al. Comparison of interstudy reproducibility of cardiovascular magnetic resonance with two-dimensional echocardiography in normal subjects and in patients with heart failure or left ventricular hypertrophy. Am J Cardiol [Internet]. 2002 Jul;90(1):29–34. Available from: https://linkinghub.elsevier.com/retrieve/pii/S0002914902023810
119. Rogers T, Dabir D, Mahmoud I, Voigt T, Schaeffter T, Nagel E, et al. Standardization of T1 measurements with MOLLI in differentiation between health and disease – the ConSept study. J Cardiovasc Magn Reson [Internet]. 2013 Dec 11;15(1):78. Available from: https://jcmr-online.biomedcentral.com/articles/10.1186/1532-429X-15-78
120. Piechnik SK, Ferreira VM, Dall'Armellina E, Cochlin LE, Greiser A, Neubauer S, et al. Shortened Modified Look-Locker Inversion recovery (ShMOLLI) for clinical myocardial T1-mapping at 1.5 and 3 T within a 9 heartbeat breathhold. J Cardiovasc

Magn Reson [Internet]. 2010 Dec 19;12(1):69. Available from: https://jcmr-online.biomedcentral.com/articles/10.1186/1532-429X-12-69

121. Messroghli DR, Plein S, Higgins DM, Walters K, Jones TR, Ridgway JP, et al. Human Myocardium: Single-Breath-hold MR T1 Mapping with High Spatial Resolution—Reproducibility Study. Radiology [Internet]. 2006 Mar;238(3):1004–12. Available from: http://pubs.rsna.org/doi/10.1148/radiol.2382041903
122. Japp AG, Gulati A, Cook SA, Cowie MR, Prasad SK. The Diagnosis and Evaluation of Dilated Cardiomyopathy. J Am Coll Cardiol [Internet]. 2016 Jun;67(25):2996–3010. Available from: https://linkinghub.elsevier.com/retrieve/pii/S0735109716329187
123. Rickers C, Wilke NM, Jerosch-Herold M, Casey SA, Panse P, Panse N, et al. Utility of Cardiac Magnetic Resonance Imaging in the Diagnosis of Hypertrophic Cardiomyopathy. Circulation [Internet]. 2005 Aug 9;112(6):855–61. Available from: https://www.ahajournals.org/doi/10.1161/CIRCULATIONAHA.104.507723
124. Dass S, Suttie JJ, Piechnik SK, Ferreira VM, Holloway CJ, Banerjee R, et al. Myocardial Tissue Characterization Using Magnetic Resonance Noncontrast T1 Mapping in Hypertrophic and Dilated Cardiomyopathy. Circ Cardiovasc Imaging [Internet]. 2012 Nov;5(6):726–33. Available from: https://www.ahajournals.org/doi/10.1161/CIRCIMAGING.112.976738
125. Alba AC, Gaztañaga J, Foroutan F, Thavendiranathan P, Merlo M, Alonso-Rodriguez D, et al. Prognostic Value of Late Gadolinium Enhancement for the Prediction of Cardiovascular Outcomes in Dilated Cardiomyopathy. Circ Cardiovasc Imaging [Internet]. 2020 Apr;13(4). Available from: https://www.ahajournals.org/doi/10.1161/CIRCIMAGING.119.010105
126. Greulich S, Seitz A, Herter D, Günther F, Probst S, Bekeredjian R, et al. Long-term risk of sudden cardiac death in hypertrophic cardiomyopathy: a cardiac magnetic

resonance outcome study. Eur Hear J - Cardiovasc Imaging [Internet]. 2021 Jun 22;22(7):732–41. Available from: https://academic.oup.com/ehjcimaging/article/22/7/732/6103204

127. Migrino RQ, Christenson R, Szabo A, Bright M, Truran S, Hari P. Prognostic implication of late gadolinium enhancement on cardiac MRI in light chain (AL) amyloidosis on long term follow up. BMC Med Phys [Internet]. 2009 Dec 5;9(1):5. Available from: http://bmcmedphys.biomedcentral.com/articles/10.1186/1756-6649-9-5

128. Murphy DT, Shine SC, Cradock A, Galvin JM, Keelan ET, Murray JG. Cardiac MRI in Arrhythmogenic Right Ventricular Cardiomyopathy. Am J Roentgenol [Internet]. 2010 Apr;194(4):W299–306. Available from: https://www.ajronline.org/doi/10.2214/AJR.09.3450

129. Tower-Rader A, Jaber WA. Multimodality Imaging Assessment of Fabry Disease. Circ Cardiovasc Imaging [Internet]. 2019 Nov;12(11). Available from: https://www.ahajournals.org/doi/10.1161/CIRCIMAGING.119.009013

130. Wendland MF. Applications of manganese-enhanced magnetic resonance imaging (MEMRI) to imaging of the heart. NMR Biomed [Internet]. 2004 Nov;17(8):581–94. Available from: http://doi.wiley.com/10.1002/nbm.943

131. KANG YS, GORE JC. Studies of Tissue NMR Relaxation Enhancement by Manganese. Invest Radiol [Internet]. 1984 Sep;19(5):399–407. Available from: http://journals.lww.com/00004424-198409000-00012

132. Jynge P, Skjold AM, Falkmer U, Andersson RGG, Seland JG, Bruvold M, et al. MnDPDP: Contrast Agent for Imaging and Protection of Viable Tissue. Contrast Media Mol Imaging [Internet]. 2020 Sep 10;2020:1–17. Available from: https://www.hindawi.com/journals/cmmi/2020/3262835/

133. Skjold A, Kristoffersen A, Vangberg TR, Haraldseth O, Jynge P, Larsson HB. An

apparent unidirectional influx constant for manganese as a measure of myocardial calcium channel activity. J Magn Reson Imaging [Internet]. 2006 Nov;24(5):1047–55. Available from: http://doi.wiley.com/10.1002/jmri.20736

134. Spath N, Tavares A, Gray GA, Baker AH, Lennen RJ, Alcaide-Corral CJ, et al. Manganese-enhanced T1 mapping to quantify myocardial viability: validation with 18F-fluorodeoxyglucose positron emission tomography. Sci Rep [Internet]. 2020 Feb 6;10(1):2018. Available from: https://www.nature.com/articles/s41598-020-58716-x

135. Spath NB, Singh T, Papanastasiou G, Baker A, Janiczek RJ, McCann GP, et al. Assessment of stunned and viable myocardium using manganese-enhanced MRI. Open Hear [Internet]. 2021 Jun 7;8(1):e001646. Available from: https://openheart.bmj.com/lookup/doi/10.1136/openhrt-2021-001646

136. Thygesen K, Alpert JS, Jaffe AS, Simoons ML, Chaitman BR, White HD, et al. Third universal definition of myocardial infarction. Eur Heart J [Internet]. 2012 Oct 1;33(20):2551–67. Available from: https://academic.oup.com/eurheartj/article/33/20/2551/447556

137. Bozkurt B, Colvin M, Cook J, Cooper LT, Deswal A, Fonarow GC, et al. Current Diagnostic and Treatment Strategies for Specific Dilated Cardiomyopathies: A Scientific Statement From the American Heart Association. Circulation [Internet]. 2016 Dec 6;134(23). Available from: https://www.ahajournals.org/doi/10.1161/CIR.0000000000000455

138. 2014 ESC Guidelines on diagnosis and management of hypertrophic cardiomyopathy. Eur Heart J [Internet]. 2014 Oct 14;35(39):2733–79. Available from: https://academic.oup.com/eurheartj/article-lookup/doi/10.1093/eurheartj/ehu284

139. Messroghli DR, Greiser A, Fröhlich M, Dietz R, Schulz-Menger J. Optimization and validation of a fully-integrated pulse sequence for modified look-locker inversion-recovery (MOLLI) T1 mapping of the heart. J Magn Reson Imaging [Internet]. 2007

Oct 25;26(4):1081–6. Available from: https://onlinelibrary.wiley.com/doi/10.1002/jmri.21119

140. Messroghli DR, Radjenovic A, Kozerke S, Higgins DM, Sivananthan MU, Ridgway JP. Modified Look-Locker inversion recovery (MOLLI) for high-resolutionT1 mapping of the heart. Magn Reson Med [Internet]. 2004 Jul;52(1):141–6. Available from: https://onlinelibrary.wiley.com/doi/10.1002/mrm.20110
141. Bulluck H, White SK, Rosmini S, Bhuva A, Treibel TA, Fontana M, et al. T1 mapping and T2 mapping at 3T for quantifying the area-at-risk in reperfused STEMI patients. J Cardiovasc Magn Reson [Internet]. 2015 Dec 12;17(1):73. Available from: http://jcmr-online.com/content/17/1/73
142. Singh T, Kite TA, Joshi SS, Spath NB, Kershaw L, Baker A, et al. MRI and CT coronary angiography in survivors of COVID-19. Heart [Internet]. 2022 Jan;108(1):46–53. Available from: https://heart.bmj.com/lookup/doi/10.1136/heartjnl-2021-319926
143. aus dem Siepen F, Baumgärtner C, Müller-Henessen M, André F, Messroghli D, Ochs M, et al. Variability of cardiovascular magnetic resonance (CMR) T1 mapping parameters in healthy volunteers during long-term follow-up. Open Hear [Internet]. 2018 Feb 24;5(1):e000717. Available from: https://openheart.bmj.com/lookup/doi/10.1136/openhrt-2017-000717
144. Kellman P, Hansen MS. T1-mapping in the heart: accuracy and precision. J Cardiovasc Magn Reson [Internet]. 2014 Dec 4;16(1):2. Available from: https://jcmr-online.biomedcentral.com/articles/10.1186/1532-429X-16-2
145. Singh A, Greenwood JP, Berry C, Dawson DK, Hogrefe K, Kelly DJ, et al. Comparison of exercise testing and CMR measured myocardial perfusion reserve for predicting outcome in asymptomatic aortic stenosis: the PRognostic Importance of MIcrovascular Dysfunction in Aortic Stenosis (PRIMID AS) Study. Eur Heart J

[Internet]. 2017 Apr 21;38(16):1222–9. Available from: https://academic.oup.com/eurheartj/article/38/16/1222/2993227

146. Lin K, Suwa K, Ma H, Collins JD, Markl M, Carr JC. Variability of native T1 values: implication for defining regional myocardial changes using MRI. Int J Cardiovasc Imaging [Internet]. 2018 Oct 22;34(10):1637–45. Available from: http://link.springer.com/10.1007/s10554-018-1371-8

147. Dabir D, Child N, Kalra A, Rogers T, Gebker R, Jabbour A, et al. Reference values for healthy human myocardium using a T1 mapping methodology: results from the International T1 Multicenter cardiovascular magnetic resonance study. J Cardiovasc Magn Reson [Internet]. 2014 Dec 21;16(1):69. Available from: https://jcmr-online.biomedcentral.com/articles/10.1186/s12968-014-0069-x

148. Gulsin GS, Athithan L, McCann GP. Diabetic cardiomyopathy: prevalence, determinants and potential treatments. Ther Adv Endocrinol Metab [Internet]. 2019 Jan 27;10:204201881983486. Available from: http://journals.sagepub.com/doi/10.1177/2042018819834869

149. Seferović PM, Paulus WJ. Clinical diabetic cardiomyopathy: a two-faced disease with restrictive and dilated phenotypes. Eur Heart J [Internet]. 2015 Jul 14;36(27):1718–27. Available from: https://academic.oup.com/eurheartj/article-lookup/doi/10.1093/eurheartj/ehv134

150. Salvatore T, Pafundi PC, Galiero R, Albanese G, Di Martino A, Caturano A, et al. The Diabetic Cardiomyopathy: The Contributing Pathophysiological Mechanisms. Front Med [Internet]. 2021 Jun 30;8. Available from: https://www.frontiersin.org/articles/10.3389/fmed.2021.695792/full

151. Piepoli MF, Adamo M, Barison A, Bestetti RB, Biegus J, Böhm M, et al. Preventing heart failure: a position paper of the Heart Failure Association in collaboration with the European Association of Preventive Cardiology. Eur J Heart Fail [Internet]. 2022

Jan 27;24(1):143–68. Available from: https://onlinelibrary.wiley.com/doi/10.1002/ejhf.2351

152. NHS. National Diabetes Audit, 2015-2016. Available from: https://digital.nhs.uk/data-and-information/publications/statistical/national-diabetes-audit/national-diabetes-audit-2015-2016-report-1-care-processes-and-treatment-targets

153. Dunlay SM, Givertz MM, Aguilar D, Allen LA, Chan M, Desai AS, et al. Type 2 Diabetes Mellitus and Heart Failure: A Scientific Statement From the American Heart Association and the Heart Failure Society of America: This statement does not represent an update of the 2017 ACC/AHA/HFSA heart failure guideline update. Circulation [Internet]. 2019 Aug 13;140(7). Available from: https://www.ahajournals.org/doi/10.1161/CIR.0000000000000691

154. Lebeche D, Davidoff AJ, Hajjar RJ. Interplay between impaired calcium regulation and insulin signaling abnormalities in diabetic cardiomyopathy. Nat Clin Pract Cardiovasc Med [Internet]. 2008 Nov 23;5(11):715–24. Available from: https://www.nature.com/articles/ncpcardio1347

155. BRACKEN N, HOWARTH FC, SINGH J. Effects of Streptozotocin-Induced Diabetes on Contraction and Calcium Transport in Rat Ventricular Cardiomyocytes. Ann N Y Acad Sci [Internet]. 2006 Nov 28;1084(1):208–22. Available from: https://nyaspubs.onlinelibrary.wiley.com/doi/10.1196/annals.1372.018

156. Gulsin GS, Swarbrick DJ, Athithan L, Brady EM, Henson J, Baldry E, et al. Effects of Low-Energy Diet or Exercise on Cardiovascular Function in Working-Age Adults With Type 2 Diabetes: A Prospective, Randomized, Open-Label, Blinded End Point Trial. Diabetes Care [Internet]. 2020 Jun 1;43(6):1300–10. Available from: https://diabetesjournals.org/care/article/43/6/1300/35663/Effects-of-Low-Energy-Diet-or-Exercise-on

157. McAllister DA, Read SH, Kerssens J, Livingstone S, McGurnaghan S, Jhund P, et al.

Incidence of Hospitalization for Heart Failure and Case-Fatality Among 3.25 Million People With and Without Diabetes Mellitus. Circulation [Internet]. 2018 Dec 11;138(24):2774–86. Available from: https://www.ahajournals.org/doi/10.1161/CIRCULATIONAHA.118.034986

158. Ohkuma T, Komorita Y, Peters SAE, Woodward M. Diabetes as a risk factor for heart failure in women and men: a systematic review and meta-analysis of 47 cohorts including 12 million individuals. Diabetologia [Internet]. 2019 Sep 18;62(9):1550–60. Available from: http://link.springer.com/10.1007/s00125-019-4926-x
159. Bozkurt B, Coats AJ, Tsutsui H, Abdelhamid M, Adamopoulos S, Albert N, et al. Universal Definition and Classification of Heart Failure. J Card Fail [Internet]. 2021 Apr;27(4):387–413. Available from: https://linkinghub.elsevier.com/retrieve/pii/S1071916421000506
160. Pop-Busui R, Januzzi JL, Bruemmer D, Butalia S, Green JB, Horton WB, et al. Heart Failure: An Underappreciated Complication of Diabetes. A Consensus Report of the American Diabetes Association. Diabetes Care [Internet]. 2022 Jul 7;45(7):1670–90. Available from: https://diabetesjournals.org/care/article/45/7/1670/147048/Heart-Failure-An-Underappreciated-Complication-of
161. Zaccardi F, Webb DR, Yates T, Davies MJ. Pathophysiology of type 1 and type 2 diabetes mellitus: a 90-year perspective. Postgrad Med J [Internet]. 2016 Feb 1;92(1084):63–9. Available from: https://academic.oup.com/pmj/article/92/1084/63/6984286
162. Bidasee KR, Nallani K, Yu Y, Cocklin RR, Zhang Y, Wang M, et al. Chronic Diabetes Increases Advanced Glycation End Products on Cardiac Ryanodine Receptors/Calcium-Release Channels. Diabetes [Internet]. 2003 Jul 1;52(7):1825–36. Available from:

https://diabetesjournals.org/diabetes/article/52/7/1825/14233/Chronic-Diabetes-Increases-Advanced-Glycation-End

163. Bidasee KR, Zhang Y, Shao CH, Wang M, Patel KP, Dincer UD, et al. Diabetes Increases Formation of Advanced Glycation End Products on Sarco(endo)plasmic Reticulum Ca2+-ATPase. Diabetes [Internet]. 2004 Feb 1;53(2):463–73. Available from: https://diabetesjournals.org/diabetes/article/53/2/463/11484/Diabetes-Increases-Formation-of-Advanced-Glycation

164. Nieves-Cintrón M, Flores-Tamez VA, Le T, Baudel MM-A, Navedo MF. Cellular and molecular effects of hyperglycemia on ion channels in vascular smooth muscle. Cell Mol Life Sci [Internet]. 2021 Jan 27;78(1):31–61. Available from: https://link.springer.com/10.1007/s00018-020-03582-z

165. Ochi R. The slow inward current and the action of manganese ions in guinea-pig's myocardium. Pfl□gers Arch Eur J Physiol [Internet]. 1970;316(1):81–94. Available from: http://link.springer.com/10.1007/BF00587898

166. Ochi R. Manganese-dependent propagated action potentials and their depression by electrical stimulation in guinea-pig myocardium perfused by sodium-free media. J Physiol [Internet]. 1976 Dec 1;263(2):139–56. Available from: https://onlinelibrary.wiley.com/doi/10.1113/jphysiol.1976.sp011625

167. Hu TC -C., Pautler RG, MacGowan GA, Koretsky AP. Manganese-enhanced MRI of mouse heart during changes in inotropy†. Magn Reson Med [Internet]. 2001 Nov 18;46(5):884–90. Available from: https://onlinelibrary.wiley.com/doi/10.1002/mrm.1273

168. Eriksson R, Johansson L, Bjerner T, Ahlström H. Dobutamine-induced stress affects intracellular uptake of manganese: A quantitative magnetic resonance imaging study in pigs. J Magn Reson Imaging [Internet]. 2005 Apr 18;21(4):360–4. Available from: https://onlinelibrary.wiley.com/doi/10.1002/jmri.20279

169. Xiao Y-F, Nikolskaya A, Jaye DA, Sigg DC. Glucagon-like peptide-1 enhances cardiac L-type Ca2+ currents via activation of the cAMP-dependent protein kinase A pathway. Cardiovasc Diabetol [Internet]. 2011;10(1):6. Available from: http://cardiab.biomedcentral.com/articles/10.1186/1475-2840-10-6
170. Khan MS, Fonarow GC, McGuire DK, Hernandez AF, Vaduganathan M, Rosenstock J, et al. Glucagon-Like Peptide 1 Receptor Agonists and Heart Failure. Circulation [Internet]. 2020 Sep 22;142(12):1205–18. Available from: https://www.ahajournals.org/doi/10.1161/CIRCULATIONAHA.120.045888
171. Joshi SS, Singh T, Newby DE, Singh J. Sodium-glucose co-transporter 2 inhibitor therapy: mechanisms of action in heart failure. Heart [Internet]. 2021 Jul;107(13):1032–8. Available from: https://heart.bmj.com/lookup/doi/10.1136/heartjnl-2020-318060
172. IDF Diabetes Atlas. Available from: https://diabetesatlas.org/
173. Deshpande AD, Harris-Hayes M, Schootman M. Epidemiology of Diabetes and Diabetes-Related Complications. Phys Ther [Internet]. 2008 Nov 1;88(11):1254–64. Available from: https://academic.oup.com/ptj/article/88/11/1254/2858146
174. Rosano GM, Vitale C, Seferovic P. Heart Failure in Patients with Diabetes Mellitus. Card Fail Rev [Internet]. 2017;03(01):52. Available from: https://www.cfrjournal.com/articleindex/cfr.2016:20:2
175. Martín-Timón I. Type 2 diabetes and cardiovascular disease: Have all risk factors the same strength? World J Diabetes [Internet]. 2014;5(4):444. Available from: http://www.wjgnet.com/1948-9358/full/v5/i4/444.htm
176. Boudina S, Abel ED. Diabetic cardiomyopathy, causes and effects. Rev Endocr Metab Disord [Internet]. 2010 Mar 24;11(1):31–9. Available from: http://link.springer.com/10.1007/s11154-010-9131-7
177. Sheikh AQ, Hurley JR, Huang W, Taghian T, Kogan A, Cho H, et al. Diabetes Alters

Intracellular Calcium Transients in Cardiac Endothelial Cells. Fadini GP, editor. PLoS One [Internet]. 2012 May 9;7(5):e36840. Available from: https://dx.plos.org/10.1371/journal.pone.0036840

178. Kong MG, Jang SY, Jang J, Cho H-J, Lee S, Lee SE, et al. Impact of diabetes mellitus on mortality in patients with acute heart failure: a prospective cohort study. Cardiovasc Diabetol [Internet]. 2020 Dec 2;19(1):49. Available from: https://cardiab.biomedcentral.com/articles/10.1186/s12933-020-01026-3

179. Bahtiyar G, Gutterman D, Lebovitz H. Heart Failure: a Major Cardiovascular Complication of Diabetes Mellitus. Curr Diab Rep [Internet]. 2016 Nov 12;16(11):116. Available from: http://link.springer.com/10.1007/s11892-016-0809-4

180. Pereira L, Matthes J, Schuster I, Valdivia HH, Herzig S, Richard S, et al. Mechanisms of [Ca2+]i Transient Decrease in Cardiomyopathy of db / db Type 2 Diabetic Mice. Diabetes [Internet]. 2006 Mar 1;55(3):608–15. Available from: https://diabetesjournals.org/diabetes/article/55/3/608/12755/Mechanisms-of-Ca2-i-Transient-Decrease-in

181. Sutanto H, Lyon A, Lumens J, Schotten U, Dobrev D, Heijman J. Cardiomyocyte calcium handling in health and disease: Insights from in vitro and in silico studies. Prog Biophys Mol Biol [Internet]. 2020 Nov;157:54–75. Available from: https://linkinghub.elsevier.com/retrieve/pii/S007961072030016X

182. Eisner D. Calcium in the heart: from physiology to disease. Exp Physiol [Internet]. 2014 Oct 1;99(10):1273–82. Available from: http://doi.wiley.com/10.1113/expphysiol.2013.077305

183. Sorrentino A, Borghetti G, Zhou Y, Cannata A, Meo M, Signore S, et al. Hyperglycemia induces defective Ca 2+ homeostasis in cardiomyocytes. Am J Physiol Circ Physiol [Internet]. 2017 Jan 1;312(1):H150–61. Available from: https://www.physiology.org/doi/10.1152/ajpheart.00737.2016

184. Belke DD, Swanson EA, Dillmann WH. Decreased Sarcoplasmic Reticulum Activity and Contractility in Diabetic db/db Mouse Heart. Diabetes [Internet]. 2004 Dec 1;53(12):3201–8. Available from: https://diabetesjournals.org/diabetes/article/53/12/3201/14450/Decreased-Sarcoplasmic-Reticulum-Activity-and

185. Sanganalmath SK, Dubey S, Veeranki S, Narisetty K, Krishnamurthy P. The interplay of inflammation, exosomes and Ca2+ dynamics in diabetic cardiomyopathy. Cardiovasc Diabetol [Internet]. 2023 Feb 20;22(1):37. Available from: https://cardiab.biomedcentral.com/articles/10.1186/s12933-023-01755-1

186. Singh T, Joshi S, Meah MN, Spath NB, Papanastasiou G, Kershaw LE, et al. Repeatability and reproducibility of cardiac manganese-enhanced magnetic resonance imaging. Sci Rep [Internet]. 2023 Feb 27;13(1):3366. Available from: https://www.nature.com/articles/s41598-023-29591-z

187. Kl□ppel G, Drenck CR, Oberholzer M, Heitz PU. Morphometric evidence for a striking B-cell reduction at the clinical onset of type 1 diabetes. Virchows Arch A Pathol Anat Histopathol [Internet]. 1984;403(4):441–52. Available from: http://link.springer.com/10.1007/BF00737292

188. Roep BO, Thomaidou S, van Tienhoven R, Zaldumbide A. Type 1 diabetes mellitus as a disease of the β-cell (do not blame the immune system?). Nat Rev Endocrinol [Internet]. 2021 Mar 8;17(3):150–61. Available from: http://www.nature.com/articles/s41574-020-00443-4

189. Madsbad S, Krarup T, Regeur L, Faber OK, Binder C. Effect of strict blood glucose control on residual B-cell function in insulin-dependent diabetics. Diabetologia [Internet]. 1981 May;20(5). Available from: http://link.springer.com/10.1007/BF00252760

190. Effects of Age, Duration and Treatment of Insulin-Dependent Diabetes Mellitus on

Residual β -Cell Function: Observations During Eligibility Testing for the Diabetes Control and Complications Trial (DCCT). J Clin Endocrinol Metab [Internet]. 1987 Jul;65(1):30–6. Available from: https://academic.oup.com/jcem/article-lookup/doi/10.1210/jcem-65-1-30

191. Sun JK, Keenan HA, Cavallerano JD, Asztalos BF, Schaefer EJ, Sell DR, et al. Protection From Retinopathy and Other Complications in Patients With Type 1 Diabetes of Extreme Duration. Diabetes Care [Internet]. 2011 Apr 1;34(4):968–74. Available from: https://diabetesjournals.org/care/article/34/4/968/38854/Protection-From-Retinopathy-and-Other
192. Gibb FW, McKnight JA, Clarke C, Strachan MWJ. Preserved C-peptide secretion is associated with fewer low-glucose events and lower glucose variability on flash glucose monitoring in adults with type 1 diabetes. Diabetologia [Internet]. 2020 May 7;63(5):906–14. Available from: http://link.springer.com/10.1007/s00125-020-05099-3
193. Saudek F, Brogren C-H, Manohar S. Imaging the Beta-Cell Mass: Why and How. Rev Diabet Stud [Internet]. 2008;5(1):6–12. Available from: http://www.soc-bdr.org/content/e4/e887/volRdsVolumes5237/issRdsIssues5238/chpRdsChapters5239/strRdsArticles5240/index_en.html?preview=preview
194. Clavijo Jordan V, Hines CDG, Gantert LT, Wang S, Conarello S, Preihs C, et al. Imaging Beta-Cell Function in the Pancreas of Non-Human Primates Using a Zinc-Sensitive MRI Contrast Agent. Front Endocrinol (Lausanne) [Internet]. 2021 May 26;12. Available from: https://www.frontiersin.org/articles/10.3389/fendo.2021.641722/full
195. Gimi B, Leoni L, Oberholzer J, Braun M, Avila J, Wang Y, et al. Functional MR microimaging of pancreatic beta-cell activation. Cell Transplant [Internet]. 2006;15(2):195–203. Available from: http://www.ncbi.nlm.nih.gov/pubmed/16719054

196. Antkowiak PF, Vandsburger MH, Epstein FH. Quantitative pancreatic β cell MRI using manganese-enhanced Look-Locker imaging and two-site water exchange analysis. Magn Reson Med [Internet]. 2012 Jun;67(6):1730–9. Available from: https://onlinelibrary.wiley.com/doi/10.1002/mrm.23139

197. Fortisip Compact [Internet]. Available from: https://www.nutricia.co.uk/hcp/pim-products/fortisip-compact.html

198. Leoni L, Serai SD, Haque ME, Magin RL, Roman BB. Functional MRI characterization of isolated human islet activation. NMR Biomed [Internet]. 2010 Dec;23(10):1158–65. Available from: http://www.ncbi.nlm.nih.gov/pubmed/21162143

199. Antkowiak PF, Tersey SA, Carter JD, Vandsburger MH, Nadler JL, Epstein FH, et al. Noninvasive assessment of pancreatic β-cell function in vivo with manganese-enhanced magnetic resonance imaging. Am J Physiol Metab [Internet]. 2009 Mar;296(3):E573–8. Available from: https://www.physiology.org/doi/10.1152/ajpendo.90336.2008

200. Meyer A, Stolz K, Dreher W, Bergemann J, Holebasavanahalli Thimmashetty V, Lueschen N, et al. Manganese-Mediated MRI Signals Correlate With Functional β-Cell Mass During Diabetes Progression. Diabetes [Internet]. 2015 Jun;64(6):2138–47. Available from: http://diabetes.diabetesjournals.org/lookup/doi/10.2337/db14-0864

201. Berkova Z, Jirak D, Zacharovova K, Kriz J, Lodererova A, Girman P, et al. Labeling of pancreatic islets with iron oxide nanoparticles for in vivo detection with magnetic resonance. Transplantation [Internet]. 2008 Jan 15;85(1):155–9. Available from: http://www.ncbi.nlm.nih.gov/pubmed/18192927

202. Tai JH, Foster P, Rosales A, Feng B, Hasilo C, Martinez V, et al. Imaging Islets Labeled With Magnetic Nanoparticles at 1.5 Tesla. Diabetes [Internet]. 2006 Nov 1;55(11):2931–8. Available from:

https://diabetesjournals.org/diabetes/article/55/11/2931/12470/Imaging-Islets-Labeled-With-Magnetic-Nanoparticles

203. Moossa AR, Altorki N. Pancreatic Biopsy. Surg Clin North Am [Internet]. 1983 Dec;63(6):1205–14. Available from: https://linkinghub.elsevier.com/retrieve/pii/S003961091643183X

204. Richardson SJ, Pugliese A. 100 YEARS OF INSULIN: Pancreas pathology in type 1 diabetes: an evolving story. J Endocrinol [Internet]. 2022 Feb 1;252(2):R41–57. Available from: https://joe.bioscientifica.com/view/journals/joe/252/2/JOE-21-0358.xml

205. Palmer WJ. Manganese-Based Contrast Agent Offers Safer, Non-Toxic Option for MRI scans. Available from: https://www.diagnosticimaging.com/view/manganese-based-contrast-agent-offers-safer-non-toxic-option-for-mri-scans

206. Dash R, Chung J, Ikeno F, Hahn-Windgassen A, Matsuura Y, Bennett M V., et al. Dual Manganese-Enhanced and Delayed Gadolinium-Enhanced MRI Detects Myocardial Border Zone Injury in a Pig Ischemia-Reperfusion Model. Circ Cardiovasc Imaging [Internet]. 2011 Sep;4(5):574–82. Available from: https://www.ahajournals.org/doi/10.1161/CIRCIMAGING.110.960591

207. Dash R, Kim PJ, Matsuura Y, Ikeno F, Metzler S, Huang NF, et al. Manganese-Enhanced Magnetic Resonance Imaging Enables In Vivo Confirmation of Peri-Infarct Restoration Following Stem Cell Therapy in a Porcine Ischemia–Reperfusion Model. J Am Heart Assoc [Internet]. 2015 Jul 17;4(7). Available from: https://www.ahajournals.org/doi/10.1161/JAHA.115.002044

208. Carbone RG, Monselise A, Bottino G, Negrini S, Puppo F. Stem cells therapy in acute myocardial infarction: a new era? Clin Exp Med [Internet]. 2021 May 23;21(2):231–7. Available from: https://link.springer.com/10.1007/s10238-021-00682-3

209. Tschöpe C, Ammirati E, Bozkurt B, Caforio ALP, Cooper LT, Felix SB, et al. Myocarditis and inflammatory cardiomyopathy: current evidence and future directions. Nat Rev Cardiol [Internet]. 2021 Mar 12;18(3):169–93. Available from: https://www.nature.com/articles/s41569-020-00435-x

210. Elmariah S. Patterns of Left Ventricular Remodeling in Aortic Stenosis: Therapeutic Implications. Curr Treat Options Cardiovasc Med [Internet]. 2015 Jul 21;17(7):31. Available from: http://link.springer.com/10.1007/s11936-015-0391-0

211. Kellum JA, Romagnani P, Ashuntantang G, Ronco C, Zarbock A, Anders H-J. Acute kidney injury. Nat Rev Dis Prim [Internet]. 2021 Jul 15;7(1):52. Available from: https://www.nature.com/articles/s41572-021-00284-z